DOC.20070530.0013

QA: QA

ANL-NBS-HS-000058 REV 00

May 2007

Calibrated Unsaturated Zone Properties

NOTICE OF OPEN CHANGE DOCUMENTS - THIS DOCUMENT IS IMPACTED BY THE LISTED CHANGE DOCUMENT AND CANNOT BE USED WITHOUT IT.

----

1) ACN-001, DATED 07/10/2007

Prepared for:
U.S. Department of Energy
Office of Civilian Radioactive Waste Management
Office of Repository Development
1551 Hillshire Drive
Las Vegas, Nevada 89134-6321

Prepared by:
Sandia National Laboratories
OCRWM Lead Laboratory for Repository Systems
1180 Town Center Drive
Las Vegas, Nevada 89144

Under Contract Number
DE-AC04-94AL85000

DISCLAIMER

This report was prepared as an account of work sponsored by an agency of the United States Government. Neither the United States Government nor any agency thereof, nor any of their employees, nor any of their contractors, subcontractors or their employees, makes any warranty, express or implied, or assumes any legal liability or responsibility for the accuracy, completeness, or any third party's use or the results of such use of any information, apparatus, product, or process disclosed, or represents that its use would not infringe privately owned rights. Reference herein to any specific commercial product, process, or service by trade name, trademark, manufacturer, or otherwise, does not necessarily constitute or imply its endorsement, recommendation, or favoring by the United States Government or any agency thereof or its contractors or subcontractors. The views and opinions of authors expressed herein do not necessarily state or reflect those of the United States Government or any agency thereof.

QA: QA

Calibrated Unsaturated Zone Properties

ANL-NBS-HS-000058 REV 00

May 2007

INTENTIONALLY LEFT BLANK

Sandia National Laboratories

Scientific Analysis/Calculation Signature Page/Change History

Complete only applicable items.

2. Document Title
Calibrated Unsaturated Zone Properties

3. DI (Including Rev. No.)
ANL-NBS-HS-000058 REV 00

	Printed Name	Signature	Date
4. Originator	Hui-Hai Liu		5/24/07
5. Checker	Charles Haukwa		5/24/07
5. QCS	Vivi Fissekidou		5/24/07
7. Responsible Manager/Lead	Cliff Ho	Clifford K. Ho	5/24/07
8. Responsible Manager	Stephanie Kuzio		5/24/07

9. Remarks
Quanlin Zhou and Yongkoo Seol contributed to Section 6 and Appendices B through E. Teamrat Ghezzehei and Peter Persoff contributed to Appendix G. Tim Vogt and Jim Houseworth contributed to Appendix C.

Change History

10. Revision No.	11. Description of Change
REV 00	Initial Issue. The report addresses CR 9885 by using corrected surface areas of core samples (Appendix G).

INTENTIONALLY LEFT BLANK

CONTENTS

Page

CONTENTS (Continued)

Page

FIGURES

Page

FIGURES (Continued)

Page

TABLES

Page

TABLES (Continued)

Page

ACRONYMS

CFu	Crater Flat undifferentiated hydrogeologic unit
CHn	Calico Hills nonwelded hydrogeologic unit
DIRS	Document Input Reference System
DKM	dual-permeability model
DTN	data tracking number
ECM	Equilibrium continuum model
ESF	Exploratory Studies Facility
FEP	feature, event, or process
HGU	hydrogeologic unit
LA	license application
NSP	Nevada State Plane
PTn	Paintbrush nonwelded hydrogeologic unit
TCw	Tiva Canyon welded hydrogeologic unit
TDMS	Technical Data Management System
TPO	technical product output
TSPA	Total System Performance Assessment
TSw	Topopah Spring welded hydrogeologic unit
TWP	technical work plan
STN	Software Tracking Number
UTM	Universal Transverse Mercator
UZ	unsaturated zone
UZ models	unsaturated zone flow and transport models

INTENTIONALLY LEFT BLANK

1. PURPOSE

The purpose of this report is to document the calibrated property sets for unsaturated zone (UZ) flow and transport process models (UZ models). The calibration of the property sets is performed through inverse modeling using a previously validated model. This work followed, and was planned in *Technical Work Plan for: Unsaturated Zone Flow, Drift Seepage and Unsaturated Zone Transport Modeling* (BSC 2006 [DIRS 177465], Sections 1 and 2.1.2). However, this analysis report deviates from the technical work plan (TWP) (BSC 2006 [DIRS 177465]), which states the calibrated property sets are to be documented as an appendix to *UZ Flow Models and Submodels* (SNL 2007 [DIRS 175177]). The deviation is that this analysis is documented as a separate analysis report. This deviation is expected to improve the efficiency of documentating the analysis activities, and reviewing and checking the document. Direct inputs to this report were derived from the following upstream analysis and model reports (Section 4):

- *Analysis of Hydrologic Properties Data* (BSC 2004 [DIRS 170038])
- *Development of Numerical Grids for UZ Flow and Transport Modeling* (BSC 2004 [DIRS 169855])
- *Simulation of Net Infiltration for Present-Day and Potential Future Climates* (SNL 2007 [DIRS 174294])
- *Geologic Framework Model (GFM2000)* (BSC 2004 [DIRS 170029].

The calibrated property sets correspond to four estimated present-day net infiltration scenarios (10th, 30th, 50th, and 90th percentiles). The calibrated property sets submitted to the Technical Data Management System (TDMS) are:

- Drift-scale calibrated parameter sets based on one-dimensional inversions
- Mountain-scale calibrated parameter sets based on one-dimensional inversions
- Calibrated fault parameters based on two-dimensional inversions.

The caveats and limitations for use of each of these property sets are documented in Sections 6.1 and 6.4. The limitations of the calibration process are also discussed in Sections 6.1, 6.3, and 6.4.

The TWP (BSC 2006 [DIRS 177465]) applicable to this work was developed in accordinance with the applicable BSC procedures and only BSC procedures are discussed there. However, calibration activities documented in this report were transferred to the Lead Lab on October 2, 2006. Therefore, the corresponding Lead Lab procedures have been followed in this study (Section 2). Also, CorpsCon V. 5.11.08 [DIRS 155082] is not listed in the TWP (BSC 2006 [DIRS 177465]), but has been used in this study to convert UTM (Universal Transverse Mercator) coordinates for infiltration maps to the NSP (Nevada State Plane) system. This conversion is necessary because locations of calibration boreholes are given using NSP coordinates.

INTENTIONALLY LEFT BLANK

2. QUALITY ASSURANCE

Development of this report and the supporting analysis activities have been determined to be subject to the Yucca Mountain Project's quality assurance program as indicated in *Technical Work Plan for: Unsaturated Zone Flow, Drift Seepage and Unsaturated Zone Transport Modeling* (BSC 2006 [DIRS 177465], Section 8.1). Approved quality assurance procedures identified in the TWP (BSC 2006 [DIRS 177465], Section 4) have been used to conduct and document the activities described in this report. Since this activity was transitioned to the Lead Laboratory QA program, the corresponding lead lab procedures were used. The methods used to control the electronic management of data during the analysis and documentation activities are described in IM-PRO-002, *Control of the Electronic Management of Information.* The analysis activities and associated calculations herein were conducted and documented following SCI-PRO-005, *Scientific Analysis and Calculations.* SCI-PRO-001, *Qualification of Unqualified Data*, was followed for qualifying data for the intended use within the report (Appendix G).

This report provides calibrated values for hydrologic properties of the unsaturated zone rocks above and below the repository. The unsaturated zone rocks above and below the reposity are natural barriers classfied in *Q-List* (BSC 2005 [DIRS 175539]) as "Safety Category" because it is important to waste isolation, as defined in LS-PRO-0203, *Q-List and Classification of Structures, Systems, and Components*. The report contributes to the analysis data used to support the Total System Performance Assessment (TSPA), but is not directly used by TSPA. The conclusions from this report do not directly impact engineered features important to preclosure safety, as defined in LS-PRO-0203.

INTENTIONALLY LEFT BLANK

3. USE OF SOFTWARE

Table 3-1 lists software used in this study. These are appropriate for the intended application and are used only within the range of validation. They were obtained from Software Configuration Management and meet the requirements of IM-PRO-003, *Software Management*. All qualified software used in this report has been run on platform version numbers consistent with those listed in the Software Baseline Report readily available through Software Configuration Management.

Table 3-1. Qualified Software Used in This Report

Software Name	Version	Software Tracking Number (STN)	Reference Number	Operating Environment
iTOUGH2	5.0	10003-5.0-00	[DIRS 160106]	Linux, Red Hat V7.3
2kgrid8.for	1.0	10503-1.0-00	[DIRS 154787]	PC, DOS V4.00.1111
infil2grid	1.7	10077-1.7-00	[DIRS 154793]	PC, DOS V4.00.1111
TBgas3D	2.0	10882-2.0-00	[DIRS 160107]	SUN, O.S.5.5.1
e9-3in	1.0	10126-1.0-00	[DIRS 146536]	Sun, UNIX
CorpsCon	5.11.08	10547-5.11.08-00	[DIRS 155082]	PC, WINDOWS NT 4.0

The use of the codes listed in Table 3-1 is documented in Section 6 and appendices. These codes have been qualified and meet the requirements of IM-PRO-003. The code iTOUGH2 V5.0 was used for property calibration against field data based on inverse modeling methodology. The codes 2kgrid8.for V1.0, infil2grid V1.7, TBgas3D V2.0, e9-3in V1.0, and CorpsCon V. 5.11.08 are used for converting an ECM (Effective Continuum Model) grid to the corresponding DKM (dual-permeability model) grid, mapping the infiltration rate data into top elements of a numerical grid, determining the top gas-flow boundary conditions for calibration simulations using pneumatic data, converting EOS9 format of initial conditions to the corresponding EOS3 format, and converting coordinate systems for the infiltration maps, respectively.

Standard spreadsheet software (Microsoft Excel® 2002 with Windows 2000 operating systems on desktop PC) is employed for simple data analyses and processing using standard functions, and plotting programs (Tecplot Version 10.0) are used for generating figures of simulation results. These programs are exempt from the software qualification requirements of IM-PRO-003. All information needed to reproduce the work using the standard spreadsheet, including the input, computation, and output, is included in this report (Appendices C and E).

The iTOUGH2 V5.0 code is selected for use in this analysis report because of its general capability in inverse modeling and in handling unsaturated zone flow and transport in fractured rock. There are no limitations on the outputs when the software is used within the range of use for simulating unsaturated flow through fractured rock. The other codes listed in Table 3-1 were developed routines to perform the simple, specific functions as previously mentioned. The validation ranges for these routines are to convert an ECM grid to the corresponding DKM grid (2kgrid8.for V1.0), to map infiltration data into the top boundary of a numerical grid (infil2grid V1.7), to determine top gas-pressure boundary condition (TBgas3D V2.0), to convert flow conditions from EOS9 to EOS3 format (e9-3in V1.0), and to convert coordinates from UTM to

NSP system (CorpsCon V. 5.11.08). The use of these codes is consistent with the intended use and within the document validation ranges of the software.

4. INPUTS

This section discusses input data and parameters used in this report.

4.1 DIRECT INPUTS

Source information on the direct inputs is summarized in Table 4-1 and is further documented below. Specific data files from each data set (Table 4-1) used in this study, are described in Section 6 and/or the related appendices. The appropriateness of the inputs is also described.

4.1.1 Output from Other Models and Analyses

Developed data include the spatially varying infiltration maps from the infiltration model and several numerical grids, which are documented in separate reports (BSC 2004 [DIRS 169855]; SNL 2007 [DIRS 174294]). These data sets are too large to reproduce here, but are listed by data tracking number (DTN) in Table 4-1. Uncalibrated properties and property-estimate uncertainties of the matrix and fractures, which are used as inputs to the calibration, are listed in Tables 4-2 and 4-3, respectively. Porosity, residual saturation, satiated saturation, and van Genuchten parameter *m* are not calibrated. All other properties and uncertainty data are used to constrain the calibration. The infiltration maps are the best estimates of unsaturated zone infiltration rate distributions currently available. The appropriateness of the numerical grids for simulating flow and transport in the unsaturated zone is presented in a scientific analysis report (BSC 2004 [DIRS 169855]).

4.1.2 Acquired Data

Acquired data include saturation; water potential; pneumatic pressure; fracture, matrix, and fault properties; infiltration maps; and numerical grids. In all cases, the data sets are too large to reproduce here, but are listed by DTN in Table 4-1. These data are developed prior to use in the inversions as documented in Sections 6.2 and 6.3.4. Data that are not used are also discussed.

4.1.2.1 Saturation Data

Saturation data measured on core from boreholes USW SD-6, USW SD-7, USW SD-9, USW SD-12, USW UZ-14, UE-25 UZ#16, USW WT-24, USW UZ-N11, USW UZ-N31, USW UZ-N 32, USW UZ-N33, USW UZ-N37, USW UZ-N38, USW UZ-N53, USW UZ-N54, USW UZ-N55, USW UZ-N57, USW UZ-N58, USW UZ-N59, and USW UZ-N61 are used for the one-dimensional inversions. The locations of these boreholes are shown in Figure 4-1. These boreholes do not intersect mapped faults, and thus the saturation data from these boreholes are representative of the rock mass of Yucca Mountain. Saturation data measured on core from Borehole USW UZ-7a (location shown in Figure 4-1) are used for the two-dimensional inversions. This borehole intersects the Ghost Dance fault, and saturation data from this borehole are judged to be representative of the faulted rock at Yucca Mountain.

Saturation data measured on core from several boreholes and tunnels at Yucca Mountain are not included in any of the inversions. Saturation data measured on core from boreholes USW NRG-6 and USW NRG-7a are not used because handling of the core caused excessive drying (Rousseau et al. 1999 [DIRS 102097], p. 125). Saturation data measured on core from the

Exploratory Studies Facility (ESF), Enhanced Characterization of Repository Block Cross-Drift, alcoves, and niches are not used, because they represent only a single layer in the stratigraphic column. Geophysical measurements of saturation are not used because of larger uncertainties associated with these data, compared with direct measurements of saturation by oven drying. A detailed discussion of the relevant geophysical measurements was presented by *Thermal Conductivity of the Potential Repository Horizon* (BSC 2004 [DIRS 169854], Appendix B) as compared with the corresponding core measurements. The iTOUGH2 input files from DTNs: LB0208UZDSCPMI.001 [DIRS 161285], LB0208UZDSCPUI.001 [DIRS 166711], LB0302AMRU0035.001 [DIRS 162378] and LB02092DSSCFPR.001 [DIRS 162422] contain the saturation data formatted for iTOUGH2 inversions. In this study, these input files are used as the direct inputs into inversion runs. These DTNs are output from *Calibrated Properties Model* (BSC 2004 [DIRS 169857]). SCI-PRO-005, Section 6.2.1 D, states 'if using a previously validated mathematical model to complete the scientific A/C [analysis or calculation], obtain the appropriate model file/product output from the Technical Data Management System (TDMS).' The justification of the appropriateness to use these data is provided in Section 4.1.3.

Table 4-1. Input Data Sources and Data Tracking Numbers

DTN	Data Description	Section Describing Data Use
LB0208HYDSTRAT.001 [DIRS 174491]	2002 UZ Model Grid Components: Supporting Files	Appendix C
GS000608312261.001 [DIRS 155891]	In situ Pneumatic Pressure Data for Borehole UE-25 NRG#5	6.2.3
GS950208312232.003 [DIRS 105572]; GS951108312232.008 [DIRS 106756]; GS031208312232.007 [DIRS 178751]	In situ Pneumatic Pressure Data for Borehole USW NRG-6 & USW NRG-7a	6.2.3
GS960908312261.004 [DIRS 106784]	In situ Pneumatic Pressure Data for Borehole USW SD-7	6.2.3
GS031208312232.008 [DIRS 178750]	In situ Pneumatic Pressure Data for Borehole USW SD-12, USW NRG-7a, and USW UZ-7a	6.2.3 6.3.3 6.3.4
SN0609T0502206.028 [DIRS 178753]	Present-Day Infiltration Maps	6.2.5 Appendix C Appendix D Appendix F
LB02081DKMGRID.001 [DIRS 160108]	One-dimensional and two-dimensional grids	6.2.1 6.3.4 Appendix B Appendix F
LB0205REVUZPRP.001 [DIRS 159525]	Uncalibrated Fracture Property Data	6.4 Appendix F
LB0207REVUZPRP.002 [DIRS 159672]	Uncalibrated Matrix Property Data	6.4
LB0207REVUZPRP.001 [DIRS 159526]	Uncalibrated Fault Property Data	6.3.4

Table 4-1. Input Data Sources and Data Tracking Numbers (Continued)

DTN	Data Description	Section Describing Data Use
LB0208UZDSCPMI.001 [DIRS 161285]	Calibrated One-Dimensional Parameter Set for the UZ flow and transport model for previous base-case infiltration map	5 6.2.2 6.2.4 6.3.2 Appendix B Appendix D
LB0208UZDSCPUI.001 [DIRS 166711]	Calibrated One-Dimensional Parameter Set for the UZ flow and transport model for previous upper-bound infiltration map	6.2.2 6.2.4 6.3.2 Appendix D
LB02091DSSCP3I.001 [DIRS 161292]	One-Dimensional, Mountain-Scale Calibration for calibrated properties model	6.2.3 6.2.4 6.2.5 Appendix B Appendix E
LB02092DSSCFPR.001 [DIRS 162422]	Two-dimensional, Fault Calibration for calibrated properties model	6.2.5 6.3.4 Appendix F
MO0012MWDGFM02.002 [DIRS 153777]	Geologic Framework Model (GFM2000)	6.2.3 6.3.4
LB0302AMRU0035.001 [DIRS 162378]	UZ Calibrated Property Model Validation	6.2.3 6.2.4 6.3.2 Appendix E
LB0210AMRU0035.002 [DIRS 166712]	UZ Parameter Uncertainty	6.4.2

Table 4-2. Uncalibrated Matrix Properties and Uncertainty Data

HGU	ϕ	k [m^2]	log(k) [log(m^2)]	$\sigma_{log(k)}$	N	N Nondetect	$SE_{log(k)}$	$1/\alpha$ [Pa]	log($1/\alpha$) [log (Pa)]	$SE_{log(1/\alpha)}$	m	SE_m	S_r
CCR & CUC	0.241	4.7×10^{-15}	−14.33	0.47	3	0	0.27	8.27×10^{4}	4.918	0.279	0.388	0.085	0.02
CUL & CW	0.088	6.4×10^{-20}	−19.20	2.74	15	25	0.43	5.46×10^{5}	5.737	0.178	0.280	0.045	0.20
CMW	0.200	1.8×10^{-16}	−15.74	2.38	5	1	0.97	2.50×10^{5}	5.398	0.188	0.259	0.042	0.31
CNW	0.387	4.0×10^{-14}	−13.40	2.05	10	0	0.65	2.03×10^{4}	4.308	0.199	0.245	0.032	0.24
BT4	0.428	4.1×10^{-13}	−12.39	1.41	11	0	0.43	4.55×10^{3}	3.658	0.174	0.219	0.019	0.13
TPY	0.233	1.3×10^{-15}	−14.90	0.64	2	0	0.46	7.63×10^{4}	4.883	0.379	0.247	0.064	0.07
BT3	0.413	1.3×10^{-13}	−12.87	1.09	11	1	0.31	8.90×10^{3}	3.950	0.088	0.182	0.008	0.14
TPP	0.498	1.1×10^{-13}	−12.96	0.39	11	0	0.12	2.12×10^{4}	4.325	0.104	0.300	0.023	0.06
BT2	0.490	6.7×10^{-13}	−12.17	1.12	21	0	0.24	1.74×10^{4}	4.239	0.170	0.126	0.013	0.05
TC	0.054	4.4×10^{-17}	−16.36	3.02	6	5	0.91	2.71×10^{5}	5.432	0.310	0.218	0.054	0.21
TR	0.157	3.2×10^{-16}	−15.50	0.94	46	1	0.14	9.43×10^{4}	4.974	0.116	0.290	0.025	0.07
TUL	0.155	2.8×10^{-17}	−16.56	1.61	37	12	0.23	1.75×10^{5}	5.244	0.111	0.283	0.024	0.12
TMN	0.111	4.5×10^{-19}	−18.34	0.97	74	35	0.09	1.40×10^{6}	6.147	0.108	0.317	0.042	0.19
TLL	0.131	3.7×10^{-17}	−16.44	1.65	51	24	0.19	6.01×10^{4}	4.779	0.521	0.216	0.061	0.12

Table 4-2. Uncalibrated Matrix Properties and Uncertainty Data (Continued)

HGU	ϕ	k [m^2]	log(*k*) [log(m^2)]	$\sigma_{log(k)}$	N	N Nondetect	$SE_{log(k)}$	$1/\alpha$ [Pa]	log(1/α) [log (Pa)]	$SE_{log(1/\alpha)}$	m	SE_m	S_r
TM2 & TM1	0.103	2.3×10^{-20}	−19.63	3.67	21	42	0.46	3.40×10^{6}	6.532	0.097	0.442	0.073	0.20
PV3	0.043	2.9×10^{-18}	−17.54	1.57	16	2	0.37	1.00×10^{6}	6.000	0.278	0.286	0.065	0.42
PV2a	0.275	a	a	a	a	a	a	2.17×10^{5}	5.336	0.156	0.059	0.007	0.36
PV2v	0.229	4.3×10^{-13}	−12.37	1.38	16	0	0.34	1.94×10^{4}	4.287	0.042	0.293	0.011	0.13
BT1a	0.285	3.5×10^{-17}	−16.45	2.74	9	1	0.87	4.72×10^{6}	6.674	0.183	0.349	0.073	0.38
BT1v	0.331	2.1×10^{-13}	−12.67	1.11	35	0	0.19	1.35×10^{4}	4.131	0.049	0.240	0.008	0.06
CHV	0.346	1.6×10^{-12}	−11.81	1.62	46	0	0.24	3.39×10^{3}	3.530	0.094	0.158	0.008	0.06
CHZ	0.322	5.2×10^{-18}	−17.28	0.91	99	17	0.08	4.45×10^{5}	5.649	0.094	0.257	0.022	0.26
BTa	0.271	8.2×10^{-19}	−18.08	2.05	9	8	0.50	6.42×10^{6}	6.808	0.043	0.499	0.036	0.36
BTv	b	b	b	b	b	b	b	5.04×10^{4}	4.703	0.207	0.147	0.020	b
PP4	0.321	1.5×10^{-16}	−15.81	2.74	6	2	0.97	5.00×10^{5}	5.699	0.401	0.474	0.224	0.29
PP3	0.318	6.4×10^{-15}	−14.20	0.75	51	0	0.11	1.32×10^{5}	5.120	0.084	0.407	0.031	0.08
PP2	0.221	5.4×10^{-17}	−16.27	1.18	34	3	0.19	6.22×10^{5}	5.794	0.147	0.309	0.041	0.10
PP1	0.297	8.1×10^{-17}	−16.09	1.52	27	1	0.29	1.13×10^{5}	5.052	0.234	0.272	0.036	0.30
BF3/TR3	0.175	1.1×10^{-15}	−14.95	1.64	7	1	0.58	8.94×10^{4}	4.951	0.931	0.193	0.117	0.11
BF2	0.234	c	c	c	c	c	c	8.46×10^{6}	6.927	0.032	0.617	0.070	0.21

DTN: LB0207REVUZPRP.002 [DIRS 159672].

NOTES: The relation between HGUs and UZ model layers is given in Table 6-1.
k is permeability; σ is standard deviation; N is number of samples; ϕ is porosity.
α and m are fitting parameters for the van Genuchten water potential relationship.
SE is standard error.
S_r is residual liquid saturation.
Nondetect means permeability too low to measure.
Lower-case characters 'a' and 'v' refer to the zeolitic and vitric portions of a given HGU (Table 6-1), respectively..

[a] BT1a was used as an analogue for permeability because only one permeability data point is available for PV2a.

[b] BT1v was used as an analogue for porosity, residual saturation, and permeability because only one sample is available for BTv.

[c] PP1 was used as an analogue for permeability because only one measurable permeability data point is available for BF2.

Table 4-3. Uncalibrated Fracture Property Data

UZ Model Layer	Permeability (m^2)				Frequency (m^{-1})			van Genuchten				
	k_G	$log(k_G)$	$\sigma_{log(kG)}$	N	f	σ_f	N	α (Pa^{-1})	log(α)	m (−)	porosity (−)	Std (−)
tcw11	3.0×10^{-11}	−10.52	–	2	0.92	0.94	76	5.0×10^{-3}	−2.30	0.633	2.4×10^{-2}	–
tcw12	5.3×10^{-12}	−11.28	0.78	80	1.91	2.09	1241	2.2×10^{-3}	−2.66	0.633	1.7×10^{-2}	-
tcw13	4.5×10^{-12}	−11.35	1.15	3	2.79	1.43	60	1.9×10^{-3}	−2.73	0.633	1.3×10^{-2}	–
ptn21	3.2×10^{-12}	−11.49	0.88	12	0.67	0.92	76	2.7×10^{-3}	−2.57	0.633	9.2×10^{-3}	–
ptn22	3.0×10^{-13}	−12.52	0.20	4	0.46	–	–	1.4×10^{-3}	−2.86	0.633	1.0×10^{-2}	–
ptn23	3.0×10^{-13}	−12.52	0.20	4	0.57	–	63	1.2×10^{-3}	−2.91	0.633	2.1×10^{-3}	–
ptn24	3.0×10^{-12}	−11.52	–	1	0.46	0.45	18	3.0×10^{-3}	−2.53	0.633	1.0×10^{-2}	–
ptn25	1.7×10^{-13}	−12.78	0.10	7	0.52	0.6	72	1.1×10^{-3}	−2.96	0.633	5.5×10^{-3}	–
ptn26	2.2×10^{-13}	−12.66	–	1	0.97	0.84	114	9.6×10^{-4}	−3.02	0.633	3.1×10^{-3}	–
tsw31	8.1×10^{-13}	−12.09	–	–	2.17	2.37	140	1.1×10^{-3}	−2.96	0.633	5.0×10^{-3}	–

Table 4-3. Uncalibrated Fracture Property Data (Continued)

UZ Model Layer	Permeability (m^2)				Frequency (m^{-1})			van Genuchten				
	k_G	$\log(k_G)$	$\sigma_{\log(kG)}$	N	f	σ_f	N	α (Pa^{-1})	$\log(\alpha)$	m (–)	porosity (–)	Std (–)
tsw32	7.1×10^{-13}	−12.15	0.66	31	1.12	1.09	842	1.4×10^{-3}	−2.86	0.633	8.3×10^{-3}	–
tsw33	7.8×10^{-13}	−12.11	0.61	27	0.81	1.03	1329	1.6×10^{-3}	−2.80	0.633	5.8×10^{-3}	–
tsw34	3.3×10^{-13}	−12.48	0.47	180	4.32	3.42	10646	6.7×10^{-4}	−3.18	0.633	8.5×10^{-3}	2.50×10^{-3}
alternate tsw34	1.5×10^{-13}	−12.81	0.75	180								
tsw35	9.1×10^{-13}	−12.04	0.54	31	3.16	–	595	1.0×10^{-3}	−2.99	0.633	9.6×10^{-3}	–
tsw3[67]	1.3×10^{-12}	−11.87	0.28	19	4.02	–	526	1.1×10^{-3}	−2.96	0.633	1.3×10^{-2}	–
tsw38	8.1×10^{-13}	−12.09	–	–	4.36	–	37	8.9×10^{-4}	−3.05	0.633	1.1×10^{-2}	–
tsw39	8.1×10^{-13}	−12.09	–	–	0.96	–	46	1.5×10^{-3}	−2.82	0.633	4.3×10^{-3}	–
ch1Ze	2.5×10^{-14}	−13.60	–	–	0.04	–	3	1.4×10^{-3}	−2.86	0.633	1.6×10^{-4}	–
ch1VI	2.2×10^{-13}	−12.66	–	–	0.10	–	11	2.1×10^{-3}	−2.69	0.633	6.1×10^{-4}	–
ch[23456]VI	2.2×10^{-13}	−12.66	–	–	0.14	–	25	1.9×10^{-3}	−2.73	0.633	7.7×10^{-4}	–
ch[2345]Ze	2.5×10^{-14}	−13.60	–	1	0.14	–	25	8.9×10^{-4}	−3.05	0.633	3.7×10^{-4}	–
ch6	2.5×10^{-14}	−13.60	–	–	0.04	–	–	1.4×10^{-3}	−2.86	0.633	1.6×10^{-4}	–
pp4	2.5×10^{-14}	−13.60	–	–	0.14	–	–	8.9×10^{-4}	−3.05	0.633	3.7×10^{-4}	–
pp3	2.2×10^{-13}	−12.66	–	–	0.20	–	–	1.6×10^{-3}	−2.78	0.633	9.7×10^{-4}	–
pp2	2.2×10^{-13}	−12.66	–	–	0.20	–	–	1.6×10^{-3}	−2.78	0.633	9.7×10^{-4}	–
pp1	2.5×10^{-14}	−13.60	–	–	0.14	–	–	8.9×10^{-4}	−3.05	0.633	3.7×10^{-4}	–
bf3	2.2×10^{-13}	−12.66	–	–	0.20	–	–	1.6×10^{-3}	−2.78	0.633	9.7×10^{-4}	–
bf2	2.5×10^{-14}	−13.60	–	–	0.14	–	–	8.9×10^{-4}	−3.05	0.633	3.7×10^{-4}	–
tr3	2.2×10^{-13}	−12.66	–	–	0.20	–	–	1.6×10^{-3}	−2.78	0.633	9.7×10^{-4}	–
tr2	2.5×10^{-14}	−13.60	–	–	0.14	–	–	8.9×10^{-4}	−3.05	0.633	3.7×10^{-4}	–
tcwf	2.7×10^{-11}	−10.57	–	–	1.90	–	–	3.8×10^{-3}	−2.42	0.633	2.9×10^{-2}	–
ptnf	3.1×10^{-12}	−11.51	–	–	0.54	–	–	2.8×10^{-3}	−2.55	0.633	1.1×10^{-2}	–
tswf	1.5×10^{-11}	−10.82	–	–	1.70	–	–	3.2×10^{-3}	−2.49	0.633	2.5×10^{-2}	–
chnf	3.7×10^{-13}	−12.43	–	–	0.13	–	–	2.3×10^{-3}	−2.64	0.633	1.0×10^{-3}	–

DTNs: LB0205REVUZPRP.001 [DIRS 159525]; LB0207REVUZPRP.001 [DIRS 159526].

NOTES: k is permeability.
G refers to geometric mean.
σ is standard deviation.
N is number of samples.
f is fracture frequency.
α and m are fitting parameters for the van Genuchten water potential relationship.
Std refers to standard deviation for fracture porosity.
tsw3[67] refers to tsw36 and tsw37.
ch[23456]VI refers to ch2VI through ch6VI.
ch[23456]Ze refers to ch2Ze through ch6Ze.

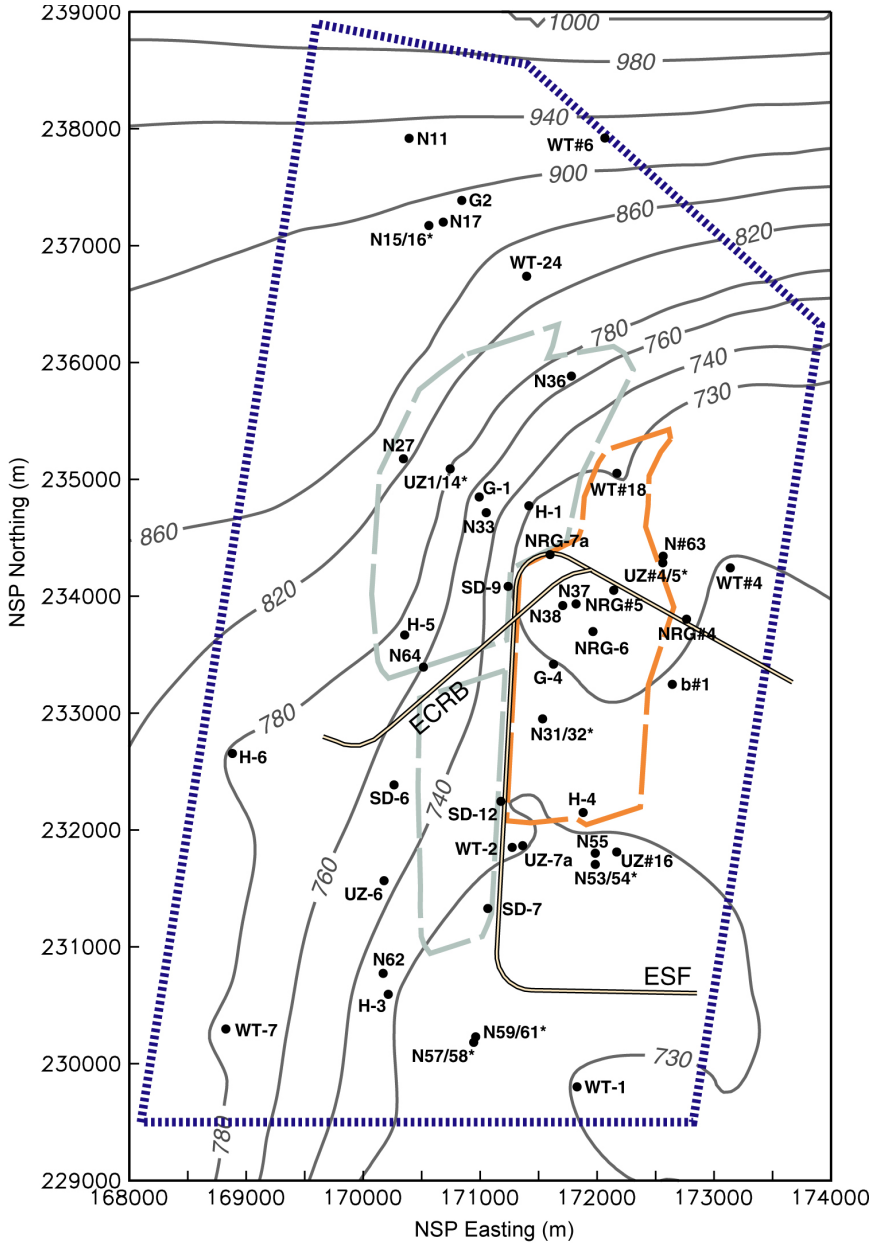

Source: BSC 2004 [DIRS 169855], Figure 6-2.
NOTE: NSP = Nevada State Plane.

Figure 4-1. Borehole Locations

4.1.2.2 Water-Potential Data

Water-potential data, measured in situ in boreholes USW NRG-6, USW NRG-7a, UE-25 UZ#4, and USW SD-12, are used in the one-dimensional inversions. These boreholes do not intersect mapped faults, and thus the water-potential data are representative of the rock mass of Yucca Mountain. Water-potential data measured in situ in Borehole USW UZ-7a are used for the two-dimensional inversions. This borehole intersects the Ghost Dance fault, and thus the water-potential data are judged to be representative of the faulted rock of Yucca Mountain. Water potential data measured in situ in Borehole UE-25 UZ#5 are not used because this borehole is very close to Borehole UE-25 UZ#4; the inversion results could be biased if both datasets (representing a smaller fraction of the whole region) were included. The iTOUGH2 input files from DTNs: LB0208UZDSCPMI.001 [DIRS 161285], LB0208UZDSCPUI.001 [DIRS 166711], LB0302AMRU0035.001 [DIRS 162378], and LB02092DSSCFPR.001 [DIRS 162422] contain the water-potential data formatted for iTOUGH2 inversions. In this study, these input files are used as direct inputs into inversion runs. Also note some recent water potential measurements were not used because the data were either similar to existing data or had a large measurement uncertainty (see Appendix A).

Water-potential data measured on cores are not used because drying during drilling and/or handling may have substantially changed the water potential. In contrast with saturation data, for which the amount of change may be estimated (see Section 6.2.2), there is no way to reliably estimate the change in water potential.

4.1.2.3 Pneumatic Pressure Data

Pneumatic pressure data measured in situ in boreholes UE-25 NRG#5, USW NRG-6, USW NRG-7a, USW SD-7, and USW SD-12 are used in the one-dimensional inversion. These boreholes do not intersect mapped faults, and thus the pneumatic pressure data from these boreholes are representative of the rock mass of Yucca Mountain. Pneumatic pressure data measured in situ in borehole USW UZ-7a are used in the two-dimensional inversion. This borehole intersects the Ghost Dance fault, and thus the pneumatic pressure data from this borehole are judged to be representative of the faulted rock of Yucca Mountain. The iTOUGH2 input files from DTNs: LB02091DSSCP3I.001 [DIRS 161292], LB0302AMRU0035.001 [DIRS 162378], and LB02092DSSCFPR.001 [DIRS 162422] contain the pressure data that are formatted for iTOUGH2 inversions. In this study, these input files are used as the direct inputs into inversion runs.

Pneumatic pressure data from Boreholes UE-25 UZ#4 and UE-25 UZ#5 are not used for the one-dimensional inversion because they are close to a small, unnamed fault which, while it does not affect the in situ water-potential data, could affect the pneumatic data. While data from these boreholes and from USW NRG-6 do show the influence of the ESF, which is transmitted via faults, they are not used for calibration of fault parameters because three-dimensional models would be required, and only a single parameter, Topopah Spring welded hydrogeologic unit (TSw) horizontal fracture permeability, could be calibrated.

4.1.2.4 Use of Established Fact Data and the Data Qualified for the Intended Use

Established fact data are used in Equations 6-8 through 6-10 (Section 6.2.2). These data include physical properties of air, the molecular weight and critical temperature and critical pressure of both air and water, and the mole fraction of water vapor in air. The data values and sources are specified in Section 6.2.2 of this report.

Data used for determining uncertainties in measurements of matrix saturation and water potential (Flint 1998 [DIRS 100033], pp. 11, and 17 to 19; Rousseau et al. 1999 [DIRS 102097], pp. 129 to 131 and 144), as discussed in Section 6.2.2, are qualified for the intended use in this report (Appendix G).

4.1.3 Use of Technical Product Outputs (TPOs) from the Calibrated Properties Model

Inputs taken from *Calibrated Properties Model* (BSC 2004 [DIRS 169857]) and their usage in this current report are given in Table 4-4. Per SCI-PRO-005, *Scientific Analyses and Calculations*, these inputs are considered suitable for their intended uses in this report, for the following reasons:

1. The inputs obtained from these TPOs are the best available data for their intended purposes as explained in Table 4-4

2. The results reported in the model report have been used in peer-reviewed journal publications (Wu et al. 2004 [DIRS 156399]; Liu et al. 2004 [DIRS 166106]).

Descriptions and specific additional justifications for using the input data files obtained from *Calibrated Properties Model* (BSC 2004 [DIRS 169857]) TPO are given in Table 4-4.

Table 4-4. Input Data from Calibrated Properties Model Report

No	DTN	Data Description	Data Use and Additional Justifications
1	LB0208UZDSCPMI.001 [DIRS 161285]	Calibrated one-dimensional parameter set for base-case infiltration scenario (*minfl7Ddri.par*), and compiled water saturation and potential data (*minfl7Ddri*).	The parameter set was used as initial guesses for inverse modeling, and the formatted water saturation and potential data were used for parameter calibration. Selecting an initial guess that is close to the final value of the calibrated parameter improves the chance of finding a good match with observed data (see Section 6.3.2 and Appendix D). These data are considered the best available guesses, because they were derived through rigorous inverse modeling exercise that met all the quality assurance requirements in place at the time.
2	LB0208UZDSCPUI.001 [DIRS 166711]	Calibrated one-dimensional parameter set for upper-bound infiltration scenario (*UinfA1i.par*), and compiled water saturation and potential data (*UinfA1i*).	

Table 4-4. Input Data from Calibrated Properties Model Report (Continued)

No	DTN	Data Description	Data Use and Additional Justifications
3	LB02091DSSCP3I.001 [DIRS 161292] LB0302AMRU0035.001 [DIRS 162378]	Formatted gas pressure data (**.txt*, *MinfGasAi, NMi*), and formatted boundary condition (*timvsp.dat*).	These compiled and formatted input files were directly used for one-dimensional, mountain-scale calibration (see Sections 6.3.3 and Appendix E). These input files were considered appropriate for their intended use in this report because they were derived from qualified data sources.
4	LB0210AMRU0035.002 [DIRS 166712]	Uncertainties for rock properties.	These property uncertainties were directly used for determining calibrated property uncertainties (section 6.4.2). They were considered appropriate for their intended use in this report because they were derived from qualified data sources.
5	LB02092DSSCFPR.001 [DIRS 162422]	Compiled saturation data and water potential data (*MFAi*), formatted pneumatic pressure data (**.prn*; *LMGi*), and boundary condition (*timvspF.dat*).	These compiled and formatted input files were directly used for calibration of fault parameters (see Section 6.3.4 and Appendix F). These input files were considered appropriate for their intended use in this report because they were derived from qualified data sources.

TPO=technical product output.

Use of TPOs from other reports is discussed in Section 4.1.1.

4.2 CRITERIA

Technical requirements to be satisfied by performance assessment are based on 10 CFR 63.114 [DIRS 173273] ("Requirements for Performance Assessment") and 10 CFR63.115 [DIRS 173273] ("Requirements for Multiple Barriers"). The acceptance criteria that will be used by the U.S. Nuclear Regulatory Commission to determine whether the technical requirements for this report have been met are identified in *Yucca Mountain Review Plan, Final Report* (YMRP) (NRC 2003 [DIRS 163274]). The pertinent requirements and criteria for this analysis report are summarized in Table 4-5.

Table 4-5. Project Requirements and Yucca Mountain Review Plan Acceptance Criteria Applicable to This Report

Requirement	YMRP Acceptance Criteria[a]
10 CFR 63.114 (a and b)	Criteria 2 and 3 for *Flow Paths in the Unsaturated Zone*

[a]From NRC 2003 [DIRS 163274], Section 2.2.1.3.6.3.

The acceptance criteria identified in Section 2.2.1.3.6.3 of the YMRP (NRC 2003 [DIRS 163274]) are included below. In cases where subsidiary criteria are listed in the Yucca Mountain Review Plan for a given criterion, only the subsidiary criteria addressed by this scientific analysis are listed below. How these components are addressed is summarized in Section 7 of this report.

Acceptance Criteria from Section 2.2.1.3.6.3, *Flow Paths in the Unsaturated Zone*

Acceptance Criterion 1, ***System Description and Model Integration Are Adequate.***

1. Total system performance assessment adequately incorporates, or bounds, important design features, physical phenomena, and couplings, and uses consistent and appropriate assumptions throughout the flow paths in the unsaturated zone abstraction process. Couplings include thermal-hydrologic-mechanical-chemical effects as appropriate;

2. The aspects of geology, hydrology, geochemistry, physical phenomena, and couplings that may affect flow paths in the unsaturated zone are adequately considered. Conditions and assumptions in the abstraction of flow paths in the unsaturated zone are readily identified and consistent with the body of data presented in the description;

9. Guidance in NUREG–1297 (Altman et al. 1988 [DIRS 103597]) and NUREG–1298 (Altman et al. 1988 [DIRS 103750]), or other acceptable approaches for peer review and data qualification is followed.

Acceptance Criterion 2, ***Data are Sufficient for Model Justification.***

1. Hydrological and thermal-hydrological-mechanical-chemical values used in the license application are adequately justified. Adequate descriptions of how the data were used, interpreted, and appropriately synthesized into the parameters are provided;

2. The data on the geology, hydrology, and geochemistry of the unsaturated zone, are collected using acceptable techniques;

3. Estimates of deep-percolation flux rates constitute an upper bound, or are based on a technically defensible unsaturated zone flow model that reasonably represents the physical system. The flow model is calibrated, using site-specific hydrologic, geologic, and geochemical data. Deep-percolation flux is estimated, using the appropriate spatial and temporal variability of model parameters, and boundary conditions that consider climate-induced change in soil depths and vegetation;

4. Appropriate thermal-hydrologic tests are designed and conducted, so that critical thermal-hydrologic processes can be observed, and values for relevant parameters estimated;

5. Sensitivity or uncertainty analyses are performed to assess data sufficiency, and verify the possible need for additional data;

6. Accepted and well-documented procedures are used to construct and calibrate numerical models.

Acceptance Criterion 3, ***Data Uncertainty is Characterized and Propagated Through the Model Abstraction.***

1. Models use parameter values, assumed ranges, probability distributions, and bounding assumptions that are technically defensible, reasonably account for uncertainties and variabilities, and do not result in an under-representation of the risk estimate;

4. The initial conditions, boundary conditions, and computational domain used in sensitivity analyses and/or similar analyses are consistent with available data. Parameter values are consistent with the initial and boundary conditions and the assumptions of the conceptual models for the Yucca Mountain site;

5. Coupled processes are adequately represented; and

6. Uncertainties in the characteristics of the natural system and engineered materials are considered.

4.3 CODES, STANDARDS, AND REGULATIONS

No codes, standards, or regulations other than those identified in Table 4-5 and determined to be applicable were used in this analysis report.

INTENTIONALLY LEFT BLANK

5. ASSUMPTIONS

The following assumptions are used to develop the calibrated property sets. This section presents the rationale for these assumptions and references the section of this report in which each assumption is used. Other assumptions basic to the UZ models of Yucca Mountain are elements of the conceptual model, which are summarized at the beginning of Section 6 and are fully documented in *Conceptual Model and Numerical Approaches for Unsaturated Zone Flow and Transport* (BSC 2004 [DIRS 170035]).

1. It is assumed that layers bf3 and bf2 have the same hydraulic properties as tr3 and tr2, respectively (Section 6.3.2).

   Justification: No data except geologic contacts exist for layers tr3 or tr2 (the Tram Tuff). Because the Tram Tuff has a structure similar to the Bullfrog Tuff and the two tuffs are divided into similar model layers (BSC 2004 [DIRS 170029], Table 6-2), the hydrologic properties should also be similar. Further, model layers tr3 and tr2 constitute only a small portion of the unsaturated zone in the northern part of the model area and along the foot wall of the Solitario Canyon fault, so the properties are not likely to have a large impact on simulations of flow and transport.

3. When the matrix saturation data is derived from a single measurement, the respective sample standard error is assumed to be 0.05 (Section 6.2.2).

   Justification: The standard deviation σ of a sample (hence, the standard error) is not defined for a single measurement (sample size N=1). The standard error for matrix saturations derived from a single measurement is assumed to be 0.05. This value is within the range of computed standard errors (0.001 to 0.268) derived from multiple measurements (N greater than 1) of saturation (DTN: LB0208UZDSCPMI.001 [DIRS 161285], *layvsat.xls*).

4. For the purpose of inversions, the standard error of uncalibrated log(α) for fractures is assumed to be 2 (Section 6.2.2).

   Justification: The uncalibrated log(α) for fractures is estimated from fracture permeability and fracture density data. This method of estimation does not provide standard error of the log(α). Therefore, a conservative estimate of 2 is chosen to represent the standard error of fracture log(α). This value is approximately double of the largest standard error of matrix fracture log(α) given in Table 4-2.

Based on the rationales stated above, these assumptions do not need to be verified.

INTENTIONALLY LEFT BLANK

6. DISCUSSION

6.1 BACKGROUND

6.1.1 Objectives

The UZ models are used to represent past, present, and future thermal-hydrological and chemical conditions within the unsaturated zone of Yucca Mountain. The UZ models consist of hydrological (flow and transport) and thermal properties, and a numerical grid, which together form input for the TOUGH family of simulators. This report documents the development of some of the hydrologic properties for the UZ models. Assumptions used in this section and their bases are presented in Section 5. The intended use of the output data developed using approaches in this section is given in Section 1.

6.1.2 Conceptual Model and Alternative Models

Property calibration of the UZ models is a key step in the model development. Property calibration is necessary to refine the property estimates derived from laboratory and field data, so they are suitable for use in the UZ models and so UZ models accurately depict hydrological conditions in the mountain. The UZ models consider large-scale hydrological processes; where properties are scale dependent, upscaling will inherently be part of the calibration process. The calibration process also reduces property-estimate uncertainty and bias. Property estimates from laboratory and field data, like any other estimates, will have uncertainty associated with them because of data limitations (e.g., sampling and measurement biases, limited number of samples). The conceptual model and numerical schemes used to develop the numerical representation of the UZ models have been documented in *Conceptual Model and Numerical Approaches for Unsaturated Zone Flow and Transport* (BSC 2004 [DIRS 170035]). The aspects of the conceptual model and numerical schemes that are most relevant to this study are highlighted in this section. Alternative models and numerical approaches are also discussed in this section.

A variety of numerical approaches have been proposed to deal with flow and transport processes in fractured media at field scale (BSC 2004 [DIRS 170035], Section 6.3.1). When classified according to the manner in which fracture networks are treated in the model structure, the approaches fall into three groups: (1) continuum approaches (including effective continuum, dual continuum, and multiple interacting continua), (2) discrete fracture-network approaches, and (3) other approaches (e.g., a combination of the continuum approaches and the discrete fracture-network approaches). Based on overall flow and transport behavior in the unsaturated zone, the scale of the problem under consideration, and a compromise between simulation accuracy and computational feasibility, the dual-permeability method (a continuum approach) is considered appropriate for describing flow and transport in the unsaturated zone (BSC 2004 [DIRS 170035], Section 6.3.2). Consequently, the dual-permeability method is used for all the simulation studies documented in this report. The alternative approaches (including discrete fracture-network approaches and other approaches) generally involve computational generation of synthetic fracture networks and subsequent simulations of flow and transport in each individual fracture. While these approaches are useful as tools for concept evaluation, they are not practically feasible for dealing with large-scale problems (BSC 2004 [DIRS 170035], Section 6.3).

Because the Paintbrush nonwelded hydrogeologic unit (PTn) greatly attenuates episodic infiltration pulses, liquid water flow below the PTn is considered to be approximately in steady state under ambient conditions (BSC 2004 [DIRS 170035], Sections 6.1.2 and 6.1.6). The ambient conditions refer to conditions under which flow and transport processes in the unsaturated zone are not disturbed by heat loading from nuclear wastes that are proposed to be stored in the repository horizons. This study focuses on flow processes and data collected under ambient conditions. Steady-state liquid flow conditions are thus used in all the studies documented in this report. Note that the existence of episodic flow through the PTn (possibly through faults) is indicated by the finding of potential "bomb-pulse" signature of ^{36}Cl in the unsaturated zone (BSC 2006 [DIRS 179489]). However, this flow component is believed to carry only a small amount of water (BSC 2004 [DIRS 170035], Sections 6.1.6 and 6.1.7).

Heterogeneities exist at different scales within both the fracture and matrix continua in the unsaturated zone at Yucca Mountain. Treatment of subsurface heterogeneity and parameterization (use of a number of parameters to represent the heterogeneous distribution) is highly relevant to calibration of hydraulic properties. A geologic-based, deterministic approach is mainly used for characterizing subsurface heterogeneity in the unsaturated zone (BSC 2004 [DIRS 170035], Section 6.3.4). This is based on the following considerations: (1) overall behavior of large-scale flow and transport processes are mainly determined by relatively large-scale heterogeneities associated with the geologic structures of the mountain, (2) the heterogeneity model needs to be consistent with the available data, and (3) this approach is also supported by field observation (e.g., matrix-saturation distributions) (BSC 2004 [DIRS 170035], Section 6.3.4). Therefore, the heterogeneity of hydrological properties in this study is treated as a function of geologic layering, shown in Table 6-3, so that any one geologic layer has homogeneous properties (referred to as layer average properties), except where faulting or variable alteration (e.g., zeolitization) is present. In these cases, two sets of properties are used for layers with variable alteration, one for the portion of the layer that is altered beyond some threshold and one for the remaining portion. *Development of Numerical Grids for UZ Flow and Transport Modeling* (BSC 2004 [DIRS 169855], Section 6) documents this process. Heterogeneity in faults is treated as a function of major hydrogeologic units shown in Table 6-1, with the Calico Hills nonwelded hydrogeologic unit (CHn) and CFu combined (i.e., only four sets of hydrological properties are used for the faults).

The van Genuchten (1980 [DIRS 100610], pp. 892 to 893) relations, originally developed for porous media, have been used as constitutive relationships for liquid flow in the unsaturated zone (BSC 2004 [DIRS 170035], Section 6.3.5). This treatment results from the use of porous-medium equivalence for describing flow in fractures. Recently, Liu and Bodvarsson (2001 [DIRS 160110]) developed a new constitutive-relationship model for unsaturated flow in fracture networks, based mainly on numerical experiments. They found that results of the van Genuchten model are close to their simulation results when the water saturation value is small, which indicates that the van Genuchten model is approximately valid for low fracture saturations corresponding to ambient conditions. Therefore, the van Genuchten model is still used in this study. Calibrations are performed using data collected under ambient conditions.

In a number of laboratory scale experiments, Glass et al. (1996 [DIRS 139237]) demonstrated that gravity-driven fingering flow is a common flow mechanism in individual fractures. Fingering flow can occur at different scales. It has been well known in the subsurface hydrology community that flow and transport processes and the related parameters are scale-dependent

(e.g., Neuman 1994 [DIRS 105731]). Fingering flow at a fracture network scale, resulting from subsurface heterogeneity and nonlinearity involved in an unsaturated system, is a more important mechanism for liquid flow in the unsaturated zone than fingering flow in individual fractures. This is because the UZ flow model deals with flow and transport at large scales consisting of a great number of fractures. The active fracture model of the report by Liu et al. (1998 [DIRS 105729]) is used for considering the mechanism of fingering flow at a fracture network scale (BSC 2004 [DIRS 170035], Section 6.3.7). The active fracture concept is based on the reasoning that, as a result of fingering flow, only a portion of fractures in a connected, unsaturated fracture network contributes to liquid water flow. A detailed evaluation of the active fracture model based on both theoretical arguments and field observations is presented in *Conceptual Model and Numerical Approaches for Unsaturated Zone Flow and Transport* (BSC 2004 [DIRS 170035], Section 7).

Liquid flow occurs predominantly in the matrix in the PTn (see Table 6-1) and the matrix in vitric portions of the CHn. The dominant matrix flow results from relatively high matrix permeabilities and low fracture densities in these units (BSC 2004 [DIRS 170035], Section 6.1.2). In the welded units (layers), liquid flow occurs predominantly in the fractures. This conceptual model is supported by UZ flow tests conducted in nonwelded tuffs at Busted Butte and in the ESF Alcove 4. The tests at Busted Butte conducted in the upper CHn(v) show that flow took place in the matrix; fracture flow was not observed, given the limits of the observational capability (even though fractures are present) (BSC 2004 [DIRS 170004], Section 6.13). Tests in ESF Alcove 4 conducted in the PTn unit also show that flow around a large, through-going fracture is matrix-dominant (BSC 2004 [DIRS 170004], Section 6.7).

It is well known that permeability is scale-dependent (Neuman 1994 [DIRS 105731]). Calibrated properties are necessary on two scales, mountain-scale and drift-scale. Calibration of the mountain-scale properties considers pneumatic pressure data that reflect the mountain-scale process of barometric pumping. Mountain-scale properties are intended for use in models of processes at the mountain scale. Calibration of the drift-scale properties does not consider the pneumatic pressure data. Drift-scale properties are intended for use in models of processes at the drift scale.

6.1.3 Simulator and Numerical Model

In this study, iTOUGH2 V5.0 [DIRS 160106] is used for calibration. This program uses the integral-finite-difference method for spatial discretization, and is a general-purpose inverse and forward numerical simulator for multidimensional, coupled fluid and heat flow of multiphase, multicomponent fluid mixtures in porous and fractured media. To the best of the authors' knowledge, iTOUGH2 represents the state of the art in the area of inverse modeling of multiphase flow processes in fractured media. This code has been comprehensively tested under different conditions (Finsterle 1998 [DIRS 103783]; 1999 [DIRS 104367]). The forward flow simulation in iTOUGH2 V5.0 [DIRS 160106] involves numerically solving the following governing equation (for an arbitrary flow domain V_n with the boundary Γ_n) (Pruess 1987 [DIRS 100684], Section 3)

$$\frac{d}{dt}\int_{V_n} M dV = \int_{\Gamma_n} F \bullet n d\Gamma + \int_{V_n} q dV \qquad \text{(Eq. 6-1)}$$

where t is time, M is the accumulation (storage) term, F is the mass flux, n is the unit vector normal to the domain boundary, and q is the source term.

The inverse modeling approach used by iTOUGH2 V5.0 [DIRS 160106] is based on the classical weighted least-squares method, which consists of minimizing the objective function

$$S = \mathbf{r}^T \mathbf{C}_{zz}^{-1} \mathbf{r} \quad \text{(Eq. 6-2)}$$

The residual vector $\mathbf{r}$ contains the differences between the measured value, z^*, and the corresponding model prediction, $z(\mathbf{p})$, which is a function of the unknown, n-dimensional parameter vector $\mathbf{p}$ (i.e., $r_i = (z_i^* - z(\mathbf{p})_i)$, $i = 1 \ldots m$, where m is the number of calibration points). The inverse of the covariance matrix, $\mathbf{C}_{zz}$, which holds the expected variances of the final residuals on its diagonal, is used as a weighting matrix. The objective function is a measure of the misfit between the simulation output and the measured data. It is automatically minimized using the Levenberg-Marquardt algorithm implemented in iTOUGH2 V5.0 (Finsterle 1999 [DIRS 104367], Section 2).

The covariance matrix of the estimated parameters is asymptotically given by:

$$\mathbf{C}_{pp} = s_0^2 \left(\mathbf{J}^T \mathbf{C}_{zz}^{-1} \mathbf{J} \right)^{-1} \quad \text{(Eq. 6-3)}$$

where $\mathbf{J}$ is an $m \times n$ Jacobian matrix holding the partial derivatives of the predicted seepage with respect to the unknown parameters, $J_{ij} = \partial z_i / \partial p_j$, and s_0^2 is the estimated error variance, which represents the variance of the mean weighted residual; it is an aggregate measure of goodness-of-fit:

$$s_0^2 = \frac{\mathbf{r}^T \mathbf{C}_{zz}^{-1} \mathbf{r}}{m - n} \quad \text{(Eq. 6-4)}$$

The impact of parameter uncertainty (expressed through matrix, $\mathbf{C}_{pp}$) on predictions can be evaluated by means of first-order-second-moment uncertainty propagation analysis. iTOUGH2 V5.0 [DIRS 160106], calculates the covariance matrix of the prediction, $\mathbf{C}_{\hat{z}\hat{z}}$, based on a linearity and normality assumption using:

$$\mathbf{C}_{\hat{z}\hat{z}} = \mathbf{J} \mathbf{C}_{pp} \mathbf{J}^T \quad \text{(Eq. 6-5)}$$

The inverse modeling methodology and its numerical implementation are described in detail in the iTOUGH2 software documentation, specifically by Finsterle (1999 [DIRS 104367], Section 2).

The upstream weighting numerical technique for the relative permeability is used for inversions. While this is considered to be an approximation for calculating flow from fractures to the matrix (matrix imbibition), it is still expected to be a reasonable scheme for this study. First, it is well known that upstream weighting is a robust approach that avoids numerical oscillations for

multiphase flow in highly heterogeneous systems (Forsyth et al. 1995 [DIRS 161743]). Simulation of unsaturated flow in the unsaturated zone is numerically challenging because of a combination of heterogeneity and nonlinearity. To perform numerical simulation for such a complex system, both numerical accuracy and computational feasibility need to be considered. It is a reasonably practical choice to use this scheme to avoid the potential numerical problems. Secondly, use of the approach is not expected to result in significant errors for simulating matrix imbibition processes in the unsaturated zone. In nonwelded units, the flow mainly occurs in the matrix, and the flow component from fractures to the matrix is expected to be small. In the welded units, flow mainly occurs in fractures (because of small matrix permeability), again resulting in a relatively small flow component from fractures to the matrix. Finally, the approximation introduced by the weighting scheme is also compensated by the calibration procedure, which includes the effects of numerical grids and numerical schemes.

Table 6-1. GFM2000 Lithostratigraphy, Unsaturated Zone Model Layer, and Hydrogeologic Unit Correlation

Major Unit (Modified from Montazer and Wilson 1984 [DIRS 100161])	GFM2000 Lithostratigraphic Nomenclature	Unsaturated Zone Model Layer	Hydrogeologic Unit (Flint 1998 [DIRS 100033], Table 1)
Tiva Canyon welded hydrogeologic unit (TCw)	Tpcr	tcw11	CCR, CUC
	Tpcp	tcw12	CUL, CW
	TpcLD		
	Tpcpv3	tcw13	CMW
	Tpcpv2		
Paintbrush nonwelded hydrogeologic unit (PTn)	Tpcpv1	ptn21	CNW
	Tpbt4	ptn22	BT4
	Tpy (Yucca)	ptn23	TPY
		ptn24	BT3
	Tpbt3		
	Tpp (Pah)	ptn25	TPP
	Tpbt2	ptn26	BT2
	Tptrv3		
	Tptrv2		
Topopah Spring welded hydrogeologic unit (TSw)	Tptrv1	tsw31	TC
	Tptrn		
		tsw32	TR
	Tptrl, Tptf	tsw33	TUL
	Tptpul, RHHtop		
	Tptpmn	tsw34	TMN
	Tptpll	tsw35	TLL
	Tptpln	tsw36	TM2 (upper 2/3 of Tptpln)

Table 6-1. GFM2000 Lithostratigraphy, UZ Model Layer, and Hydrogeologic Unit Correlation (Continued)

Major Unit (Modified from Montazer and Wilson 1984 [DIRS 100161])	GFM2000 Lithostratigraphic Nomenclature	Unsaturated Zone Model Layer	Hydrogeologic Unit (Flint 1998 [DIRS 100033], Table 1)
		tsw37	TM1 (lower 1/3 of Tptpln)
	Tptpv3	tsw38	PV3
	Tptpv2	tsw39 (vit, zeo)	PV2
Calico Hills nonwelded hydrogeologic unit (CHn)	Tptpv1	ch1 (vit, zeo)	BT1 or BT1*a* (altered)
	Tpbt1		
	Tac (Calico)	ch2 (vit, zeo)	CHV (vitric) or CHZ (zeolitic)
		ch3 (vit, zeo)	
		ch4 (vit, zeo)	
		ch5 (vit, zeo)	
	Tacbt (Calicobt)	ch6 (vit, zeo)	BT
	Tcpuv (Prowuv)	pp4	PP4 (zeolitic)
	Tcpuc (Prowuc)	pp3	PP3 (devitrified)
	Tcpmd (Prowmd)	pp2	PP2 (devitrified)
	Tcplc (Prowlc)		
	Tcplv (Prowlv)	pp1	PP1 (zeolitic)
	Tcpbt (Prowbt)		
	Tcbuv (Bullfroguv)		
Crater Flat undifferentiated (CFu)	Tcbuc (Bullfroguc)	bf3	BF3 (welded)
	Tcbmd (Bullfrogmd)		
	Tcblc (Bullfroglc)		
	Tcblv (Bullfroglv)	bf2	BF2 (nonwelded)
	Tcbbt (Bullfrogbt)		
	Tctuv (Tramuv)		
	Tctuc (Tramuc)	tr3	Not Available
	Tctmd (Trammd)		
	Tctlc (Tramlc)		
	Tctlv (Tramlv)	tr2	Not Available
	Tctbt (Trambt)and below		

Source: BSC 2004 [DIRS 169855], Table 6-5.

6.2 ANALYSIS INPUTS

This section discusses inputs for parameter calibration activities documented in this report. These inputs include numerical grids, infiltration rates, matrix-saturation and water-potential data, pneumatic pressure data and rock-hydraulic-property data. Some inputs for fault property calibration are documented in Section 6.3.4.

6.2.1 Numerical Grids

One-dimensional, vertical-column numerical grids and a two-dimensional, cross-sectional numerical grid are used for the corresponding calibrations. Numerical grids under DTN: LB02081DKMGRID.001 [DIRS 160108] are slightly modified in this study. The eight-character element-name format in this DTN is not compatible with all necessary iTOUGH2

V5.0 [DIRS 160106] features. In response, the element names are converted to a five-character format. The details of the grid modification are provided in Appendix B.

6.2.2 Matrix-Saturation and Water-Potential Data

Saturation and water-potential data, which are inverted to obtain the calibrated parameter sets, were developed so that they can be compared to the numerical predictions. To compare core saturation data to the saturation profiles predicted by the numerical simulations on intervals as large as several tens of meters (corresponding to model layer thickness), the data need to be averaged. The averaged data and their uncertainties are used for calibrating unsaturated zone parameters (Section 6.3). In situ water-potential data are measured at depth intervals equal to or greater than the numerical grid spacing, so these data do not need to be averaged. Inversions using iTOUGH2 V5.0 (LBNL 2002 [DIRS 160106]) need both averaged (gridblock scale) matrix saturation and water-potential data and their uncertainties as inputs. These data and uncertainties are documented in *minfI7Ddri* (DTN: LB0208UZDSCPMI.001 [DIRS 161285]) and *UinfA1i* (DTN: LB0208UZDSCPUI.001 [DIRS 166711]). These files are used as direct input into the calibration activities for this study.

iTOUGH2 V5.0 [DIRS 160106] allows the data to be weighted. The weight of each saturation data point is estimated from the number of measurements, the standard deviation of the measurements, and estimates of handling and measurement error. The total error, *TE*, which is equal to the inverse of the weight, is:

$$TE = SE + ME + HE \quad \text{(Eq. 6-6)}$$

where *SE* is the standard error, *ME* is the measurement error, and *HE* is the handling error.

Standard error, *SE*, is defined here as

$$SE = \frac{\sigma}{\sqrt{N}} \quad \text{(Eq. 6-7)}$$

where σ is the unbiased estimate of the standard deviation and *N* is the number of measurements. For N=1, σ and thus *SE* are assumed to be 0.05 (Assumption 3, in Section 5). Flint (1998 [DIRS 100033], p. 17) reports that the measurement error for bulk properties is less than 0.5%. The measurement error for saturation is thus taken to be 0.005, which is qualified for the intended use for this study in Appendix G.

Drying of core during handling is a potential source of error for saturation data (Flint 1998 [DIRS 100033], pp. 18 to 19; Rousseau et al. 1999 [DIRS 102097], pp. 129 to 131). The *HE* is estimated for the core drying effects. Saturation is not easily quantifiable because of the variable nature of the forces controlling the drying. Drying during handling at the surface is related to saturation, water potential (and variation of water potential with saturation), and temperature of the core—as well as temperature, pressure, relative humidity, and speed of the air around the core. Drying of the core during drilling is related to similar factors. Rather than correct the measured saturation data by an uncertain drying estimate, a contribution to the total uncertainty

of the saturation data is made by an estimate of drying losses. This contribution is included as the handling error, *HE*, in Equation 6-6.

A simplified model of core drying during handling is used to estimate the rate of evaporation from the core. A fully saturated core is approximated as a spherical rock with a surface that is always completely wet and that has the same area as the core. A solution for evaporation from a spherical drop of water in an air stream is given by Bird et al. (1960 [DIRS 103524], p. 648) as

$$W = \eta \pi \delta^2 \frac{x_0 - x_\infty}{1 - x_\infty} \qquad \text{(Eq. 6-8)}$$

where W is the evaporation rate, η is the mass-transfer coefficient of water vapor in air, δ is the diameter of a sphere with the same surface area as the core, x_0 is the water mole fraction in the air at the surface of the core, and x_∞ is the water mole fraction in air far away from the core. The mass-transfer coefficient of water vapor in air, η, is given by Bird et al. (1960 [DIRS 103524], p. 649) as

$$\eta = \frac{cD}{\delta}\left[2 + 0.6\left(\frac{v\delta\rho}{\mu}\right)^{1/2}\left(\frac{\mu}{D\rho}\right)^{1/3}\right] \qquad \text{(Eq. 6-9)}$$

where c is the total molar concentration of the air-water mixture, D is the effective binary diffusivity of water vapor in air, v is air speed, ρ is density of air, and μ is viscosity of air.

Effective binary diffusivity, D [cm^2/s], for an air and water-vapor (components A and B) mixture is given by Bird et al. (1960 [DIRS 103524], p. 505) as

$$D = \frac{3.64\times10^{-4}}{p}\left(\frac{T}{\sqrt{T_{cA}T_{cB}}}\right)^{2.334}\left(p_{cA}p_{cB}\right)^{1/3}\left(T_{cA}T_{cB}\right)^{5/12}\left(\frac{1}{M_A}+\frac{1}{M_B}\right)^{1/2} \qquad \text{(Eq. 6-10)}$$

where p is pressure (atm), T is temperature (K), and p_c, T_c, and M are the critical pressure (atm), critical temperature (K), and molecular weight (g/g-mole), respectively, of components A and B.

The evaporation rate is estimated by setting the temperature of the core at 25°C and the temperature, pressure, relative humidity, and speed of the air far from the core at 30°C, 1 atm, 25%, and 3 km/h, respectively. These are all reasonable values for field conditions at Yucca Mountain and qualified for the intended use for this study in Appendix G. Neglecting the small effect of the water vapor in the air, the physical properties of air at 27.5°C (the average temperature) are $c = 4.05 \times 10^{-5}$ g-mole/cm^3, $\rho = 0.00118$ g/cm^3, and $\mu = 1.84 \times 10^{-4}$ g/cm/s (Roberson and Crowe 1990 [DIRS 124773], p. A-22). The molecular weight, critical temperature and critical pressure of air are 28.97 g/g-mole, 132 K, and 36.4 atm, respectively (Bird et al. 1960 [DIRS 103524], p. 744). The molecular weight and critical temperature and pressure of water are 18.02 g/g-mole, 647.25 K, and 218.3 atm, respectively (Weast 1987 [DIRS 114295], pp. B-94, F-66). The mole fraction of water vapor in air at the surface of the core, x_0, is 0.0313 (Weast 1987 [DIRS 114295], p. D-190). Given a relative humidity of 25%,

the mole fraction of water vapor in air far from the core, x_∞, is 0.0126 (Weast 1987 [DIRS 114295], p. D-190). The core surface area is approximately 297 cm^2 that is qualified for the intended use for this study in Appendix G. Using these values, an evaporation rate of 2.69×10^{-4} g-mole/s is calculated based on Equations 6-8 to 6–10.

At this evaporation rate, the saturation of a fully saturated core of matrix porosity 22.3% (a typical value for tuff matrix (Table 4-3)) will be reduced by 2.2% after 5 minutes, which is the handling time given by Flint (1998 [DIRS 100033], p. 11). A fully dry core will have no reduction in saturation. Using these two points, the linear dependence of saturation change on saturation yields the relation

$$\Delta S = 0.022S \qquad \text{(Eq. 6-11)}$$

where S is the uncorrected saturation value and ΔS is saturation change resulting from handling, or *HE*. Although the actual relation between ΔS and S may be much more complex than Equation 6-11, this equation is in practice adequate for estimating *HE* here. Average porosity for the entire mountain is calculated as a layer-thickness weighted average of individual layer porosities. Also, water lost to drilling air is not considered here, because an approach to accurately estimate water loss is not available. However, the estimation of *HEs* does not consider the effect of matrix water potential, resulting in overestimated handling errors. This may partially compensate for the effects of water lost to drilling air.

Rousseau et al. (1999 [DIRS 102097], p. 144) give ± 0.2 MPa as the 95% confidence interval (two standard deviations) for the in situ water-potential measurements. One standard deviation, 0.1 MPa, is used as an estimate for the uncertainty for the water potential. Also, the equilibrium (steady-state) water potential values used for calibration in this analysis report are consistent with more recent water potential data collected from April 1998 to December 2001 as shown in Appendix A.

6.2.3 Pneumatic Pressure Data

Thirty days of data from each borehole are used for the inversions. Several criteria are used to select data for the inversions: The data must include diurnal pressure changes and longer-period, weather-associated pressure changes; and must have been obtained prior to any influence from construction of the ESF. Table 6-2 shows the starting and ending dates for the data that were used in the inversion. Data from the instrument station or port nearest the bottom of the Tiva Canyon welded hydrogeologic unit (TCw) are included because they show the lack of attenuation and lag in the barometric signal through the TCw. Data from stations between the lowermost in the TCw and the surface are not included, because they would not add information to the inversion and would weight the TCw data more than other data. Data from all instrument stations or ports in the PTn are included because there is substantial attenuation and lag in the barometric pumping signal through the PTn. Individual layers in the PTn are expected to have widely variable permeability, so it is important to include data that show the amount of barometric-signal attenuation and lag in different layers of the PTn. Data from the uppermost and lowermost instrument stations or ports in the TSw are included, because they show the lack of significant attenuation and lag in the barometric pumping signal characteristics through the TSw. Data from the stations in between the uppermost and lowermost stations in the TSw unit

are not included, for the same reason cited above for the TCw data. Data from the two lowest instrument stations in Borehole USW SD-12 are not included because these data are affected by the presence of perched water, which is not adequately reproduced in the one-dimensional simulations. Data from the third-lowest instrument station in USW SD-12 are not included because it was not properly isolated from the surface (Rousseau et al. 1997 [DIRS 100178], p. 31). The elevation of a location where gas pressure was monitored is determined by the ground surface elevation of the corresponding boreholes (available from *Contacts00md.dat* of DTN: MO0012MWDGFM02.002 [DIRS 153777]) minus depths of the measurement locations (available from DTNs in Table 6-2). During the determination procedure, 1 ft =0.3048 m was used [*Standard for Use of the International System of Units (SI): The Modern Metric System* (IEEE/ASTM SI 10-1997 [DIRS 151762], pp. 18 and 25]. The files with an extension *.txt* from DTNs: LB02091DSSCP3I.001 [DIRS 161292] and LB0302AMRU0035.001 [DIRS 162378] contain the pressure data for the calibration boreholes formatted for iTOUGH2 inversions. In this study, these data files are used as the direct inputs into inversion runs.

Table 6-2. Boreholes with Pneumatic Pressure Data Used for Inversion

Borehole	Dates	Elevation[a] (m)	DTNs
UE-25 NRG#5	7/17 to 8/16/95	1,211.9	GS000608312261.001 [DIRS 155891]
	7/17 to 8/16/95	1,195.4	
	7/17 to 8/16/95	1,178.4	
	7/17 to 8/16/95	1,161.6	
	7/17 to 8/16/95	1,144.5	
	7/17 to 8/16/95	1,008.9	
USW NRG-7a	3/27 to 4/26/95	1,277.4	GS950208312232.003 [DIRS 105572]; GS951108312232.008 [DIRS 106756]; GS031208312232.008 [DIRS 178750]; GS031208312232.007 [DIRS 178751]
	3/27 to 4/26/95	1,236.3	
	3/27 to 4/26/95	1,164.6	
	3/27 to 4/26/95	1,079.3	
USW SD-7	4/5 to 5/5/96	1,272.5	GS960908312261.004 [DIRS 106784]
	4/5 to 5/5/96	1,257.3	
	4/5 to 5/5/96	1,242.1	
	4/5 to 5/5/96	1,120.1	
USW SD-12	12/1 to 12/31/95	1,258.5	GS031208312232.008 [DIRS 178750]
	12/1 to 12/31/95	1,232.0	
	12/1 to 12/31/95	1,217.1	
	12/1 to 12/31/95	1,001.3	
USW NRG-6	3/27 to 4/26/95	1,207.9	GS950208312232.003 [DIRS 105572] GS951108312232.008 [DIRS 106756]
	3/27 to 4/26/95	1,192.7	
	3/27 to 4/26/95	1,162.2	
	3/27 to 4/26/95	1,028.1	

[a] Elevation derived from DTN: MO0012MWDGFM02.002 [DIRS 153777], *Contacts00md.dat*.

6.2.4 Prior Information

Uncalibrated rock-property data (Tables 4-3 and 4-4) are used as prior information. (Prior information refers to property data collected from both field and laboratory measurements.) In the inversing calculations reported in this report, the prior information is also used as data to be calibrated against. These data are just as important to the parameter calibration as data on the state of the system (e.g., saturation). The combination of the two types of information allows the calibration to match the data as close as possible, while simultaneously estimating rock parameters that are reasonable according to the prior information. Standard errors of parameters for weighting the prior information are taken from Tables 4-2 and 4-3. Matrix permeability data are weighted by the inverse of the standard error (Equation 6-7), giving more weight to the more certain measurements (Finsterle 1999 [DIRS 104367], Sections 1.5 and 2.5.3). Because permeability is lognormally distributed, σ and thus *SE* are estimated for the log-transformed permeabilities (i.e., log(k)). The number of samples used for calculation of the standard error does not include nondetect samples (i.e., N in Equation 6-7 is the total number of samples minus the number of nondetect samples, as shown in Table 4-3). As discussed below, drift-scale fracture permeabilities are directly assigned from the prior information, and therefore standard error data are not needed for calibration of drift-scale fracture permeabilities. Mountain-scale fracture permeabilities, however, are calibrated using the pneumatic data, because the pneumatic data correspond to a mountain-scale process. In inversions of pneumatic pressure data, prior information does not significantly contribute to the objective function (Section 6.3.1) because the number of data points is considerably larger than the number of calibrated fracture permeabilities. Therefore, the choice of standard error used to weigh the prior information is inconsequential to the inversion. For simplicity, a standard error of two orders of magnitude is assigned to fracture permeabilities in TCw and PTn for calibrating mountain-scale nonfault property sets, and a standard error of one order of magnitude for calibrating fault property sets. For layers tsw31 through tsw37, fracture permeabilities are calibrated by a technique that does not require weighting, so no standard errors are used (see Section 6.3.3). Standard error is given for log(α) because α is lognormally distributed. For fracture properties, the uncalibrated value of α_F is estimated based on fracture permeability and fracture frequency data (BSC 2004 [DIRS 170038], Section 6). Since a directly measured α_F value is not available, a relatively large value of 2 (or two orders of magnitude, compared with values for matrix log(α)) is assigned as standard error for log(α_F) in inversions. These prior information data were incorporated and formatted in *minfI7Ddri* from DTN: LB0208UZDSCPMI.001 [DIRS 161285], *UinfA1i* from DTN: LB0208UZDSCPUI.001 [DIRS 166711], *MinfGasAi* from DTN: LB02091DSSCP3I.001 [DIRS 161292], and *NMi* from DTN: LB0302AMRU0035.001 [DIRS 162378]. These files are used as direct inputs to inversion runs (Appendices D and E).

6.2.5 Boundary and Initial Conditions

Infiltration rates (DTN: SN0609T0502206.028 [DIRS 178753]) are used as top boundary conditions during calibration activities. To consider the uncertainty in infiltration rates, four infiltration maps (corresponding to the 10th, 30th, 50th, and 90th percentiles of probability distribution of the average infiltration rate) are used in this study. For each infiltration map (DTN: SN0609T0502206.028 [DIRS 178753]), the infiltration rate at each calibration borehole, shown in Table 6-3, is determined as an averaged infiltration-rate value over a circular area with a 200-m radius with the center at the borehole location (Appendix C). A relatively large value

for the radius (compared with the lateral gridblock sizes) is used because of capillary-dispersion considerations (lateral redistribution of moisture resulting from a capillary gradient from wet areas under high infiltration zones to dry areas under low infiltration zones) within the PTn unit. This treatment is supported by the fact that vertical matrix saturation and water potential distributions (corresponding to calibration boreholes) simulated from the three-dimensional site-scale UZ model (SNL 2007 [175177], Section 6) are similar to those for one-dimensional studies documented in this report. Note that a three-dimensional model can explicitly capture the capillary-dispersion process within the PTn unit. During fault-parameter calibration involving the two-dimensional numerical grid, the infiltration rates are directly calculated using infil2grid V1.7 [DIRS 154793], based on the corresponding sizes of top elements of the grid. In all the simulations in this study, bottom boundaries correspond to the water table. The four different infiltration boundary conditions were used here for inversions, to examine alternative models and the corresponding parameter sets. For inversions of matrix saturation and water potential data, steady-state water flow fields are simulated.

Table 6-3. Area-Averaged Infiltration Rates (mm/yr) Used in the One-Dimensional Inversions

Borehole	10th Percentile of Infiltration Rate	30th Percentile of Infiltration Rate	50th Percentile of Infiltration Rate	90th Percentile of Infiltration Rate
UE-25 NRG#5	0.80	3.42	6.20	16.09
USW NRG-6	0.50	2.19	3.77	9.71
USW NRG-7	1.38	3.83	5.95	14.00
USW SD-6	6.44	15.22	20.72	45.49
USW SD-7	3.37	9.04	15.03	34.61
USW SD-9	2.40	6.87	11.17	26.89
USW SD-12	3.18	8.47	12.78	30.51
UE-25 UZ#4	0.78	3.74	7.25	17.22
USW UZ-14	1.89	4.81	6.94	16.36
UE-25 UZ#16	0.25	1.72	3.11	7.87
USW UZ-N11	9.77	21.30	35.42	51.07
USW UZ-N31	1.72	5.43	9.63	23.03
USW UZ-N33	1.60	4.01	5.59	12.56
USW UZ-N37	0.66	2.38	3.85	9.95
USW UZ-N38	1.17	4.03	6.62	16.96
USW UZ-N53	0.63	2.94	5.28	13.15
USW UZ-N55	0.47	2.56	4.63	11.76
USW UZ-N57	1.48	4.31	7.32	17.19
USW UZ-N61	1.41	4.32	7.63	18.03
USW WT-24	6.01	14.20	21.97	45.23

Source: Appendix C.

The time-varying pneumatic pressure boundary condition used to simulate barometric pumping is a combination of records from the surface at boreholes USW NRG-6 and USW NRG-7a. The record from USW NRG-7a is used as the basis for the surface signal. Where there are gaps in the data from USW NRG-7a, data from USW NRG-6 are used to fill them. Four discontinuous 60-day periods are concatenated into a 240-day record of barometric pressure. The four 60-day

periods cover the four 30-day periods selected for data inversion and the 30 days immediately preceding each. The 30 days preceding the data sets are included in the simulations to develop a dynamic pressure history in the simulation. Because pressures are constantly changing in the real system, pneumatic pressure is never in equilibrium (i.e., pneumatically static conditions are never achieved). Initial conditions for pneumatic simulations are either pneumatically static conditions or dynamic conditions from a previous simulation. When the barometric signal is applied to the upper boundary of the unsaturated zone, the pressure variations within the unsaturated zone quickly equilibrate to the boundary condition, because propagation of the pressure fronts from the upper boundary is all that is necessary. The mean pressure, however, takes slightly longer to equilibrate, because flow from the upper boundary must reach the entire unsaturated zone. Previous work with the Yucca Mountain models have shown that after 30 days, the effects of the initial conditions are insignificant (i.e., dynamic pneumatic conditions corresponding to the current dynamic boundary conditions are developed) (Ahlers et al. 1998 [DIRS 124842], p. 224). This is also true when the initial conditions are the dynamic conditions at the end of a 60-day period (i.e., when switching from one 60-day boundary condition period to the next). The mean pressure at the collar (surface) of each borehole is different because each borehole is at a different elevation. The mean pressure of the pneumatic bounding condition for each boundary node is calculated based on the initial condition. The formatted gas pressure data (files with an extension *.txt*) and top boundary condition (*timvsp.dat* for calibration boreholes and *timvspF.dat* for fault) from DTNs: LB02091DSSCP3I.001 [DIRS 161292] and LB02092DSSCFPR.001 [DIRS 162422] are directly used in the relevant simulation studies (Section 6.3). Observed pneumatic pressure data (input files) were taken at irregular time intervals. Therefore, iTOUGH2 V5.0 [DIRS 160106] automatically interpolates the data to obtain a data set suitable for inversions. These interpolated data are plotted in Figures 6-9 and 6-12.

6.3 UZ FLOW MODEL PARAMETER CALIBRATION

6.3.1 General Calibration Approach

Inversion is an iterative process in which predictions from a numerical simulation are compared to data. The rock parameters are adjusted (calibrated) to improve the match between the prediction and the data. Data that are inverted to provide the calibrated properties documented in this report include saturation in the rock matrix, water potential in the rock matrix, and pneumatic pressure in the fractures. Hydrologic-property estimates from laboratory and field measurements, which provide initial estimates (prior information) for rock parameters, are included as data in the inversion (initial estimates for rock properties are different from initial guesses for inversions in this study). These data, which are referred to as “prior information” in this report, are just as important to the inversion as data about the state of the system (e.g., saturation). The combination of the two types of information allows the inversion to match the data as close as possible, while simultaneously estimating rock parameters that are reasonable according to the prior information. Three different kinds of parameter sets—drift-scale, mountain-scale and fault parameter sets—are determined from these calibration activities.

iTOUGH2 V5.0 [DIRS 160106] is used to carry out the automatic portion of the inversion process by considering weighted data and prior information according to the uncertainty of the estimated value. iTOUGH2 V5.0 [DIRS 160106] attempts to minimize the sum of the squared,

weighted residuals (called the objective function) by iteratively adjusting (calibrating) selected rock parameters. Finsterle (1998 [DIRS 103783]; 1999 [DIRS 104367]) describes further details of the inversion approach. The objective function is an indicator of goodness-of-fit. Changes in the objective function value and rock properties for each inversion iteration are provided in output files for a given calibration activity (Appendices D, E, and F).

6.3.2 Calibration of Drift-Scale Parameters

Calibration Procedure—One-dimensional inversion of the matrix-saturation and water-potential data is carried out for drift-scale parameters. The EOS9 module (Richards' equation) of iTOUGH2 V5.0 [DIRS 160106] is used for the inversion. The one-dimensional submodels correspond to 16 surface-based boreholes from which saturation and water potential have been measured. Table 6-4 shows the types of data used from each borehole, and Figure 4-1 shows the locations of some selected boreholes. Steady-state water flow is simulated simultaneously in all columns. Layer-averaged effective parameters are estimated (i.e., the same set of parameter values is used for each geologic layer in all columns).

Table 6-4. Data Used for One-Dimensional Calibration of Drift-Scale Properties from Each Borehole

Borehole	Matrix Liquid Saturation (core)	Matrix Liquid Water Potential (in situ)	Data Tracking Numbers
USW NRG-6	—	X	LB0208UZDSCPUI.001 [DIRS 161285]; LB0302AMRU0035.001 [DIRS 162378]
USW SD-7	X	—	
USW SD-9	X	—	
USW SD-12	—	X	
UE-25 UZ#4	—	X	
USW UZ-14	X	—	
UE-25 UZ#16	X	—	
USW UZ-N11	X	—	
USW UZ-N31	X	—	
USW UZ-N33	X	—	
USW UZ-N37	X	—	
USW UZ-N53	X	—	
USW UZ-N57	X	—	
USW UZ-N61	X	—	
USW UZ-N38	X	—	
USW UZ-N55	X	—	
USW SD-6	X	—	
USW WT-24	X	—	
USW NRG-7a	—	X	

Four calibrated parameter sets are produced, one for each present-day infiltration case (Section 6.2.5). The infiltration scenarios are key inputs to the UZ models because flow and transport are dependent on the amount of water infiltrating into the mountain. Appendix D provides a more-detailed discussion of calibration procedure and the use of the direct inputs.

Choice of Parameters for Calibration—Rock parameters to be estimated are matrix permeability, *k*, matrix van Genuchten parameter α (van Genuchten 1980 [DIRS 100610], pp. 892 to 893), fracture van Genuchten parameters α and an active-fracture-model parameter, γ (Liu et al. 1998 [DIRS 105729]) (values for log(k) and log(α) are adjusted in inversions). Other parameters are not changed in the calibration. These parameters are calibrated for model layers shown in Table 6-1 (except the zeolitic portion of CHn), though in some cases a common parameter value is estimated for groups of layers. (Details regarding which layers are grouped for parameter estimation are discussed below.) Inverse modeling involves iterations through many forward simulations and is therefore computationally intensive. For computational efficiency, one-dimensional simulations are used because the time required for each forward simulation is relatively short (on the order of one minute) compared to two- and three-dimensional simulations. Thus, many simulations, thousands in this case, can be accomplished in a reasonably short period. The effect of using one-dimensional simulations is that all flow is forced to be vertical; no lateral flow is considered in these calibrations. From the surface to the repository, lateral flow is not expected to be significant because perched water has not been found here. Below the repository, in the Calico Hills nonwelded hydrogeologic unit (CHn: see Table 6-1) and the Crater Flat undifferentiated unit (CFu), areas of perched water exist where lateral flow may be significant. Properties needed to produce perched water and varying degrees of lateral flow within the CHn and CFu units are further refined during three-dimensional calibrations performed in *UZ Flow Models and Submodels* (SNL 2007 [DIRS 175177], Section 6). Properties for the zeolitic portion of CHn, the unit where perched water is observed, are not calibrated here. Fracture permeability and van Genuchten *m* are not calibrated here because they are expected to be relatively insensitive to simulated matrix-saturation and water-potential distributions. Also, in the vatric part of the CHn, the fracture van Genuchten parameters α and an active-fracture-model parameter, γ, are not calibrated, because under the ambient conditions, water flow occurs mainly in the matrix (Section 6.1), and therefore these two parameters are not sensitive to simulated matrix saturation and water potential values. Furthermore, the field data in the vitric part of CHn are very limited. (For example, there are only 23 [out of total 298] matrix saturation data points in the vitric part of the CHn.) For a model layer where parameter γ is not calibrated, a parameter value of 0.25 is assigned to the layer, because the reasonable range of the parameter is between 0.2 and 0.4 for the unsaturated zone (BSC 2004 [DIRS 170035] Section 7) and 0.25 is close to the middle of the range. A detailed discussion on sensitivities of rock properties to the relevant simulation results is provided by Bandurraga and Bodvarsson (1999 [DIRS 103949], Section 5). Based on available data and previous calibrations (Bandurraga and Bodvarsson 1999 [DIRS 103949], Section 5), the set of parameters chosen for calibration has been shown to be adequate in representing ambient conditions in the unsaturated zone at Yucca Mountain.

Residual and satiated saturation are parameters that do not influence the calibration to ambient data as strongly as the van Genuchten parameter α. This is because ambient saturation and water-potential data are generally not at the extremes of the relationships where these bounding values play a stronger role. Like matrix porosity, matrix residual saturation is another property that is simple to measure with low error, so it makes more sense to calibrate the parameters that are not well constrained.

The matrix van Genuchten *m* parameter, which is essentially a pore-size distribution index, is well constrained by directly fitting the desaturation data to the van Genuchten function (Table 4-2), whereas the same data may give an estimate of the van Genuchten α that is biased toward the drainage condition. In this study, matrix van Genuchten *m* parameters are not calibrated.

Other hydrological parameters not calibrated are fracture and matrix porosity, residual saturation, and satiated saturation. Liquid flow simulations, because they are in steady state, are insensitive to porosity variations, so porosity could not be calibrated by inversion of saturation and water-potential data. Further, matrix porosity is a well-constrained property because the techniques used to measure porosity are simple and the measurement error is low.

Because there are no data for model layers tr3 and tr2, they are assigned the same properties as model layers bf3 and bf2, respectively (Assumption 1, in Section 5). This assignment is based on the common depositional profile of the Tram and Bullfrog Tuffs. Because the Bullfrog Tuff represents a very small portion of the unsaturated zone within the UZ model boundaries (it is present above the water table only immediately next to the Solitario Canyon fault and in the extreme northern portion of the UZ models) (BSC 2004 [DIRS 169855], Section 6), the impact of this approximation is not significant.

Common values of k_M, α_M, α_F, are used for the vitric Tac (material types ch2v, ch3v, ch4v, and ch5v) and for the zeolitic Tac (material types ch2z, ch3z, ch4z, and ch5z), respectively. The common value refers to a property value shared by several model layers. As reflected in Table 6-1, these layers do not represent actual geologic or hydrogeologic divisions, but are employed to better characterize which portions of the Tac are vitric or zeolitic, as documented in *Development of Numerical Grids for UZ Flow and Transport Modeling* (BSC 2004 [DIRS 169855], Section 6).

The lower nonlithophysal layer of the TSw (Tptpln) is subdivided into two layers based on matrix property development consistent with the report by Flint (1998 [DIRS 100033], pp. 27 to 29). This division does not exist for the fracture properties (see Table 4-3), so common values of fracture properties are used for material types tsw36 and tsw37.

The fracturing characteristics of the rocks of Yucca Mountain are considered to be primarily dependent on the degree of welding and alteration. Data in Table 4-3 show that this is true of fracture frequency. The welded rocks have higher fracture frequencies than nonwelded rocks. Because of the general division between the fracture characteristics of welded and nonwelded rocks, model layers are grouped together, based on welding, to estimate common values of the active fracture parameter. Alteration is believed to possibly influence the active fracture parameter, so it is also used as a criterion for grouping layers. In inversions, common values of γ are estimated for the TCw, PTn, some layers of the TSw, zeolitic portions of the TSw and Cfu, and devitrified/welded portions of CFu. The initial guesses for the γ factor are assigned in a range of 0.2 to 0.4 for the welded units (BSC 2004 [DIRS 170035], Section 7). Table 6-5 shows the material types included in each of these groups. The value of γ is estimated individually for tsw31 because matrix-to-fracture flow is expected to be high in this layer, as a result of the transition from matrix-dominated flow in the PTn to fracture-dominated flow in the TSw.

Table 6-5. Material Groups of the Active Fracture Parameter, γ, for Saturation and Water-Potential Data Inversion

Material Type (group)
tcw11, tcw12, tcw13
ptn21, ptn22, ptn23, ptn24, ptn25, ptn26
tsw31
tsw32 and tsw33
tsw34, tsw35, tsw36, tsw37, tsw38, tsw39
pp4, pp1, bf2, and tswz (zeolitic portion of tsw39)
pp3, pp2, bf3

Source: Output DTNs: LB0610UZDSCP10.001 (*Sandia2R218i*); LB0610UZDSCP30.001 (*Sandia2R113i*); LB0611UZDSCP50.001 (*Sandia2R118i*); LB0612UZDSCP90.001 (*Sandia2R217i*).

To speed up the calibration simulations by employing properties that are close to final calibration results, property sets from the previous version of calibrated sets (DTNs: LB0208UZDSCPMI.001 [DIRS 161285] and LB0208UZDSCPUI.001 [DIRS 166711]) were used as initial guesses of inversions in this study. A detailed description of the input and output files for the inversions is given in Appendix D.

Calibration Results—The one-dimensional calibrated drift-scale parameter sets for the 10th, 30th, 50th, and 90th percentile infiltration scenarios are presented in Tables 6-6 to 6-9, respectively. Matches to the saturation data achieved with these parameter sets for several calibration boreholes are shown in Figures 6-1, 6-3, 6-5, and 6-7, respectively. The fracture flux fraction is defined as the ratio of the vertical fracture flux to the total water flux. Note that saturation data in the zeolitic portion of CHn (where perched water was observed) are not used for calibration. Figures 6-2, 6-4, 6-6, and 6-8 show matches to the water-potential data for two calibration boreholes. The boreholes used in these figures generally have more data points for vertical distributions of matrix saturation and/or water potential. Also, in those figures, an error bar corresponds to one standard deviation (characterizing data uncertainty) on each side of the given data point.

Table 6-6. Calibrated Parameters from One-Dimensional Inversion of Saturation, and Water-Potential Data for the 10th Percentile Infiltration Scenario

Model Layer	K_M (m^2)	α_M (1/Pa)	m_M (−)	K_F (m^2)	α_F (1/Pa)	m_F (−)	γ (−)
tcw11	3.74×10^{-15}	1.01×10^{-5}	0.388	3.0×10^{-11}	5.27×10^{-3}	0.633	0.400
tcw12	5.52×10^{-20}	2.56×10^{-6}	0.280	5.3×10^{-12}	1.57×10^{-3}	0.633	0.400
tcw13	5.65×10^{-17}	2.26×10^{-6}	0.259	4.5×10^{-12}	1.24×10^{-3}	0.633	0.400
ptn21	4.60×10^{-15}	7.76×10^{-5}	0.245	3.2×10^{-12}	8.70×10^{-4}	0.633	0.001
ptn22	5.45×10^{-12}	1.16×10^{-4}	0.219	3.0×10^{-13}	1.57×10^{-3}	0.633	0.001
ptn23	1.69×10^{-14}	2.47×10^{-5}	0.247	3.0×10^{-13}	5.18×10^{-3}	0.633	0.001
ptn24	6.94×10^{-12}	9.03×10^{-4}	0.182	3.0×10^{-12}	1.86×10^{-3}	0.633	0.001
ptn25	2.35×10^{-13}	6.77×10^{-5}	0.300	1.7×10^{-13}	1.33×10^{-3}	0.633	0.001
ptn26	3.16×10^{-11}	1.00×10^{-3}	0.126	2.2×10^{-13}	1.34×10^{-3}	0.633	0.001
tsw31	9.78×10^{-17}	2.80×10^{-5}	0.218	8.1×10^{-13}	1.82×10^{-5}	0.633	0.129

Table 6-6. Calibrated Parameters from One-Dimensional Inversion of Saturation, and Water-Potential Data for the 10th Percentile Infiltration Scenario (Continued)

Model Layer	K_M (m^2)	α_M (1/Pa)	m_M (−)	K_F (m^2)	α_F (1/Pa)	m_F (−)	γ (−)
tsw32	4.55×10^{-16}	1.71×10^{-5}	0.290	7.1×10^{-13}	4.20×10^{-5}	0.633	0.400
tsw33	1.86×10^{-17}	7.26×10^{-6}	0.283	7.8×10^{-13}	1.59×10^{-3}	0.633	0.400
tsw34	3.16×10^{-18}	2.55×10^{-6}	0.317	3.3×10^{-13}	3.16×10^{-4}	0.633	0.400
tsw35	1.09×10^{-17}	4.45×10^{-6}	0.216	9.1×10^{-13}	3.16×10^{-4}	0.633	0.400
tsw36	3.16×10^{-18}	2.51×10^{-6}	0.442	1.3×10^{-12}	7.44×10^{-4}	0.633	0.400
tsw37	3.16×10^{-18}	2.51×10^{-6}	0.442	1.3×10^{-12}	7.44×10^{-4}	0.633	0.400
tsw38	3.79×10^{-18}	1.88×10^{-6}	0.286	8.1×10^{-13}	2.12×10^{-3}	0.633	0.400
tswz (zeolitic portion of tsw39)	3.50×10^{-17}	4.61×10^{-6}	0.059	8.1×10^{-13}	1.50×10^{-3}	0.633	0.250
tswv (vitric portion of tsw39)	1.49×10^{-13}	4.72×10^{-5}	0.293	8.1×10^{-13}	1.50×10^{-3}	0.633	0.250
ch1z	3.50×10^{-17}	2.12×10^{-7}	0.349	2.5×10^{-14}	1.40×10^{-3}	0.633	0.250
ch1v	2.21×10^{-12}	1.20×10^{-4}	0.240	2.2×10^{-13}	2.10×10^{-3}	0.633	0.250
ch2v	1.55×10^{-12}	3.36×10^{-4}	0.158	2.2×10^{-13}	1.90×10^{-3}	0.633	0.250
ch3v	1.55×10^{-12}	3.36×10^{-4}	0.158	2.2×10^{-13}	1.90×10^{-3}	0.633	0.250
ch4v	1.55×10^{-12}	3.36×10^{-4}	0.158	2.2×10^{-13}	1.90×10^{-3}	0.633	0.250
ch5v	1.55×10^{-12}	3.36×10^{-4}	0.158	2.2×10^{-13}	1.90×10^{-3}	0.633	0.250
ch6v	3.92×10^{-13}	1.72×10^{-5}	0.147	2.2×10^{-13}	1.90×10^{-3}	0.633	0.250
ch2z	5.20×10^{-18}	2.25×10^{-6}	0.257	2.5×10^{-14}	8.90×10^{-4}	0.633	0.250
ch3z	5.20×10^{-18}	2.25×10^{-6}	0.257	2.5×10^{-14}	8.90×10^{-4}	0.633	0.250
ch4z	5.20×10^{-18}	2.25×10^{-6}	0.257	2.5×10^{-14}	8.90×10^{-4}	0.633	0.250
ch5z	5.20×10^{-18}	2.25×10^{-6}	0.257	2.5×10^{-14}	8.90×10^{-4}	0.633	0.250
ch6z	8.20×10^{-19}	1.56×10^{-7}	0.499	2.5×10^{-14}	1.40×10^{-3}	0.633	0.250
pp4	3.01×10^{-17}	6.31×10^{-6}	0.474	2.5×10^{-14}	2.82×10^{-4}	0.633	0.146
pp3	9.24×10^{-14}	1.72×10^{-5}	0.407	2.2×10^{-13}	2.47×10^{-3}	0.633	0.199
pp2	1.68×10^{-15}	4.84×10^{-6}	0.309	2.2×10^{-13}	3.17×10^{-3}	0.633	0.199
pp1	5.01×10^{-17}	3.16×10^{-5}	0.272	2.5×10^{-14}	1.53×10^{-4}	0.633	0.146
bf3	1.00×10^{-14}	3.20×10^{-5}	0.193	2.2×10^{-13}	2.93×10^{-3}	0.633	0.199
bf2	8.10×10^{-17}	1.18×10^{-7}	0.617	2.5×10^{-14}	8.90×10^{-4}	0.633	0.250

NOTES: Correlation of the UZ model grid layers given above with the major units [modified from the report by Montazer and Wilson (1984 [DIRS 100161])], the lithostratigraphic nomenclature (see Table 6-1) (BSC 2004 [DIRS 170029]), and the hydrogeologic units (Flint 1998 [DIRS 100033], Table 1) are given in Table 6-1. These data have been developed as documented in this report and submitted under output DTN: LB0610UZDSCP10.001 (*Calibrated Parameters_R218.doc*).

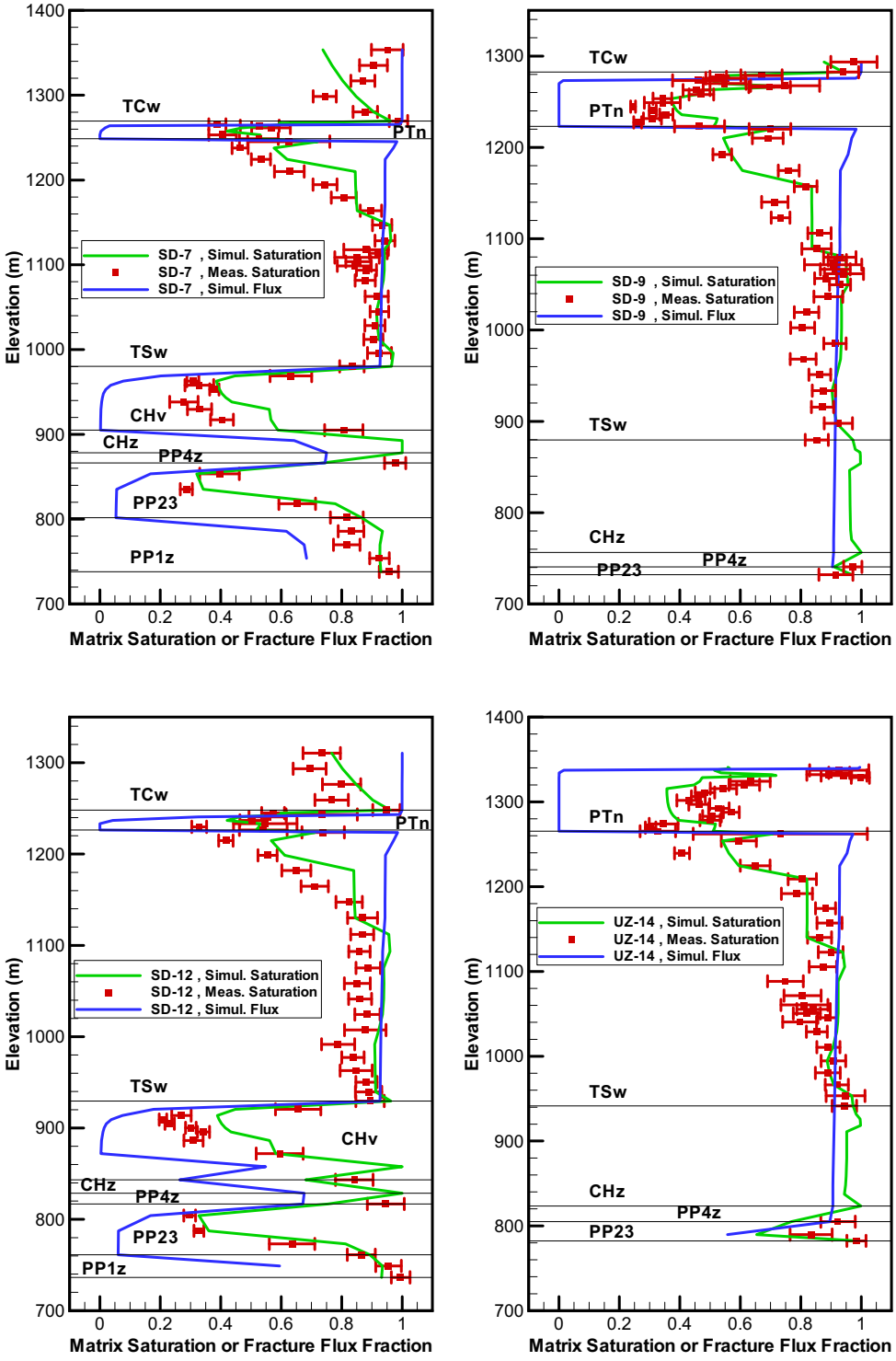

Output DTN: LB0610UZDSCP10.001 (*Sandia2R218D, Sandia2R218D.out* and *Sandia2R218i.out*).

Figure 6-1. Saturation Matches and Fracture Flux Fraction at Selected Boreholes for the One-Dimensional, Drift-Scale, Calibrated Parameter Set for the 10th Percentile Infiltration Scenario

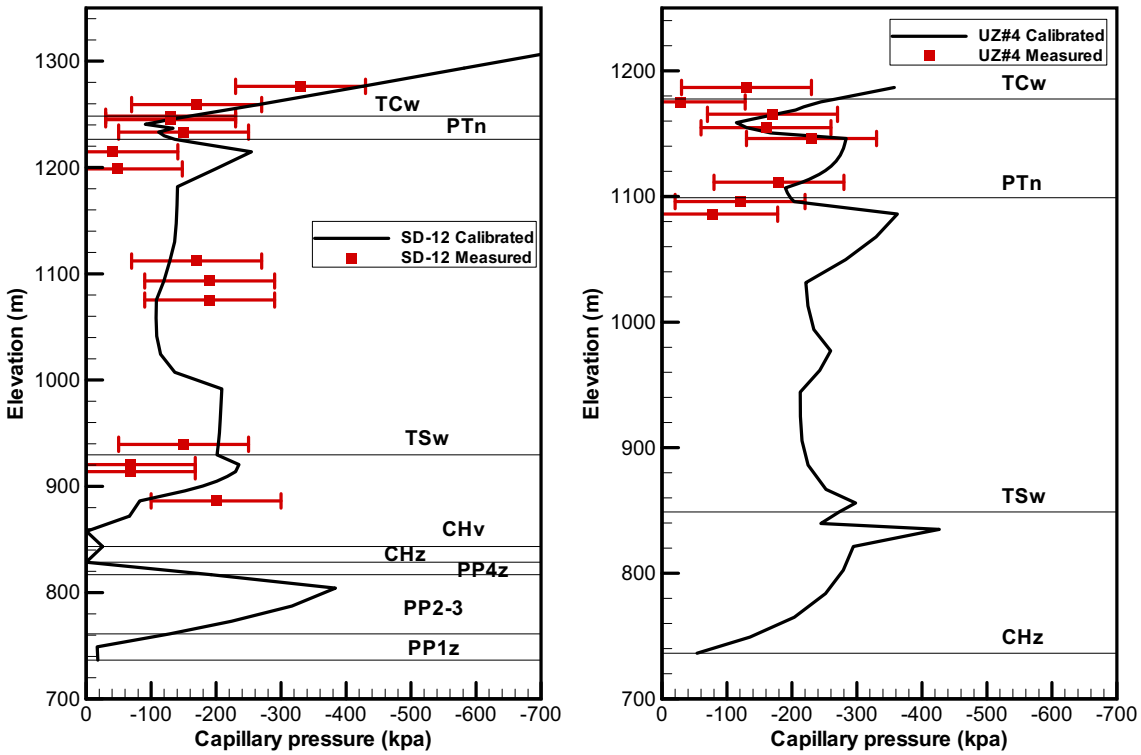

Output DTN: LB0610UZDSCP10.001 (*Sandia2R218D, Sandia2R218D.out* and *Sandia2R218i.out*).

Figure 6-2. Water-Potential Matches at Selected Boreholes for the One-Dimensional, Drift-Scale, Calibrated Parameter Set for the 10th Percentile Infiltration Scenario

Table 6-7. Calibrated Parameters from One-Dimensional Inversion of Saturation, and Water-Potential Data for the 30th Percentile Infiltration Scenario

Model Layer	K_M (m^2)	α_M (1/Pa)	m_M (–)	K_F (m^2)	α_F (1/Pa)	m_F (–)	γ (–)
tcw11	3.88×10^{-15}	1.22×10^{-5}	0.388	3.0×10^{-11}	4.99×10^{-3}	0.633	0.400
tcw12	1.15×10^{-19}	2.88×10^{-6}	0.280	5.3×10^{-12}	2.18×10^{-3}	0.633	0.400
tcw13	4.39×10^{-16}	2.61×10^{-6}	0.259	4.5×10^{-12}	1.85×10^{-3}	0.633	0.400
ptn21	2.13×10^{-14}	9.82×10^{-5}	0.245	3.2×10^{-12}	2.68×10^{-3}	0.633	0.001
ptn22	1.28×10^{-11}	1.22×10^{-4}	0.219	3.0×10^{-13}	1.37×10^{-3}	0.633	0.001
ptn23	4.06×10^{-14}	2.41×10^{-5}	0.247	3.0×10^{-13}	1.22×10^{-3}	0.633	0.001
ptn24	7.64×10^{-12}	7.44×10^{-4}	0.182	3.0×10^{-12}	2.94×10^{-3}	0.633	0.001
ptn25	9.63×10^{-13}	6.28×10^{-5}	0.300	1.7×10^{-13}	1.09×10^{-3}	0.633	0.001
ptn26	1.86×10^{-11}	8.11×10^{-4}	0.126	2.2×10^{-13}	9.51×10^{-4}	0.633	0.001
tsw31	3.21×10^{-17}	2.90×10^{-5}	0.218	8.1×10^{-13}	2.08×10^{-5}	0.633	0.088
tsw32	3.01×10^{-16}	1.59×10^{-5}	0.290	7.1×10^{-13}	5.65×10^{-5}	0.633	0.400
tsw33	1.86×10^{-17}	6.56×10^{-6}	0.283	7.8×10^{-13}	1.58×10^{-3}	0.633	0.400
tsw34	3.16×10^{-18}	1.71×10^{-6}	0.317	3.3×10^{-13}	3.16×10^{-4}	0.633	0.400
tsw35	1.11×10^{-17}	3.38×10^{-6}	0.216	9.1×10^{-13}	5.75×10^{-4}	0.633	0.400
tsw36	3.16×10^{-18}	7.32×10^{-7}	0.442	1.3×10^{-12}	1.09×10^{-3}	0.633	0.400

Table 6-7. Calibrated Parameters from One-Dimensional Inversion of Saturation, and Water-Potential Data for the 30th Percentile Infiltration Scenario (Continued)

Model Layer	K_M (m^2)	α_M (1/Pa)	m_M (−)	K_F (m^2)	α_F (1/Pa)	m_F (−)	γ (−)
tsw37	3.16×10^{-18}	7.32×10^{-7}	0.442	1.3×10^{-12}	1.09×10^{-3}	0.633	0.400
tsw38	1.27×10^{-17}	3.11×10^{-6}	0.286	8.1×10^{-13}	8.87×10^{-4}	0.633	0.400
tswz (zeolitic portion of tsw39)	3.50×10^{-17}	4.61×10^{-6}	0.059	8.1×10^{-13}	1.50×10^{-3}	0.633	0.250
tswv (vitric portion of tsw39)	2.23×10^{-13}	4.69×10^{-5}	0.293	8.1×10^{-13}	1.50×10^{-3}	0.633	0.250
ch1z	3.50×10^{-17}	2.12×10^{-7}	0.349	2.5×10^{-14}	1.40×10^{-3}	0.633	0.250
ch1v	2.59×10^{-12}	1.11×10^{-4}	0.240	2.2×10^{-13}	2.10×10^{-3}	0.633	0.250
ch2v	6.77×10^{-11}	3.33×10^{-4}	0.158	2.2×10^{-13}	1.90×10^{-3}	0.633	0.250
ch3v	6.77×10^{-11}	3.33×10^{-4}	0.158	2.2×10^{-13}	1.90×10^{-3}	0.633	0.250
ch4v	6.77×10^{-11}	3.33×10^{-4}	0.158	2.2×10^{-13}	1.90×10^{-3}	0.633	0.250
ch5v	6.77×10^{-11}	3.33×10^{-4}	0.158	2.2×10^{-13}	1.90×10^{-3}	0.633	0.250
ch6v	2.71×10^{-13}	1.84×10^{-5}	0.147	2.2×10^{-13}	1.90×10^{-3}	0.633	0.250
ch2z	5.20×10^{-18}	2.25×10^{-6}	0.257	2.5×10^{-14}	8.90×10^{-4}	0.633	0.250
ch3z	5.20×10^{-18}	2.25×10^{-6}	0.257	2.5×10^{-14}	8.90×10^{-4}	0.633	0.250
ch4z	5.20×10^{-18}	2.25×10^{-6}	0.257	2.5×10^{-14}	8.90×10^{-4}	0.633	0.250
ch5z	5.20×10^{-18}	2.25×10^{-6}	0.257	2.5×10^{-14}	8.90×10^{-4}	0.633	0.250
ch6z	8.20×10^{-19}	1.56×10^{-7}	0.499	2.5×10^{-14}	1.40×10^{-3}	0.633	0.250
pp4	3.51×10^{-17}	6.31×10^{-6}	0.474	2.5×10^{-14}	2.82×10^{-4}	0.633	0.400
pp3	1.02×10^{-13}	1.48×10^{-5}	0.407	2.2×10^{-13}	1.65×10^{-3}	0.633	0.400
pp2	1.69×10^{-15}	3.89×10^{-6}	0.309	2.2×10^{-13}	1.65×10^{-3}	0.633	0.400
pp1	2.57×10^{-17}	3.16×10^{-5}	0.272	2.5×10^{-14}	1.58×10^{-4}	0.633	0.400
bf3	6.31×10^{-14}	6.18×10^{-5}	0.193	2.2×10^{-13}	1.65×10^{-3}	0.633	0.400
bf2	8.10×10^{-17}	1.18×10^{-7}	0.617	2.5×10^{-14}	8.90×10^{-4}	0.633	0.250

NOTES: Correlation of the UZ model grid layers given above with the major units [modified from the report by Montazer and Wilson (1984 [DIRS 100161])], the lithostratigraphic nomenclature (see Table 6-1) (BSC 2004 [DIRS 170029]), and the hydrogeologic units (Flint 1998 [DIRS 100033], Table 1) are given in Table 6-1. These data have been developed as documented in this report and submitted under output DTN: LB0610UZDSCP30.001 (*Calibrated Parameter_R113_30%.doc*).

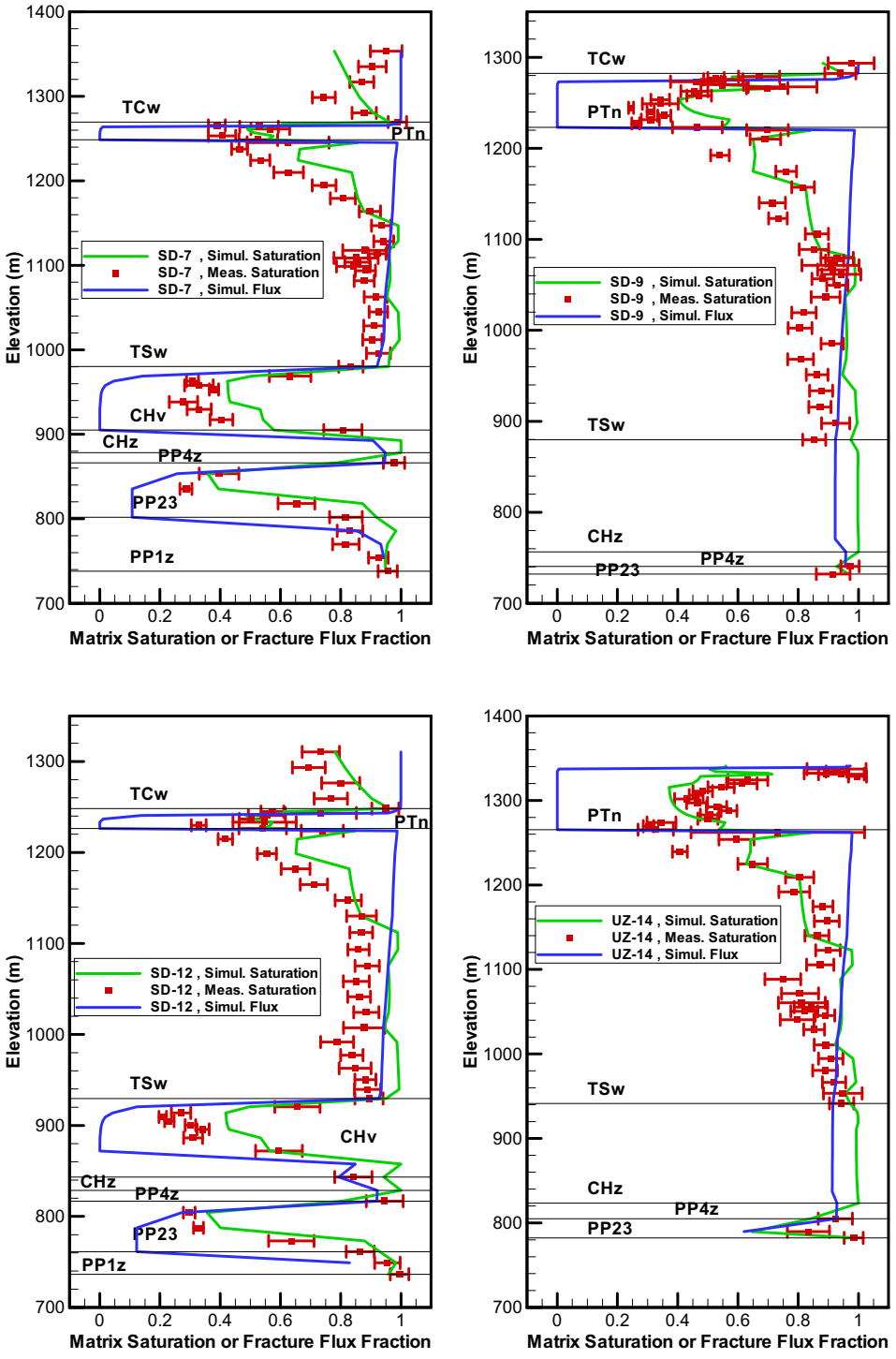

Output DTN: LB0610UZDSCP30.001 (*Sandia2R113A, Sandia2R113A.out* and *Sandia2R113Ai.out*).

Figure 6-3. Saturation Matches and Fracture Flux Fraction at Selected Boreholes for the One-Dimensional, Drift-Scale, Calibrated Parameter Set for the 30th Percentile Infiltration Scenario

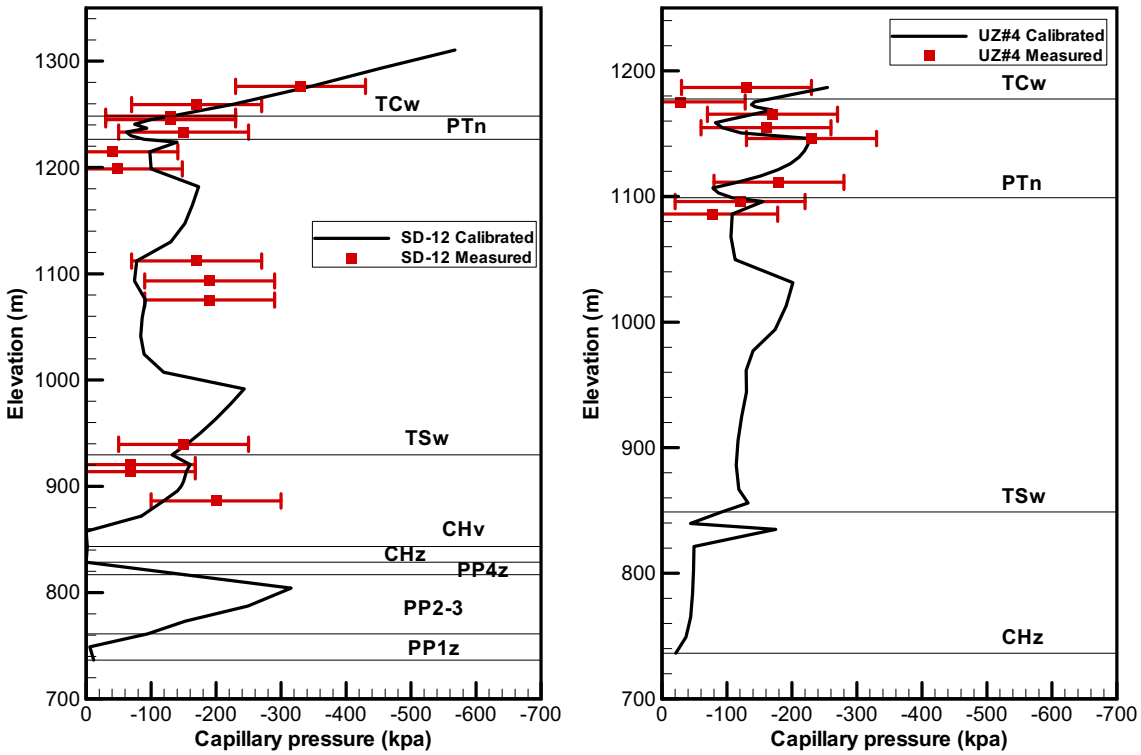

Output DTN: LB0610UZDSCP30.001 (*Sandia2R113A, Sandia2R113A.out* and *Sandia2R113Ai.out*).

Figure 6-4. Water-Potential Matches at Selected Boreholes for the One-Dimensional, Drift-Scale, Calibrated Parameter Set for the 30th Percentile Infiltration Scenario

Table 6-8. Calibrated Parameters from One-Dimensional Inversion of Saturation and Water-Potential Data for the 50th Percentile Infiltration Scenario

Model Layer	K_M (m^2)	α_M (1/Pa)	m_M (−)	K_F (m2)	α_F (1/Pa)	m_F (−)	γ (−)
tcw11	3.90×10^{-15}	1.23×10^{-5}	0.388	3.0×10^{-11}	5.01×10^{-3}	0.633	0.400
tcw12	1.16×10^{-19}	3.04×10^{-6}	0.280	5.3×10^{-12}	2.19×10^{-3}	0.633	0.400
tcw13	4.41×10^{-16}	2.71×10^{-6}	0.259	4.5×10^{-12}	1.86×10^{-3}	0.633	0.400
ptn21	2.14×10^{-14}	8.82×10^{-5}	0.245	3.2×10^{-12}	2.69×10^{-3}	0.633	0.001
ptn22	1.70×10^{-11}	1.23×10^{-4}	0.219	3.0×10^{-13}	1.38×10^{-3}	0.633	0.001
ptn23	6.15×10^{-14}	2.39×10^{-5}	0.247	3.0×10^{-13}	1.23×10^{-3}	0.633	0.001
ptn24	2.30×10^{-11}	8.08×10^{-4}	0.182	3.0×10^{-12}	2.95×10^{-3}	0.633	0.001
ptn25	6.41×10^{-13}	5.71×10^{-5}	0.300	1.7×10^{-13}	1.10×10^{-3}	0.633	0.001
ptn26	3.16×10^{-11}	9.92×10^{-4}	0.126	2.2×10^{-13}	9.55×10^{-4}	0.633	0.001
tsw31	1.04×10^{-16}	1.07×10^{-5}	0.218	8.1×10^{-13}	2.00×10^{-5}	0.633	0.075
tsw32	1.70×10^{-16}	2.70×10^{-5}	0.290	7.1×10^{-13}	5.01×10^{-5}	0.633	0.393
tsw33	3.78×10^{-17}	6.42×10^{-6}	0.283	7.8×10^{-13}	1.58×10^{-3}	0.633	0.393
tsw34	3.16×10^{-18}	1.50×10^{-6}	0.317	3.3×10^{-13}	3.16×10^{-4}	0.633	0.400
tsw35	1.94×10^{-17}	3.72×10^{-6}	0.216	9.1×10^{-13}	5.78×10^{-4}	0.633	0.400

Table 6-8. Calibrated Parameters from One-Dimensional Inversion of Saturation and Water-Potential Data for the 50th Percentile Infiltration Scenario (Continued)

Model Layer	K_M (m^2)	α_M (1/Pa)	m_M (−)	K_F (m2)	α_F (1/Pa)	m_F (−)	γ (−)
tsw36	4.45×10^{-18}	6.58×10^{-7}	0.442	1.3×10^{-12}	1.10×10^{-3}	0.633	0.400
tsw37	4.45×10^{-18}	6.58×10^{-7}	0.442	1.3×10^{-12}	1.10×10^{-3}	0.633	0.400
tsw38	2.16×10^{-17}	3.69×10^{-6}	0.286	8.1×10^{-13}	8.91×10^{-4}	0.633	0.400
tswz (zeolitic portion of tsw39)	3.50×10^{-17}	4.61×10^{-6}	0.059	8.1×10^{-13}	1.50×10^{-3}	0.633	0.250
tswv (vitric portion of tsw39)	2.24×10^{-13}	4.84×10^{-5}	0.293	8.1×10^{-13}	1.50×10^{-3}	0.633	0.250
ch1z	3.50×10^{-17}	2.12×10^{-7}	0.349	2.5×10^{-14}	1.40×10^{-3}	0.633	0.250
ch1v	3.16×10^{-12}	1.35×10^{-4}	0.240	2.2×10^{-13}	2.10×10^{-3}	0.633	0.250
ch2v	1.58×10^{-11}	3.19×10^{-4}	0.158	2.2×10^{-13}	1.90×10^{-3}	0.633	0.250
ch3v	1.58×10^{-11}	3.19×10^{-4}	0.158	2.2×10^{-13}	1.90×10^{-3}	0.633	0.250
ch4v	1.58×10^{-11}	3.19×10^{-4}	0.158	2.2×10^{-13}	1.90×10^{-3}	0.633	0.250
ch5v	1.58×10^{-11}	3.19×10^{-4}	0.158	2.2×10^{-13}	1.90×10^{-3}	0.633	0.250
ch6v	5.14×10^{-13}	1.67×10^{-5}	0.147	2.2×10^{-13}	1.90×10^{-3}	0.633	0.250
ch2z	5.20×10^{-18}	2.25×10^{-6}	0.257	2.5×10^{-14}	8.90×10^{-4}	0.633	0.250
ch3z	5.20×10^{-18}	2.25×10^{-6}	0.257	2.5×10^{-14}	8.90×10^{-4}	0.633	0.250
ch4z	5.20×10^{-18}	2.25×10^{-6}	0.257	2.5×10^{-14}	8.90×10^{-4}	0.633	0.250
ch5z	5.20×10^{-18}	2.25×10^{-6}	0.257	2.5×10^{-14}	8.90×10^{-4}	0.633	0.250
ch6z	8.20×10^{-19}	1.56×10^{-7}	0.499	2.5×10^{-14}	1.40×10^{-3}	0.633	0.250
pp4	1.89×10^{-17}	6.54×10^{-6}	0.474	2.5×10^{-14}	2.82×10^{-4}	0.633	0.365
pp3	1.79×10^{-13}	1.78×10^{-5}	0.407	2.2×10^{-13}	1.66×10^{-3}	0.633	0.400
pp2	1.00×10^{-15}	4.58×10^{-6}	0.309	2.2×10^{-13}	1.66×10^{-3}	0.633	0.400
pp1	2.57×10^{-17}	3.16×10^{-5}	0.272	2.5×10^{-14}	1.41×10^{-4}	0.633	0.365
bf3	6.11×10^{-14}	1.00×10^{-4}	0.193	2.2×10^{-13}	1.66×10^{-3}	0.633	0.400
bf2	8.10×10^{-17}	1.18×10^{-7}	0.617	2.5×10^{-14}	8.90×10^{-4}	0.633	0.250

NOTES: Correlation of the UZ model grid layers given above with the major units [modified from the report by Montazer and Wilson (1984 [DIRS 100161])], the lithostratigraphic nomenclature (see Table 6-1) (BSC 2004 [DIRS 170029]), and the hydrogeologic units (Flint 1998 [DIRS 100033], Table 1) are given in Table 6-1. These data have been developed as documented in this report and submitted under output DTN: LB0611UZDSCP50.001 (*CalibratedDriftScaleParameters_R118For50case.doc*).

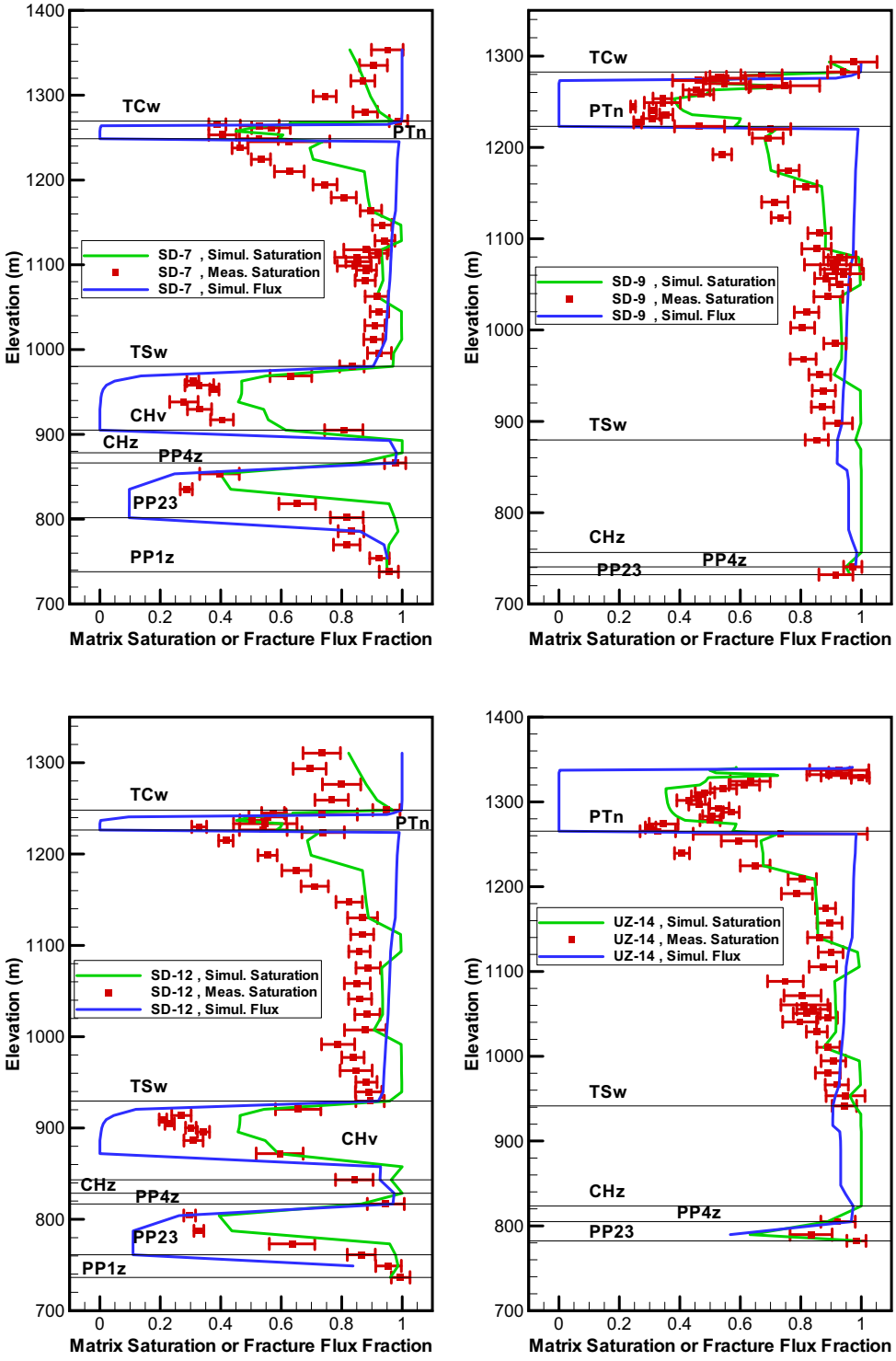

Output DTN: LB0610UZDSCP50.001 (*Sandia2R118B, Sandia2R118B.out* and *Sandia2R118Bi.out*).

Figure 6-5. Saturation Matches and Fracture Flux Fraction at Selected Boreholes for the One-Dimensional, Drift-Scale, Calibrated Parameter Set for the 50th Percentile Infiltration Scenario

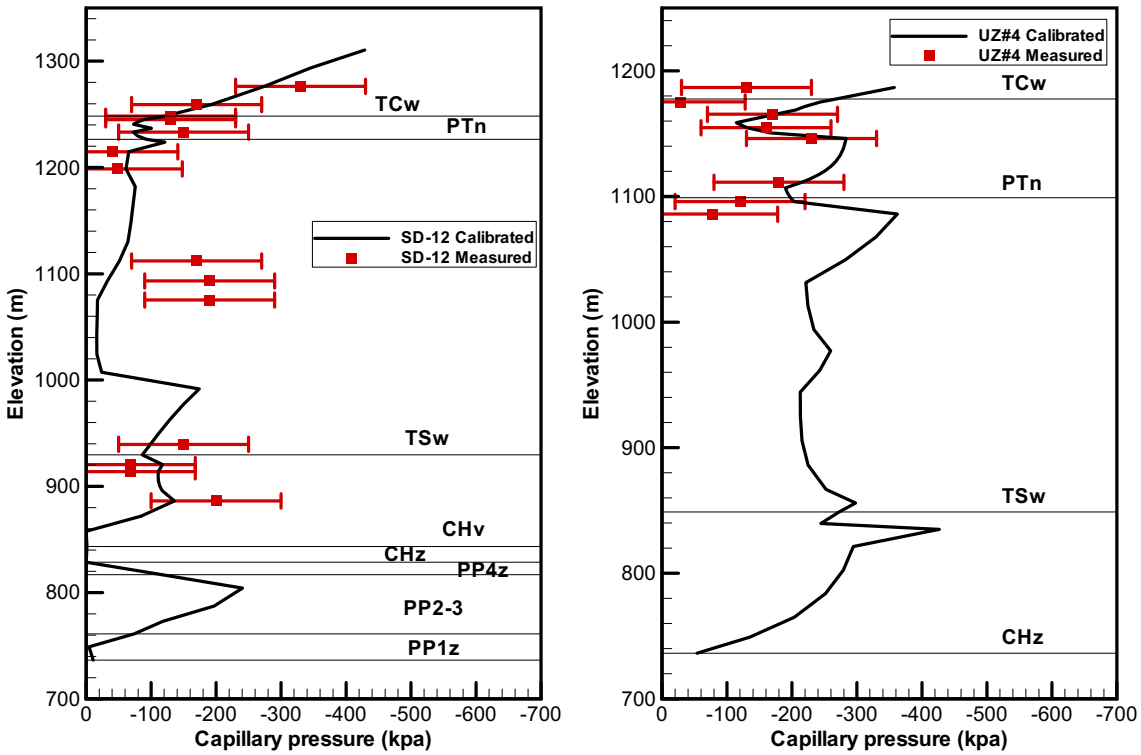

Output DTN: LB0611UZDSCP50.001 (*Sandia2R118B, Sandia2R118B.out,* and *Sandia2R118Bi.out*).

Figure 6-6. Water-Potential Matches at Selected Boreholes for the One-Dimensional, Drift-Scale, Calibrated Parameter Set for the 50th Percentile Infiltration Scenario

Table 6-9. Calibrated Parameters from One-Dimensional Inversion of Saturation and Water-Potential Data for the 90th Percentile Infiltration Scenario

Model Layer	K_M (m^2)	α_M (1/Pa)	m_M (–)	K_F (m^2)	α_F (1/Pa)	m_F (–)	γ (–)
tcw11	3.90×10^{-15}	1.23×10^{-5}	0.388	3.0×10^{-11}	5.01×10^{-3}	0.633	0.400
tcw12	3.16×10^{-19}	3.05×10^{-6}	0.280	5.3×10^{-12}	2.19×10^{-3}	0.633	0.400
tcw13	4.41×10^{-16}	2.45×10^{-6}	0.259	4.5×10^{-12}	1.86×10^{-3}	0.633	0.400
ptn21	2.14×10^{-14}	7.83×10^{-5}	0.245	3.2×10^{-12}	2.69×10^{-3}	0.633	0.001
ptn22	3.16×10^{-11}	1.37×10^{-4}	0.219	3.0×10^{-13}	1.38×10^{-3}	0.633	0.001
ptn23	8.68×10^{-14}	2.39×10^{-5}	0.247	3.0×10^{-13}	1.23×10^{-3}	0.633	0.001
ptn24	3.16×10^{-11}	6.92×10^{-4}	0.182	3.0×10^{-12}	2.95×10^{-3}	0.633	0.001
ptn25	2.21×10^{-12}	7.38×10^{-5}	0.300	1.7×10^{-13}	1.10×10^{-3}	0.633	0.001
ptn26	3.16×10^{-11}	5.71×10^{-4}	0.126	2.2×10^{-13}	9.55×10^{-4}	0.633	0.001
tsw31	2.62×10^{-15}	3.38×10^{-5}	0.218	8.1×10^{-13}	2.00×10^{-5}	0.633	0.001
tsw32	2.30×10^{-16}	3.43×10^{-5}	0.290	7.1×10^{-13}	6.37×10^{-5}	0.633	0.400
tsw33	3.97×10^{-17}	1.09×10^{-5}	0.283	7.8×10^{-13}	1.58×10^{-3}	0.633	0.400
tsw34	6.31×10^{-18}	1.35×10^{-6}	0.317	3.3×10^{-13}	3.16×10^{-4}	0.633	0.400
tsw35	7.54×10^{-17}	3.08×10^{-5}	0.216	9.1×10^{-13}	3.16×10^{-4}	0.633	0.400

Table 6-9. Calibrated Parameters from One-Dimensional Inversion of Saturation and Water-Potential Data for the 90th Percentile Infiltration Scenario (Continued)

Model Layer	K_M (m^2)	α_M (1/Pa)	m_M (−)	K_F (m^2)	α_F (1/Pa)	m_F (−)	γ (−)
tsw36	7.50×10^{-18}	4.18×10^{-7}	0.442	1.3×10^{-12}	1.10×10^{-3}	0.633	0.400
tsw37	7.50×10^{-18}	4.18×10^{-7}	0.442	1.3×10^{-12}	1.10×10^{-3}	0.633	0.400
tsw38	4.40×10^{-17}	4.78×10^{-6}	0.286	8.1×10^{-13}	8.91×10^{-4}	0.633	0.400
tswz (zeolitic portion of tsw39)	3.50×10^{-17}	4.61×10^{-6}	0.059	8.1×10^{-13}	1.50×10^{-3}	0.633	0.250
tswv (vitric portion of tsw39)	2.24×10^{-13}	4.86×10^{-5}	0.293	8.1×10^{-13}	1.50×10^{-3}	0.633	0.250
ch1z	3.50×10^{-17}	2.12×10^{-7}	0.349	2.5×10^{-14}	1.40×10^{-3}	0.633	0.250
ch1v	2.51×10^{-12}	1.28×10^{-4}	0.240	2.2×10^{-13}	2.10×10^{-3}	0.633	0.250
ch2v	3.16×10^{-11}	2.42×10^{-4}	0.158	2.2×10^{-13}	1.90×10^{-3}	0.633	0.250
ch3v	3.16×10^{-11}	2.42×10^{-4}	0.158	2.2×10^{-13}	1.90×10^{-3}	0.633	0.250
ch4v	3.16×10^{-11}	2.42×10^{-4}	0.158	2.2×10^{-13}	1.90×10^{-3}	0.633	0.250
ch5v	3.16×10^{-11}	2.42×10^{-4}	0.158	2.2×10^{-13}	1.90×10^{-3}	0.633	0.250
ch6v	3.40×10^{-13}	2.20×10^{-5}	0.147	2.2×10^{-13}	1.90×10^{-3}	0.633	0.250
ch2z	5.20×10^{-18}	2.25×10^{-6}	0.257	2.5×10^{-13}	8.90×10^{-4}	0.633	0.250
ch3z	5.20×10^{-18}	2.25×10^{-6}	0.257	2.5×10^{-14}	8.90×10^{-4}	0.633	0.250
ch4z	5.20×10^{-18}	2.25×10^{-6}	0.257	2.5×10^{-14}	8.90×10^{-4}	0.633	0.250
ch5z	5.20×10^{-18}	2.25×10^{-6}	0.257	2.5×10^{-14}	8.90×10^{-4}	0.633	0.250
ch6z	7.20×10^{-19}	1.56×10^{-7}	0.499	2.5×10^{-14}	1.40×10^{-3}	0.633	0.250
pp4	1.00×10^{-17}	6.31×10^{-6}	0.474	2.5×10^{-14}	2.82×10^{-4}	0.633	0.001
pp3	1.71×10^{-13}	1.90×10^{-5}	0.407	2.2×10^{-13}	1.66×10^{-3}	0.633	0.400
pp2	6.31×10^{-16}	2.42×10^{-6}	0.309	2.2×10^{-13}	1.66×10^{-3}	0.633	0.400
pp1	5.01×10^{-17}	3.16×10^{-5}	0.272	2.5×10^{-14}	1.41×10^{-4}	0.633	0.001
bf3	1.58×10^{-14}	1.58×10^{-4}	0.193	2.2×10^{-13}	1.58×10^{-4}	0.633	0.400
bf2	8.10×10^{-17}	1.18×10^{-7}	0.617	2.5×10^{-14}	8.90×10^{-4}	0.633	0.250

NOTES: Correlation of the UZ model grid layers given above with the Major Units [modified from the report by Montazer and Wilson (1984 [DIRS 100161])], the lithostratigraphic nomenclature (see Table 6-1) (BSC 2004 [DIRS 170029]), and the hydrogeologic units (Flint 1998 [DIRS 100033], Table 1) are given in Table 6-1. These data have been developed as documented in this report and submitted under output DTN: LB0612UZDSCP90.001 (*CalibratedDriftScaleParameters_R217For90Case.doc*).

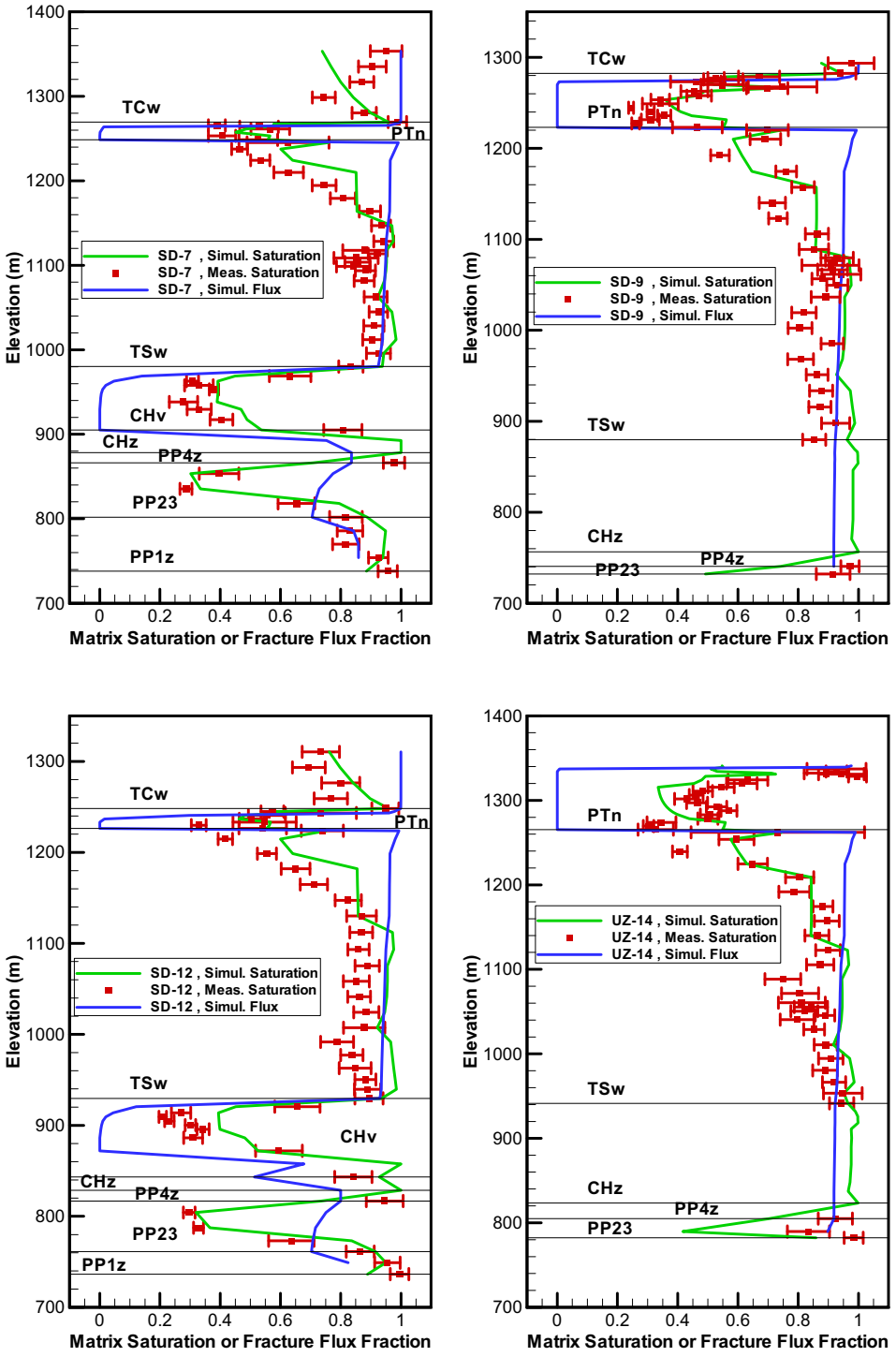

Output DTN: LB0612UZDSCP90.001 (*Sandia2R217C, Sandia2R217C.out,* and *Sandia2R217Ci.out*).

Figure 6-7. Saturation Matches and Fracture Flux Fraction at Selected Boreholes for the One-Dimensional, Drift-Scale, Calibrated Parameter Set for the 90th Percentile Infiltration Scenario

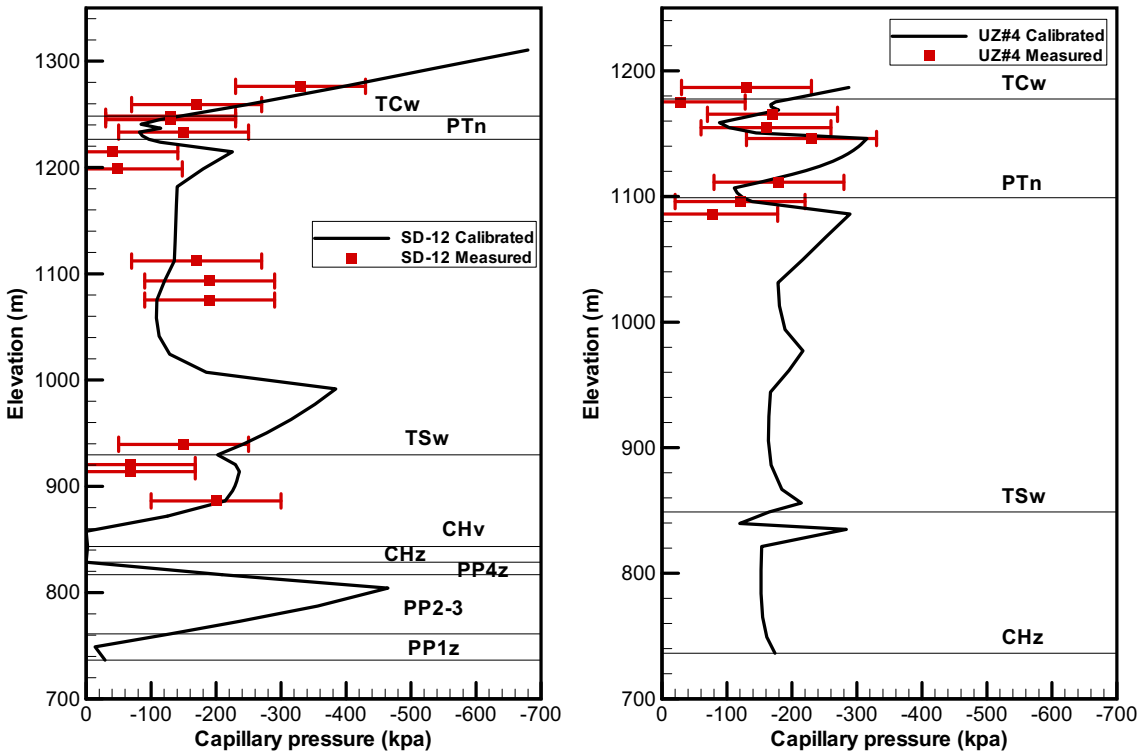

Output DTN: LB0612UZDSCP90.001 (*Sandia2R217C, Sandia2R217C.out* and *Sandia2R217Ci.out*).

Figure 6-8. Water-Potential Matches at Selected Boreholes for One-Dimensional, Drift-Scale, Calibrated Parameter Set for the 90th Percentile Infiltration Scenario

6.3.3 Calibration of Mountain-Scale Parameters

Scale Dependence of Fracture Permeability—It is well documented in the literature that large-scale effective permeabilities are generally larger than smaller-scale permeabilities (Neuman 1994 [DIRS 105731]). An intuitive explanation for this scale-dependent behavior is that a large observation scale, in an average sense, corresponds to a larger opportunity to encounter more permeable zones or paths when observations are made, which considerably increases the values of the observed permeability. Because of the scale difference, drift-scale fracture permeabilities, determined from air-injection tests, cannot be applied to mountain-scale simulations. Therefore, development of mountain-scale properties is needed. In addition to matching matrix-saturation and water-potential data, the determination of mountain-scale parameters also involves matching pneumatic pressure data measured in surface boreholes. In the drift-scale parameter sets, fracture permeabilities correspond to those determined from air-injection tests. The pneumatic pressure data result from mountain-scale gas-flow processes, whereas air-injection tests correspond to scales on an order of several meters or less.

Unlike the connected fracture networks and soils, studies on the scale-dependent behavior of matrix properties in unsaturated fractured rocks are very limited. However, it is reasonable to believe that the scale-dependent behavior of the matrix is different from fracture networks. For example, relatively large fractures can act as capillary barriers for flow between matrix blocks

separated by these fractures, even when the matrix is essentially saturated (water potential is close to the air entry value). This might limit the matrix scale-dependent behavior to a relatively small scale associated with the spacing between relatively large fractures. Although it is expected that estimated large-scale matrix permeabilities should be larger than those measured on a core scale, no evidence exists to indicate that matrix properties should be very different on both the site and drift scales, which are much larger than the scale characterized by the fracture spacing. This point is also supported by the inversion results for the drift-scale properties. For example, the estimated matrix permeabilities are generally much closer to prior information than estimated site-scale fracture permeabilities.

Based on the above discussions, only fracture permeabilities for the mountain-scale property sets are recalibrated, whereas other properties remain the same as those in the corresponding drift-scale properties.

Calibration Procedure Using Pneumatic Pressure Data—The EOS3 module of iTOUGH2 V5.0 [DIRS 160106] is used for transient pneumatic simulations. Both the gas phase and the liquid phase are considered in the flow calculations. The pneumatic inversion is carried out in two steps. First, the fracture permeabilities for layers tcw11 through ptn26 are calibrated. Then, the permeabilities for layers tsw31 through tsw37 are calibrated as a group by multiplying the prior information for all seven layers by the same factor. The input and output data files for the calibration are documented in Appendix E in detail.

The calibrated fracture permeabilities resulting from inversion of pneumatic data are expected to be higher than the prior information, owing to the scale dependency of fracture permeabilities as described above. Therefore, the initial guesses for the fracture permeabilities are log*(k)* = −10.5 for tcw11, tcw12, and tcw13, and log(*k*) = −11.5 for ptn21 through ptn26. These estimates are higher than the corresponding prior information (Table 4-4). The permeabilities of layers tsw31 through 37 are set to the values previously calibrated using the pneumatic data (Appendix E).

The lack of significant attenuation in the TSw unit is considered an important feature shown by the gas pressure data. The calibrated fracture permeabilities for the model layers in the TSw unit need to be consistent with this feature. Therefore, fracture permeabilities in the TSw need to be determined in such a way that the simulated and observed gas pressure signals at the upper and lower sensor locations in the TSw have similar degrees of attenuation for Borehole USW SD-12. Borehole USW SD-12 is chosen for this analysis because the distance between the two TSw sensors within this borehole is the largest among all the relevant boreholes. The degree of attenuation of the barometric signal through the TSw in USW SD-12, or the relative difference between the signals at the two sensor locations, was determined by using standard functions of Excel® software (see description of *R113_d_factor_gascalibration.xls* in Section E3.5) to evaluate:

$$F = \frac{1}{N}\left\{\sum_{i=1}^{N}\left[\left(P_u(t_i) - P_u(t_1)\right) - \left(P_b(t_i) - P_b(t_1)\right)\right]^2\right\}^{1/2} \qquad \text{(Eq. 6-12)}$$

where N is the total number of calibration time points, P is the gas pressure, and subscripts u and b refer to the sensors in the upper and lower (bottom) portions of the TSw within Borehole USW

SD-12. Obviously, if the gas signals from the two sensors are identical, *F* should be equal to zero. In this study, fracture permeabilities need to be determined that will predict *F* values similar to the value calculated from the data, such that the simulated and observed gas-pressure signals have similar degrees of attenuation (Appendix E).

Since the gas-pressure data from the TSw are relatively limited compared to the TCw and PTn units and the insignificant attenuation and time lag between the uppermost and lowermost sensors are used for calibration, the fracture permeabilities for different model layers in this unit could not be independently estimated in a reliable manner. Note that the attenuation and time lag are determined by the overall hydraulic properties between the two sensors, rather than by properties in a single model layer. Therefore, the ratios of the permeabilities of layers tsw31 through tsw37 are held constant, and the prior information permeability values are multiplied by a single factor, *d*. For a given infiltration map, a number of values, log(*d*), between 1 and 2 with an interval of 0.1 are tested to determine the *d* resulting in an *F* value closest to the *F* value corresponding to the data. To calculate an *F* value for a *d* factor, investigators used the outputs from the TCw and PTn fracture permeability calibrations to run the forward simulation using iTOUGH2 V5.0 [DIRS 160106] for generating gas pressures used in Equation 6-10. In a forward simulation, all the rock properties are the same as those determined from the corresponding TCw and PTn fracture permeability calibration, except the fracture permeabilities for model layers tsw31 to tsw37 are determined using the *d* factor and the prior information.

The determined log(*d*) values based on the above procedure are shown in Table 6-10 for the three infiltration maps (Appendix E). The log(*d*) values range from 1.9 to 2.0, indicating that the fracture permeabilities for the relevant model layers are increased by about two orders of magnitude compared to the prior information. This results from scale effects, as previously discussed. As previously discussed, there are two steps in the pneumatic-pressure calibration. After the *d* factor is determined, a forward run with the new fracture permeability values for tsw31 through tsw37 (considering the *d* factor) is performed to check the matches with pneumatic pressure data, compared with the matches from the first step. The comparison is satisfactory in terms of the change in the objective function (Appendix E).

Table 6-10. The Calculated log(*d*) Factors for the Four Infiltration Maps

10th Percentile	30th Percentile	50th Percentile	90th Percentile
2.0	2.0	1.9	1.9

Source: Appendix E.

Table 6-11 provides mountain-scale fracture permeabilities calibrated with pneumatic pressure data for different infiltration scenarios.

Table 6-11. Calibrated Mountain-Scale Fracture Permeabilities (m^2)

Model Layer[a]	10th Percentile	30th Percentile	50th Percentile	90th Percentile
tcw11	1.00×10^{-12}	1.21×10^{-12}	1.32×10^{-12}	9.06×10^{-13}
tcw12	1.00×10^{-10}	1.00×10^{-10}	1.00×10^{-10}	1.00×10^{-10}
tcw13	1.00×10^{-12}	6.66×10^{-13}	5.77×10^{-13}	5.55×10^{-13}
ptn21	1.00×10^{-11}	2.55×10^{-12}	1.15×10^{-12}	2.51×10^{-13}
ptn22	1.00×10^{-13}	1.00×10^{-14}	1.00×10^{-14}	1.00×10^{-14}
ptn23	2.14×10^{-13}	1.51×10^{-13}	1.10×10^{-13}	1.13×10^{-13}
ptn24	1.17×10^{-12}	1.39×10^{-12}	4.81×10^{-12}	1.00×10^{-11}
ptn25	3.08×10^{-13}	1.00×10^{-14}	1.00×10^{-14}	1.00×10^{-14}
ptn26	1.00×10^{-13}	8.38×10^{-14}	3.74×10^{-14}	1.00×10^{-14}
tsw31	8.13×10^{-11}	8.13×10^{-11}	6.46×10^{-11}	6.46×10^{-11}
tsw32	7.08×10^{-11}	7.08×10^{-11}	5.62×10^{-11}	5.62×10^{-11}
tsw33	7.76×10^{-11}	7.76×10^{-11}	6.17×10^{-11}	6.17×10^{-11}
tsw34	3.31×10^{-11}	3.31×10^{-11}	2.63×10^{-11}	2.63×10^{-11}
tsw35	9.12×10^{-11}	9.12×10^{-11}	7.24×10^{-11}	7.24×10^{-11}
tsw36	1.35×10^{-10}	1.35×10^{-10}	1.07×10^{-10}	1.07×10^{-10}
tsw37	1.35×10^{-12}	1.35×10^{-10}	1.07×10^{-10}	1.07×10^{-10}

NOTES: Correlation of the UZ model grid layers given above with the major units [modified from the report by Montazer and Wilson (1984 [DIRS 100161])], the lithostratigraphic nomenclature (see Table 6-1) (BSC 2004 [DIRS 170029]), and the hydrogeologic units (Flint 1998 [DIRS 100033], Table 1) are given in Table 6-1. These data have been developed as documented in this report and submitted under outputDTNs: LB0611MTSCHP10.001 (*CalibratedMountainScaleParameters_R218For10Case.doc*); LB0611MTSCHP30.001 (*Calibrated Mountain Scale Parameters_R113_30Percent.doc*); LB0612MTSCHP50.001(*CalibratedMountainScaleParameters_R118For50case.doc*); LB0612MTSCHP90.001 (*CalibratedMountainScaleParameters_R217For90Case.doc*).

[a] In the numerical grids used in inversions, the name of (fracture) model layer is the same as the corresponding model layer name in the table except that the 4th character is "F."

Figure 6-9 shows pneumatic pressure matches at USW SD-12 for a one-dimensional, mountain-scale, calibrated parameter set for the 10th percentile infiltration scenario. Similar matches are obtained for other boreholes and for three other infiltration scenarios. In Figure 6-9, both simulated and observed pressure curves for a given geologic layer (tsw32 and ptn26) are shifted some distance along the vertical axis to better display the matches. The shifted pressure values are also shown in the figure. The standard deviations characterizing measurement errors for pneumatic pressure are on the order of 0.001 kpa (DTN: GS031208312232.008 [DIRS 178750]). Because these errors are very small, they are not shown in Figure 6-9.

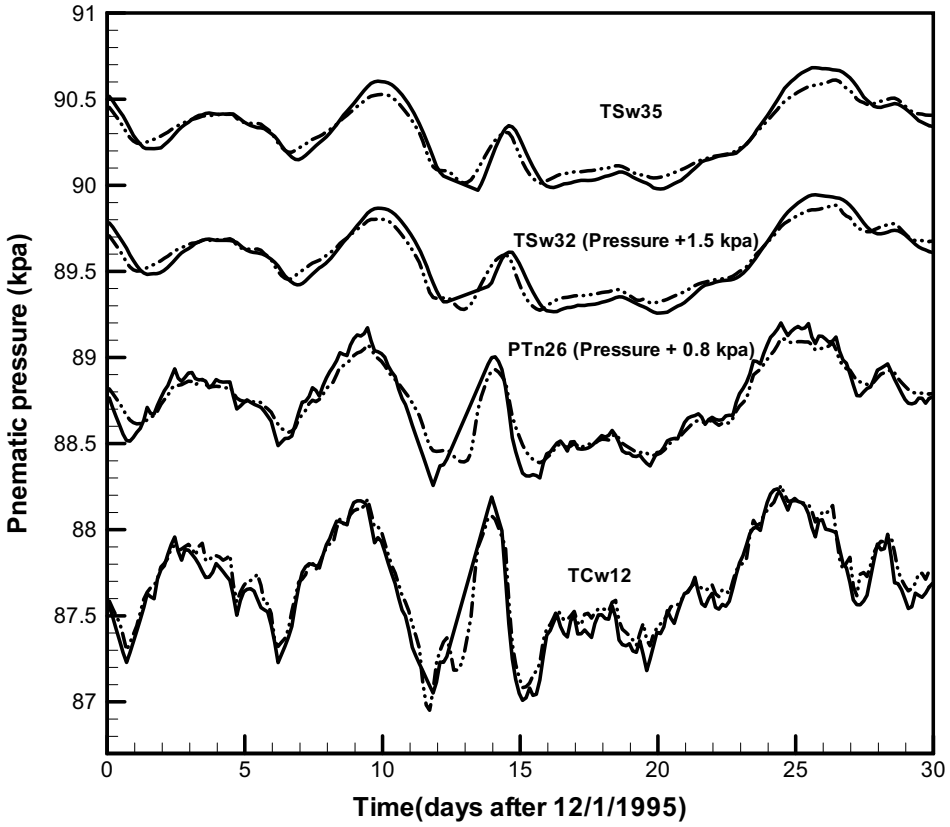

Output DTN: LB0611MTSCHP10.001 (*TtgasR218checki.tec*).

NOTE: Solid lines correspond to the interpolated raw data and dashed lines to simulated results.

Figure 6-9. Pneumatic Pressure Matches at USW SD-12 for the One-Dimensional, Mountain-Scale, Calibrated Parameter Set for the 10th Percentile Infiltration Scenario

6.3.4 Calibration of Fault Parameters

Two-dimensional flow (vertical and east—west) is considered to adequately describe the flow patterns around Borehole USW UZ-7a, used for fault property calibration. Inverse modeling is computationally intensive. For this reason, it is necessary to use the simplest approach that will adequately simulate the system being analyzed. As faults are relatively planar in geometry, flow in and around a fault zone (including interaction of the hanging wall, foot zone, and foot wall) can be sufficiently captured by a two-dimensional simulation. An east—west, vertical cross section through USW UZ-7a and the Ghost Dance fault captures this interaction. This cross section is aligned approximately parallel to the dip of the beds and parallel to the dip of the fault (perpendicular to the strike). Any lateral flow in or around the fault zone should follow the dip of the beds and the fault.

The data from Borehole USW UZ-7a represent the most complete data set from within a fault zone. Saturation, water potential, and pneumatic data are available from the surface down into the TSw. Other data sets that are influenced by faults, from Boreholes USW NRG-6, UE-25 UZ#4, and UE-25 UZ#5, include only pneumatic pressure data and are only relevant to

the TSw. Because of the limited amount of data, it is best to characterize one fault as completely as possible and apply these properties to all other faults. This treatment is necessary because not enough data are available for other faults. The Ghost Dance fault, located near the east boundary of a repository block, is an important hydrogeological feature as a potential flow path for receiving lateral flows along eastwardly tilted layer interfaces.

Use of the Input Data— USW UZ-7a data are the most comprehensive with respect to faults. Saturation, water potential, and pneumatic pressure data are available within the Ghost Dance fault zone from the surface to the upper layers of the TSw. Pneumatic-only data (that show fault influence) are available from three other boreholes, but are not used in this analysis (rationale documented in Section 4.1.2.3). Because the data on faults are limited, they are grouped into four layers to reduce the number of parameters used to characterize the fault zones. The layers are the TCw, PTn, TSw, and CHn/CFu. Data for inversion are available for only the first three layers, so only the parameters of these layers are calibrated. Minimization of the objective function is the only criterion used for a successful calibration. The proportion of fracture flow to matrix flow specifically in the fault is not an element of the conceptual model.

Saturation, water potential, and pneumatic pressure data, which are inverted to obtain the calibrated parameter sets, are developed from files with extension prn, *MFAi*, and *LMGi* from DTN: LB02092DSSCFPR.001 [DIRS 162422]. Criteria identical to those used in selecting an appropriate time interval for the pneumatic data as described in Section 6.2.3 are used to select data from USW UZ-7a. Table 6-12 shows the dates and elevations for the data that were used in the inversion. The procedure to calculate elevations is the same as that given in Section 6.2.3. Elevations in Table 6-12 (in a descending order) correspond to sensors TCP1319, TCP 1325, TCP 1331, TCP 1337, and TCP 1343, respectively (DTN: GS031208312232.008 [DIRS 178750]). As with the one-dimensional pneumatic inversion, data are taken from the lowest TCw instrument station, all instrument stations in the PTn, and in the TSw within the fault zone. Three instrument stations in the footwall (below the fault zone) are not included in the inversion because they represent interactions at the edge of the fault on a subgridblock scale not captured by the UZ models. The calibration activities are documented in Appendix F.

Table 6-12. USW UZ-7a Sensor Locations for Pneumatic Data Used for Inversion

Borehole	Dates	Elevation (m)
USW UZ-7a	12/1 to 12/31/95	1,243.6
	12/1 to 12/31/95	1,232.9
	12/1 to 12/31/95	1,222.2
	12/1 to 12/31/95	1,214.0
	12/1 to 12/31/95	1,178.4

Source: DTNs: GS031208312232.008 [DIRS 178750]; MO0012MWDGFM02.002 [DIRS 153777].

Calibration Procedure—Data inversion for calibration of the fault parameters is carried out in the same sequence of steps used for the one-dimensional mountain-scale inversion. First, the saturation and water-potential data are inverted. Second, the pneumatic data are inverted.

Fault properties to be calibrated are fracture properties, whereas matrix properties within fault zones are the same as those in nonfault zones, as indicated by property identifiers in the numerical grid (DTN: LB02081DKMGKID.001 [DIRS 160108]). Fracture permeabilities are fixed during the saturation and water-potential inversion, and are the only parameters calibrated to the pneumatic data. Parameters to be calibrated against matrix-saturation and water-potential data are fracture, α, and active-fracture-model parameter, γ. The same fracture, m (0.633), as that for the nonfault zone (Table 4-4) is used here for the fault zone, because no specific fracture m data are available for the fault zone. As discussed in Section 6.3.2, fracture m is not expected to be sensitive to simulated matrix saturation and water potential distributions.

Using the parameter set from the matrix-saturation and water-potential calibration step, fracture permeabilities are calibrated by inversion of the pneumatic data for the different infiltration scenarios. Automated inversion successfully improves the objective function and provides a good match to the pneumatic data.

Finally, the calibrated fault parameters are used to check the matches with matrix-saturation and water-potential data for the four infiltration scenarios (Appendix F). For each infiltration scenario, the resulting objective function value is almost identical to that obtained from the matrix saturation and water-potential calibration step. Therefore, the matches are satisfactory.

Calibration Results—Calibrated fault parameter sets are presented in Tables 6-13 to 6-16. As an example, matches to the data achieved with the parameter set corresponding to the 10th percentile infiltration for USW UZ-7a are shown for saturation in Figure 6-10, for water potential in Figure 6-11, and for pneumatic pressure in Figure 6-12. In Figures 6-10 and 6-11, an error bar corresponds to one standard deviation (characterizing data uncertainty) on each side of the given data point. In Figure 6-12, simulated and observed pressure curves for a given geologic layer are shifted along the vertical axis an identical distance to better display the matches. The shifted pressure values are also shown in the figure. (The standard deviations characterizing measurement errors for pneumatic pressure are on the order of 0.001 kpa (DTN: GS031208312232.008 [DIRS 178750]). Because these errors are very small, they are not shown in Figure 6-12.) The matches between data and calculation results are characterized by the corresponding objective function values for the different infiltration scenarios (Appendix F). The calibrated fracture permeabilities in the fault zone are generally higher than those for nonfault zones (Table 6-11), which is consistent with measurement results of the report by LeCain et al. (2000 [DIRS 144612], Summary). Also, properties for layer Chnf are not calibrated because no data available for calibration for this layer. In this case, the properties are assigned to be prior information. In addition, changes (within a reasonable range) in fault fracture permeability do not significantly alter flow fields in the unsaturated zone (BSC 2005 [DIRS 174116], Section 7).

Table 6-13. Calibrated Fault Parameters for the 10th Percentile Infiltration Scenario from Two-Dimensional Inversions of Saturation, Water Potential, and Pneumatic Data

Model Layer	k_F (m^2)	α_F (1/Pa)	m_F (–)	γ (–)
Tcwf	1.00×10^{-10}	1.00×10^{-2}	0.633	0.38
Ptnf	3.94×10^{-11}	2.87×10^{-3}	0.633	0.10
Tswf	1.00×10^{-10}	3.20×10^{-3}	0.633	0.20
Chnf	3.70×10^{-13}	2.30×10^{-3}	0.633	0.20

NOTES: Parameters for layer chnf are not calibrated. The prior information is taken from DTN: LB0207REVUZPRP.001 [DIRS 159526]. These data have been developed as documented in this report and submitted under output DTN: LB0612MTSCHPFT.001 (*Check10i.par*).

Table 6-14. Calibrated Fault Parameters for the 30th Percentile Infiltration Scenario from Two-Dimensional Inversions of Saturation, Water Potential, and Pneumatic Data

Model Layer	k_F (m^2)	α_F (1/Pa)	m_F (–)	γ (–)
Tcwf	1.00×10^{-10}	1.00×10^{-2}	0.633	0.21
Ptnf	5.00×10^{-11}	4.65×10^{-3}	0.633	0.17
Tswf	9.80×10^{-11}	3.73×10^{-4}	0.633	0.39
Chnf	3.70×10^{-13}	2.30×10^{-3}	0.633	0.20

NOTES: Parameters for layer chnf are not calibrated. The prior information is taken from DTN: LB0207REVUZPRP.001 [DIRS 159526]. These data have been developed as documented in this report and submitted under output DTN: LB0612MTSCHPFT.001 (*Check30i.par*).

Table 6-15. Calibrated Fault Parameters for the 50th Percentile Infiltration Scenario from Two-Dimensional Inversions of Saturation, Water Potential, and Pneumatic Data

Model Layer	k_F (m^2)	α_F (1/Pa)	m_F (–)	γ (–)
Tcwf	1.00×10^{-10}	1.00×10^{-2}	0.633	0.29
Ptnf	1.00×10^{-10}	4.65×10^{-3}	0.633	0.17
Tswf	1.00×10^{-10}	3.16×10^{-4}	0.633	0.20
Chnf	3.70×10^{-13}	2.30×10^{-3}	0.633	0.20

NOTES: Parameters for layer chnf are not calibrated. The prior information is taken from DTN: LB0207REVUZPRP.001 [DIRS 159526]. These data have been developed as documented in this report and submitted under output DTN: LB0612MTSCHPFT.001 (*Check50i.par*).

Table 6-16. Calibrated Fault Parameters for the 90th Percentile Infiltration Scenario from Two-Dimensional Inversions of Saturation, Water Potential, and Pneumatic Data

Model Layer	k_F (m^2)	α_F (1/Pa)	m_F (–)	γ (–)
Tcwf	1.00×10^{-10}	4.87×10^{-3}	0.633	0.28
Ptnf	2.98×10^{-11}	2.80×10^{-3}	0.633	0.20
Tswf	6.31×10^{-11}	4.56×10^{-4}	0.633	0.34
Chnf	3.70×10^{-13}	2.30×10^{-3}	0.633	0.20

NOTES: Parameters for layer chnf are not calibrated. The prior information is taken from DTN: LB0207REVUZPRP.001 [DIRS 159526]. These data have been developed as documented in this report and submitted under output DTN: LB0612MTSCHPFT.001 (*Check90i.par*).

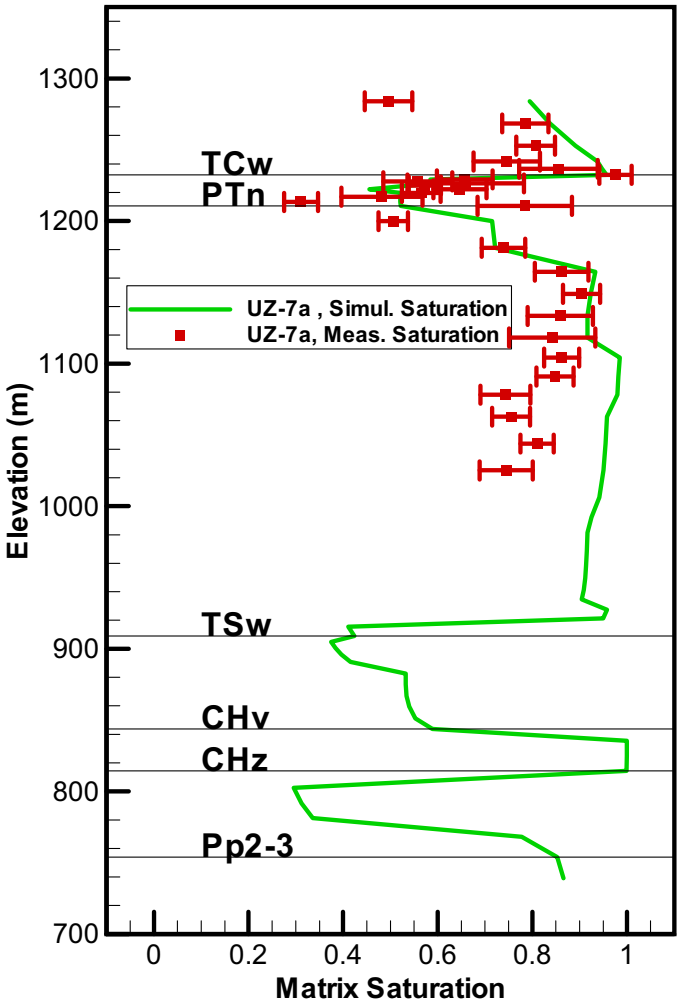

Output DTN: LB0612MTSCHPFT.001 (*test10, test10.out*, and *test10i.out*).

Figure 6-10. Saturation Matches at USW UZ-7a Used in the Two-Dimensional Calibrated Fault Parameter Set for the 10th Percentile Infiltration Scenario

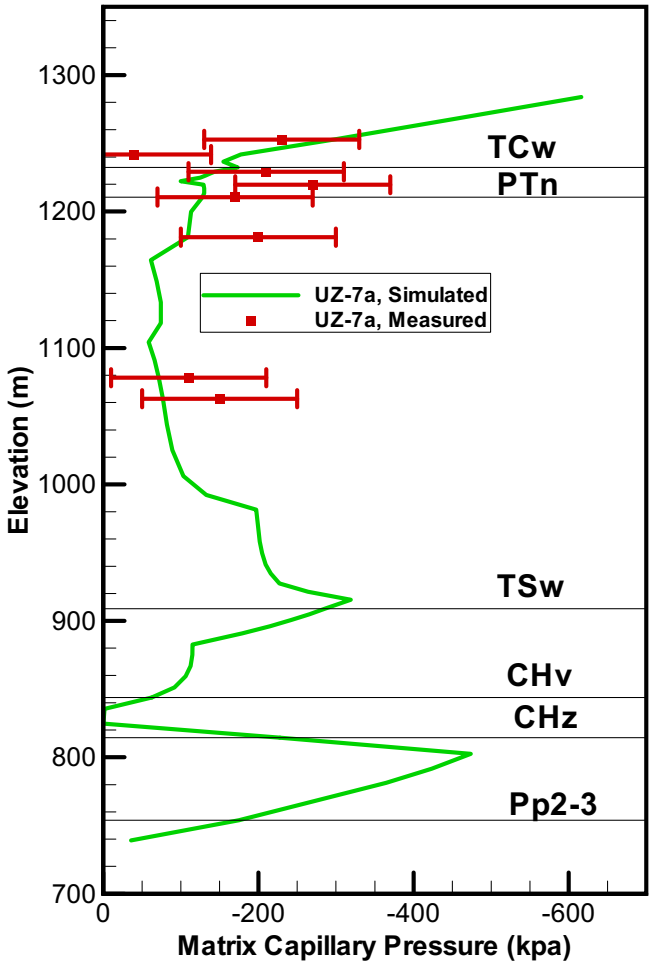

Output DTN: LB0612MTSCHPFT.001 (*test10, test10.out*, and *test10i.out*).

Figure 6-11. Water-Potential Matches at USW UZ-7a Used in the Two-Dimensional Calibrated Fault Parameter Set for the 10th Percentile Infiltration Scenario

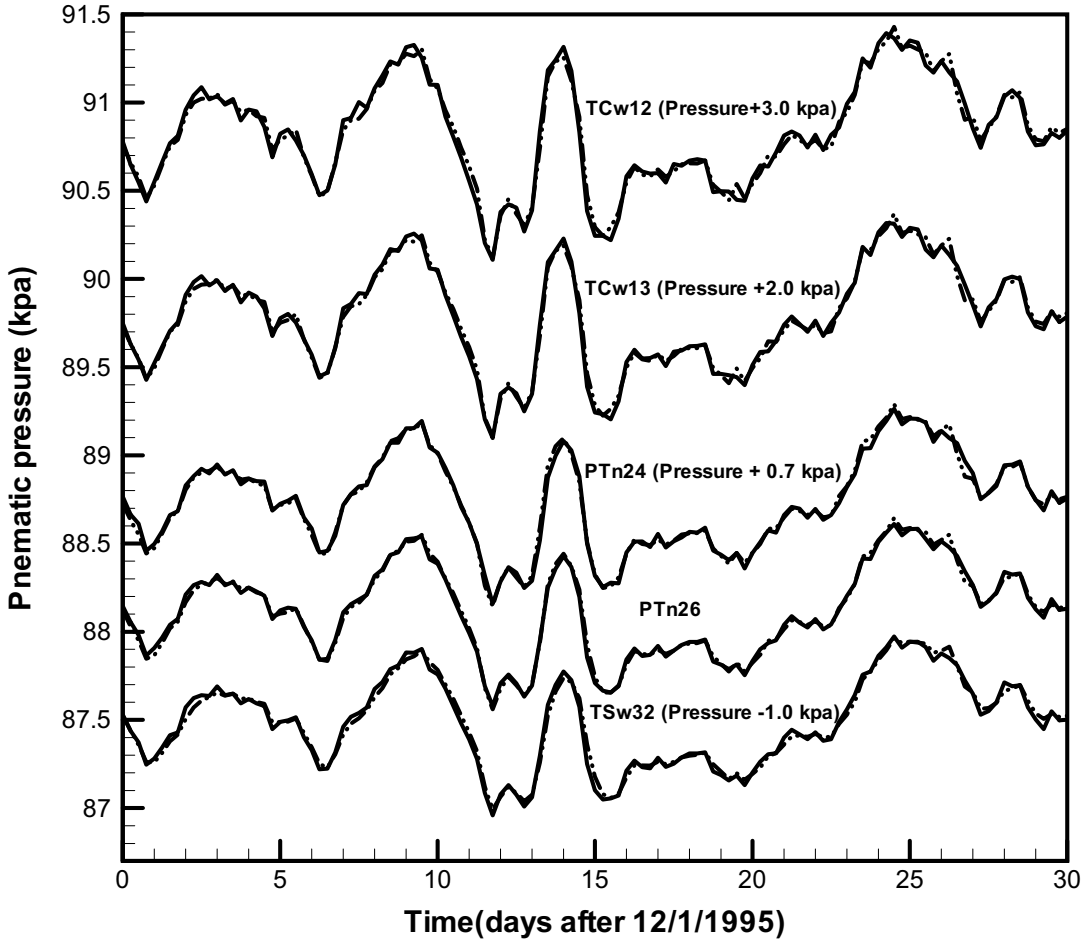

Output DTN: LB0612MTSCHPFT.001 (*testGAS10Ai.tec*).

NOTE: Solid lines correspond to the interpolated raw data and dashed lines to simulation results.

Figure 6-12. Pneumatic Pressure Matches at USW UZ-7a Used in the Two-Dimensional Calibrated Fault Parameter Set for the 10th Percentile Infiltration Scenario

6.4 DISCUSSION OF PARAMETER UNCERTAINTY

This section discusses sources and quantification of uncertainties for the calibrated parameters.

6.4.1 Sources of Parameter Uncertainty

A major source of parameter uncertainty is the conceptual model. As previously discussed, the parameter calibration is based on the conceptual model for UZ flow and transport documented in *Conceptual Model and Numerical Approaches for Unsaturated Zone Flow and Transport* (BSC 2004 [DIRS 170035]). Some aspects of the conceptual model that are important for parameter calibration are presented in Section 6.1. Conceptual simplifications used in this study will also contribute to parameter uncertainty. For example, one-dimensional simulations are used for calibrating drift-scale and mountain-scale property sets. As a result, lateral flow

behavior in the unsaturated zone may not be captured by property sets determined from one-dimensional simulations.

Infiltration-rate uncertainty also contributes to parameter uncertainty, because flow processes in the unsaturated zone are largely determined by top boundary conditions. Using the four infiltration scenarios for the parameter calibration documented in this study captures this uncertainty.

In addition, scale effects are a well-known source of parameter uncertainty. This is especially true for determination of UZ model parameters. For example, matrix parameters are measured in the unsaturated zone at core scale on the order of several centimeters, whereas in the UZ flow and transport model, numerical gridblocks are on the order of a few meters to hundreds of meters. Scale dependence of hydrologic parameters has been widely recognized in the scientific community (e.g., Neuman 1994 [DIRS 105731]). This is also clearly indicated by the differences between calibrated and uncalibrated matrix properties, as shown in Table 6-17. Although upscaling is partially considered in developing uncalibrated matrix properties (DTN: LB0207REVUZPRP.002 [DIRS 159672]), the calibrated matrix permeabilities are on average higher than uncalibrated permeabilities for all three infiltration scenarios (Table 6-17). The general increase in permeability with scale is consistent with findings reported in the literature (e.g., Neuman 1994 [DIRS 105731]). Consequently, the calibrated matrix α values are on average also larger than uncalibrated values. A larger permeability is generally expected to correspond to a larger van Genuchten α. For example, fracture α values are significantly larger than matrix values. Scale-dependent behavior for fracture permeability is considered in this study by developing parameter sets at two different scales (mountain scale and drift scale). The residuals for each layer (uncalibrated log x minus calibrated log x, where $x = k_M$ or $\alpha_{M)}$ from output DTNs: LB0610UZDSCP10.001 (*Sandia2R218Di.out*), LB0610UZDSCP30.001 (*Sandia2R113Ai.out*), LB0611UZDSCP50.001 (*Sandia2R118Bi.out*), and LB0612UZDSCP90.001 (*Sandia2R217Ci.out*) were averaged to calculate the values shown in Table 6-17. It should be emphasized that because of the difference between measurement scale and modeling scale, uncalibrated properties are not directly measured, but are in fact estimated values for the scales used in the UZ models. As a result, residuals cannot be used to evaluate the uncertainty as to the true parameter value, although they may be used to bound this uncertainty (as will be discussed later).

Table 6-17. Average Residual for Calibrated Matrix Properties for Three Infiltration Scenarios

Infiltration Scenario	Residual for log(k_M)	Residual for log(α_M)
10th Percentile	–0.43	–0.29
30th Percentile	–0.64	–0.27
50th Percentile	–0.70	–0.28
90th Percentile	–0.85	–0.33

Output DTNs: LB0610UZDSCP10.001, LB0610UZDSCP30.001, LB0611UZDSCP50.001, and LB0612UZDSCP90.001

NOTE: The residual refers to an uncalibrated matrix property minus the corresponding calibrated property.

Calibrated properties are nonunique because of data limitation. Further complicating the calibrating process, many of the parameters are cross-correlated; that is, variations in two or more parameters may have the same effect on predicted system response. Because the problem is poorly constrained, there is no well-defined global minimum in the objective function. Rather, there are likely to be many equivalent local minima. With respect to moisture and water-potential data, any of these minima provide an equally good parameter set. To address this issue, this study uses uncalibrated parameters as prior information in most inversions.

Table 6-18 shows the average absolute residual for calibrated matrix properties for four infiltration scenarios.

Table 6-18. Average Absolute Residual for Calibrated Matrix Properties for Three Infiltration Scenarios

Infiltration Scenario	Absolute Residual for $\log(k_M)$	Absolute Residual for $\log(\alpha_M)$
10th Percentile	0.72	0.39
30th Percentile	0.85	0.37
50th Percentile	0.91	0.38
90th Percentile	1.02	0.38

Output DTNs: LB0610UZDSCP10.001, LB0610UZDSCP30.001, LB0611UZDSCP50.001, and LB0612UZDSCP90.001.

NOTE: The residual refers to an uncalibrated matrix property minus the corresponding calibrated property.

The absolute value of the residual is always positive, and therefore the average absolute residual is greater than the average residual, as shown in Table 6-18. The average standard deviation of $\log(k_M)$ for uncalibrated matrix property sets (prior information) (Table 4-2) is 1.61. The standard deviation for $\log(\alpha_M)$ is not available from Table 4-3. The standard errors for $\log(\alpha_M)$ in Table 4-3 are determined from curve fitting (DTN: LB0207REVUZPRP.002 [DIRS 159672]) and cannot be directly related to the corresponding standard deviations. Wang and Narasimhan (1993 [DIRS 106793], pp. 374 to 376) reported that permeability could be approximately related to α by:

$$k \propto \alpha^2 \qquad \text{(Eq. 6-13)}$$

This yields:

$$\sigma_{\log(\alpha)} = \frac{1}{2}\sigma_{\log(k)} \qquad \text{(Eq. 6-14)}$$

where σ refers to standard deviation. Based on Equation 6-13, $\log(\alpha)$ can be expressed as $\log(k)/2$ plus a constant (for a given model layer), resulting in Equation 6-14. For each model layer, a standard deviation for $\log(\alpha_M)$ can be estimated from the corresponding standard deviation of $\log(k_M)$ based on Equations 6-13 and 6-14. The average standard deviation (calculated by hand) for $\log(\alpha_M)$ for the uncalibrated matrix property set (Table 4-3) is 0.81. The absolute residual values (Table 6-18) for the matrix properties are smaller than the corresponding average standard deviations. All these support the appropriateness of the calibrated property sets

documented in this report, which results from the use of uncalibrated rock properties as prior information in most inversions.

6.4.2 Quantification of Parameter Uncertainty

Quantifiable uncertainties are difficult to establish for the estimated parameter sets. In principle, these uncertainties could be evaluated either by Monte Carlo simulation or by linear error analysis, both of which are capabilities of iTOUGH2 V5.0 [DIRS 160106].

Because of the large numbers of parameters and the high nonlinearity of the unsaturated flow process, the linear error analysis is not reliable (Finsterle 1999 [DIRS 104367]). The linear uncertainty analysis quantifies the parameter uncertainty by linearization (based on its first-order Taylor series expansion). This method is a powerful tool only for problems that have sufficiently small parameter uncertainties (e.g., a small number of parameters and a large number of data points for calibration) or are linear (Finsterle 1999 [DIRS 104367], Section 2.8.7). However, the problem under consideration is characterized by a large number of parameters (on the same order of data point numbers for drift-scale parameter calibrations) and high nonlinearity. Criteria for the linear uncertainty analysis to apply are not met for the problem under consideration. The sensitivity matrix evaluated at the solution and the resulting covariance matrix provides insight into the correlation structure of the estimated parameters, revealing strong interdependencies. This information is used to support the qualitative statements regarding estimation uncertainty. It also indicates that probabilistic statements about the confidence region around the best-estimate parameter set cannot be based on a linear uncertainty analysis, which assumes linearity and normality within that region (as previously discussed). Such statements would have no defensible basis. Evaluating the correct shape and extent of the confidence region would require mapping the objective function in the n-dimensional parameter space and determining the hypersurface corresponding to the appropriate confidence level. Such an approach is outlined (for two parameters only) in the report by Finsterle and Pruess (1995 [DIRS 161750]). Alternatively, Monte Carlo type methods (such as the bootstrap method) would be required. (The large number of parameters make uncertainty analysis by Monte Carlo simulation prohibitively time consuming.) Based on these considerations, the uncertainty information from prior information is believed to be more reliable (and practical) for determining uncertainties for the calibrated property sets.

In this study, parameter uncertainties (standard deviations) for the uncalibrated parameter sets (Tables 4-2 and 4-3) are directly used for the calibrated parameter sets, because these uncertainties are determined from measurements. The parameter uncertainty of the uncalibrated property sets are largely a result of small-scale spatial variability. Because the degree of spatial variability decreases with scale (subgrid scale [or high frequency] spatial variability is removed at a large scale), this is likely to provide the upper limits of uncertainty on calibrated parameters for the given conceptual model and infiltration rates.

Table 6-19 gives the parameter uncertainties for the calibrated parameters. They are applied to both drift-scale and mountain-scale property sets, because both scales are larger than those on which uncalibrated parameters were measured. Uncertainties for $\log(k_M)$, and $\log(k_F)$ are taken directly from Tables 4-2 and 4-3. When a $\log(k_F)$ uncertainty is not available in Table 4-3 for a model layer, the largest value among the uncertainties (standard deviations) in all the layers for

which uncertainty values are available is used. Uncertainties for log(α_M) and log(α_F) are approximated from uncertainty values of the corresponding permeability, based on Equation 6-14. Uncertainties of the active-fracture-model parameter γ are difficult to obtain here and have not been calculated, because prior information for γ is not available. No information is available for quantifying uncertainties for m_F that is not a calibrated parameter (Section 6.3.2).

Table 6-19 also shows estimated uncertainties for calibrated fault properties taken from Table 4-3. Because fault properties are calibrated with limited data points (Section 6.3.4), the parameter uncertainties are expected to be relatively large. For each parameter type, the largest parameter uncertainty within the corresponding hydrogeologic unit for the nonfault property set is used as the corresponding fault parameter uncertainty. The fault property set does not include matrix parameters. Because complete measured data were available only for borehole UZ-7a, which crosses the Ghost Dance fault, the calibrated fault properties of the Ghost Dance fault are considered as representative of all other faults in the UZ flow model. These considerations are expected to be supported by the large uncertainties of the fault parameters.

Finally, it should be indicated that the propagation of uncertainty in the calibration is addressed in this study. The uncertainty data for measurements are used as inputs into inversions (Equation 6-2). The uncertainty in boundary conditions is reflected by developing property sets for different infiltration scenarios. The uncertainty in prior information has been used for characterizing uncertainties for calibrated properties.

Table 6-19. Uncertainties of Calibrated Parameters

Model layer	Matrix Property		Fracture Property	
	Log(k_M)	Log(α_M)	Log(k_F)	Log(α_F)
tcw11	0.47	0.24	1.15	0.58
tcw12	2.74	1.37	0.78	0.39
tcw13	2.38	1.19	1.15	0.58
ptn21	2.05	1.03	0.88	0.44
ptn22	1.41	0.71	0.20	0.10
ptn23	0.64	0.32	0.20	0.10
ptn24	1.09	0.55	1.15	0.58
ptn25	0.39	0.20	0.10	0.05
ptn26	1.12	0.56	1.15	0.58
tsw31	3.02	1.51	1.15	0.58
tsw32	0.94	0.47	0.66	0.33
tsw33	1.61	0.81	0.61	0.31
tsw34	0.97	0.49	0.47	0.24
tsw35	1.65	0.83	0.75	0.38
tsw36	3.67	1.84	0.54	0.27
tsw37	3.67	1.84	0.28	0.14
tsw38	1.57	0.79	1.15	0.58
tswz (zeolitic portion of tsw39)	2.74	1.37	1.15	0.58
tswv (vitric portion of tsw39)	1.38	0.69	1.15	0.58
ch1z	2.74	1.37	1.15	0.58
ch1v	1.11	0.56	1.15	0.58
ch2v	1.62	0.81	1.15	0.58

Table 6-19. Uncertainties of Calibrated Parameters (Continued)

Model layer	Matrix Property		Fracture Property	
	Log(k_M)	Log(α_M)	Log(k_F)	Log(α_F)
ch3v	1.62	0.81	1.15	0.58
ch4v	1.62	0.81	1.15	0.58
ch5v	1.62	0.81	1.15	0.58
ch6v	1.11	0.56	1.15	0.58
ch2z	0.91	0.46	1.15	0.58
ch3z	0.91	0.46	1.15	0.58
ch4z	0.91	0.46	1.15	0.58
ch5z	0.91	0.46	1.15	0.58
ch6z	2.05	1.03	1.15	0.58
pp4	2.74	1.37	1.15	0.58
pp3	0.75	0.38	1.15	0.58
pp2	1.18	0.59	1.15	0.58
pp1	1.52	0.76	1.15	0.58
bf3	1.64	0.82	1.15	0.58
bf2	1.52	0.76	1.15	0.58
Tcwf	[a]	[a]	1.15	0.58
Ptnf	[a]	[a]	1.15	0.58
Tswf	[a]	[a]	1.15	0.58
Chnf	[a]	[a]	1.15	0.58

Input DTNs: LB0210AMRU0035.002 [DIRS 166712]; LB0207REVUZPRP.002 [DIRS 159672]; LB0205REVUZPRP.001 [DIRS 159525].

NOTE: These uncertainty values are taken or developed from Tables 4-2 and 4-4.

[a]Fault property set does not include matrix properties.

7. CONCLUSION

7.1 PARAMETER CALIBRATIONS AND UNCERTAINTIES

This report has documented the methodologies and the data used for developing rock property sets for the unsaturated zone flow and transport models. The calibration is necessary to obtain parameter values appropriate for the scale of the process being analyzed. Although some hydrogeologic property data (prior information) are available, they cannot be directly used to predict flow and transport processes because they were measured on scales smaller than those characterizing property distributions in models used for the prediction. Since calibrations were done directly on the scales of interest, the upscaling issue was automatically considered. On the other hand, joint use of data and the prior information in inversions can further increase the reliability of the developed parameters compared with those for prior information.

Rock parameter sets were developed for both the mountain and drift scales because of the scale-dependent behavior of fracture permeability. These parameter sets, except those for faults (which were determined using two-dimensional simulation), were determined using one-dimensional simulations. If the parameters are directly used in three-dimensional simulations, they may not predict lateral flow or water perching in the unsaturated zone of Yucca Mountain. Therefore, the calibrated parameters developed in this report were further adjusted in the downstream report using the mountain-scale *UZ Flow Models and Submodels* (SNL 2007 [DIRS 175177]).

As discussed in Section 6.4, uncertainties for these calibrated properties are difficult to accurately determine, because of the inaccuracy of simplified methods for this complex problem or the extremely large computational expense of more rigorous methods. One estimate of uncertainty that may be useful to investigators using these properties is the uncertainty used for the prior information. The validity of the developed parameter sets is partially supported by the reasonable comparisons between three-dimensional simulation results from the UZ flow model and field observations including matrix saturations, water potentials, and pneumatic pressures. These three-dimensional simulations are largely based on these property sets (with further adjustments) (SNL 2007 [DIRS 175177], Section 6).

The output DTNs (including the input and output files for all runs) from this study are given in Section 8.4.

7.2 HOW THE ACCEPTANCE CRITERIA ARE ADDRESSED

The following information describes how this analysis addresses the acceptance criteria in the Yucca Mountain Review Plan (NRC 2003 [DIRS 163274], Section 2.2.1.3.6.3). Only those acceptance criteria that are applicable to this report (see Section 4.2) are discussed. In most cases, the applicable acceptance criteria are not addressed solely by this report; rather, the acceptance criteria are fully addressed when this report is considered in conjunction with other analysis and model reports that describe flow and transport in the saturated zone.

Acceptance Criteria from Section 2.2.1.3.6, *Flow Paths in the Unsaturated Zone*

Acceptance Criterion 1, *System Description and Model Integration Are Adequate*

Subcriterion (1): Total system performance assessment adequately incorporates, or bounds, important design features, physical phenomena, and couplings, and uses consistent and appropriate assumptions throughout the flow paths in the unsaturated zone abstraction process. Couplings include thermal-hydrologic-mechanical-chemical effects as appropriate.

> The analysis described in this report adequately incorporates physical phenomena related to unsaturated zone flow including the various mechanisms involved in fracture-matrix interaction, major faults, transient flow, and focused flow (discussed in Section 6.1.2). The analysis described in this report is used by UZ flow and transport models that support TSPA.

Subcriterion (2): The aspects of geology, hydrology, geochemistry, physical phenomena, and couplings that may affect flow paths in the unsaturated zone are adequately considered. Conditions and assumptions in the abstraction of flow paths in the unsaturated zone are readily identified and consistent with the body of data presented in the description.

> An adequate and detailed discussion of water flow paths and the associated processes is presented in Section 6.1.2. This discussion includes consideration of effects of rock properties, infiltration, major faults, flow focusing, and fracture-matrix interaction on the UZ flow paths.

Subcriterion (9): Guidance in NUREG–1297 (Altman et al. 1988 [DIRS 103597]) and NUREG-1298 (Altman et al. 1988 [DIRS 103750]), or other acceptable approaches for peer review and data qualification is followed.

> This report was developed in accordance with the QARD, which commits to NUREGs 1297 and 1298. Moreover, compliance with the DOE procedures, which are designed to ensure compliance with the QARD, is verified by audits by QA and other oversight activities. Accordingly, the guidance in NUREGs 1297 and 1298 has been followed as appropriate.

Acceptance Criterion 2, *Data are Sufficient for Model Justification*

Subcriterion (1): Hydrological and thermal-hydrological-mechanical-chemical values used in the license application are adequately justified. Adequate descriptions of how the data were used, interpreted, and appropriately synthesized into the parameters are provided.

> Sufficiency and applicability of input data used in this report for parameter calibration are discussed in Section 6.2 (numerical grids, infiltration rates, matrix-saturation and water-potential data, pneumatic pressure data and rock-hydraulic-property data) and Section 6.3.4 (data of the fault zone). Adequate descriptions of data use and interpretation are provided throughout Section 6.

Subcriterion (2): The data on the geology, hydrology, and geochemistry of the unsaturated zone, are collected using acceptable techniques.

Collection of input data used in this report was accomplished via acceptable techniques under the QARD. Table 4-1 in Section 4.1 provides a listing of sources of input data. Each of these source documents describe the techniques employed in collection of the data covered by the document.

Subcriterion (3): Estimates of deep-percolation flux rates constitute an upper bound, or are based on a technically defensible unsaturated zone flow model that reasonably represents the physical system. The flow model is calibrated, using site-specific hydrologic, geologic, and geochemical data. Deep-percolation flux is estimated, using the appropriate spatial and temporal variability of model parameters, and boundary conditions that consider climate-induced change in soil depths and vegetation.

The inputs from this report into the unsaturated zone flow model are calibrated from site-specific data as noted in Sections 4.1 (Data and Parameters), 6.2 (Inputs), and 6.3 (UZ Flow Model Parameter Calibration). The resulting output of this calibration activity document rock property sets for several infiltration maps that represent a good match with observed data.

Subcriterion (4): Appropriate thermal-hydrologic tests are designed and conducted, so that critical thermal-hydrologic processes can be observed, and values for relevant parameters estimated.

Hydrologic-property estimates from laboratory and field measurements provide prior information for rock parameters (Section 6.3.1), from which more accurate estimates are derived through the data inversion process.

Subcriterion (5): Sensitivity or uncertainty analyses are performed to assess data sufficiency, and verify the possible need for additional data.

The laboratory and field data and prior information (rock matrix data, water potential in the rock matrix, and pneumatic pressure) are weighted according to the uncertainty of their estimated value in the inversion process (Section 6.3.1).

Subcriterion (6): Accepted and well-documented procedures are used to construct and calibrate numerical models.

Approved QA procedures have been used to conduct and document the activities described in this report. The calibration was accomplished by the data inversion technique. Inverted data include saturation in the rock matrix, water potential in the rock matrix, and pneumatic pressure in the fractures. Hydrologic-property estimates from laboratory and field measurements, which provide initial estimates for rock parameters, also are included as data in the inversion. The combination of the two types of information allows the simulations to reproduce the data as well as possible, while simultaneously estimating reasonable rock parameters as discussed in Section 6.3.1.

Acceptance Criterion 3, *Data Uncertainty is Characterized and Propagated Through the Model Abstraction*

Subcriterion (1): Models use parameter values, assumed ranges, probability distributions, and bounding assumptions that are technically defensible, reasonably account for uncertainties and variabilities, and do not result in an under-representation of the risk estimate.

> The calibrations described in this report employs applicable Yucca Mountain borehole information and parameters (Section 4.1), bounding assumptions (Section 6.2.5), ranges and distributions (Sections 6.1 to 6.4) that are technically defensible. Parametric uncertainties are expected to be in line with the uncertainties in the prior information because, in most cases, the inversions did not change the properties very much with respect to the prior information (Section 7.1). Therefore, the output of this study is not expected to contribute to an under-representation of the risk estimate.

Subcriterion (4): The initial conditions, boundary conditions, and computational domain used in sensitivity analyses and/or similar analyses are consistent with available data. Parameter values are consistent with the initial and boundary conditions and the assumptions of the conceptual models for the Yucca Mountain site.

> Infiltration rates are used as the top boundary conditions for calibration. Four different infiltration boundary conditions were used for inversions to examine alternative models and the corresponding parameter sets (Section 6.2.5). A time-varying pneumatic pressure boundary condition, based on a combination of records from the surface at boreholes, was used to simulate barometric pumping (Section 6.2.5).

Subcriterion (5): Coupled processes are adequately represented.

> The effects of coupled processes are adequately represented through the inversion and incorporation of different types of field and laboratory data, which, taken together, represent the combination of various processes that influence flow in the unsaturated zone (see Section 6.3.1).

Subcriterion (6): Uncertainties in the characteristics of the natural system and engineered materials are considered.

> The major sources of uncertainty (conceptual model, infiltration rate, and scale effects) and their propagation to the calibrated parameters are discussed in detail in Section 6.4. Uncertainties in measured data and uncertainty propagation through inversion were also addressed (Section 6.4).

8. INPUTS AND REFERENCES

The following is a list of the references cited in this document. Column 2 represents the unique six digit numerical identifier (the Document Input Reference System [DIRS] number), which is placed in the text following the reference callout (e.g., BSC 2004 [DIRS 167969]). The purpose of these numbers is to assist in locating a specific reference. Within the reference list, multiple sources by the same author (e.g., BSC 2004) are sorted alphabetically by title.

8.1 DOCUMENTS CITED

124842 Ahlers, C.F.; Finsterle, S.; and Bodvarsson, G.S. 1998. "Characterization and Prediction of Subsurface Pneumatic Pressure Variations at Yucca Mountain, Nevada." *Proceedings of the TOUGH Workshop '98, Berkeley, California, May 4-6, 1998.* Pruess, K., ed. LBNL-41995. Pages 222-227. Berkeley, California: Lawrence Berkeley National Laboratory. TIC: 247159.

103597 Altman, W.D.; Donnelly, J.P.; and Kennedy, J.E. 1988. *Peer Review for High-Level Nuclear Waste Repositories: Generic Technical Position.* NUREG-1297. Washington, D.C.: U.S. Nuclear Regulatory Commission. TIC: 200651.

103750 Altman, W.D.; Donnelly, J.P.; and Kennedy, J.E. 1988. *Qualification of Existing Data for High-Level Nuclear Waste Repositories: Generic Technical Position.* NUREG-1298. Washington, D.C.: U.S. Nuclear Regulatory Commission. TIC: 200652.

159569 ASTM C 127-01. 2001. *Standard Test Method for Density, Relative Density (Specific Gravity), and Absorption of Coarse Aggregate*. West Conshohocken, Pennsylvania: American Society for Testing and Materials. TIC: 253073.

103949 Bandurraga, T.M. and Bodvarsson, G.S. 1999. "Calibrating Hydrogeologic Parameters for the 3-D Site-Scale Unsaturated Zone Model of Yucca Mountain, Nevada." *Journal of Contaminant Hydrology, 38,* (1-3), 25-46. New York, New York: Elsevier. TIC: 244160.

103524 Bird, R.B.; Stewart, W.E.; and Lightfoot, E.N. 1960. *Transport Phenomena.* New York, New York: John Wiley & Sons. TIC: 208957.

169857 BSC 2004. *Calibrated Properties Model.* MDL-NBS-HS-000003 REV 02. Las Vegas, Nevada: Bechtel SAIC Company. ACC: DOC.20041006.0004.

174116 BSC 2005. *Parameter Sensitivity Analysis for Unsaturated Zone Flow.* ANL-NBS-HS-000049 REV 00. Las Vegas, Neveda: Bechtel SAIC Company. ACC: DOC.20050808.0005; DOC.20060329.0020.

175539 BSC 2005. *Q-List.* 000-30R-MGR0-00500-000-003. Las Vegas, Nevada: Bechtel SAIC Company. ACC: ENG.20050929.0008.

177465 BSC 2006. *Technical Work Plan for: Unsaturated Zone Flow, Drift Seepage and Unsaturated Zone Transport Modeling.* TWP-MGR-HS-000004 REV 04. Las Vegas, Nevada: Bechtel SAIC Company. ACC: DOC.20060824.0001.

179489 BSC 2006. *Chlorine-36 Validation Study at Yucca Mountain, Nevada.* TDR-NBS-HS-000017 REV 00. Las Vegas, Nevada: Bechtel SAIC Company. ACC: DOC.20060829.0002.

170038 BSC (Bechtel SAIC Company) 2004. *Analysis of Hydrologic Properties Data*. ANL-NBS-HS-000042 REV 00. Las Vegas, Nevada: Bechtel SAIC Company. ACC: DOC.20041005.0004; DOC.20050815.0003.

170035 BSC 2004. *Conceptual Model and Numerical Approaches for Unsaturated Zone Flow and Transport*. MDL-NBS-HS-000005 REV 01. Las Vegas, Nevada: Bechtel SAIC Company. ACC: DOC.20040922.0006; DOC.20050307.0009.

169855 BSC 2004. *Development of Numerical Grids for UZ Flow and Transport Modeling.* ANL-NBS-HS-000015 REV 02. Las Vegas, Nevada: Bechtel SAIC Company. ACC: DOC.20040901.0001.

170029 BSC 2004. *Geologic Framework Model (GFM2000).* MDL-NBS-GS-000002 REV 02. Las Vegas, Nevada: Bechtel SAIC Company. ACC: DOC.20040827.0008.

170004 BSC (Bechtel SAIC Company) 2004. *In Situ Field Testing of Processes.* ANL-NBS-HS-000005 REV 03. Las Vegas, Nevada: Bechtel SAIC Company. ACC: DOC.20041109.0001; DOC.20051010.0001.

169854 BSC (Bechtel SAIC Company) 2004. *Thermal Conductivity of the Potential Repository Horizon.* MDL-NBS-GS-000005 REV 01. Las Vegas, Nevada: Bechtel SAIC Company. ACC: DOC.20040928.0006.

178718 Edwards, D.L. 1992. " *Special Handling for Core Samples from Borehole USW NRG-6.*" Letter from D.L. Edwards (USGS) to J.H. Peck (SMF, YMP), December 15, 1992. ACC: DRC.19960509.0110.

103783 Finsterle, S. 1998. *ITOUGH2 V3.2 Verification and Validation Report.* LBNL-42002. Berkeley, California: Lawrence Berkeley National Laboratory. ACC: MOL.19981008.0014.

104367 Finsterle, S. 1999. *ITOUGH2 User's Guide.* LBNL-40040. Berkeley, California: Lawrence Berkeley National Laboratory. TIC: 243018.

161750 Finsterle, S. and Pruess, K. 1995. "Solving the Estimation-Identification Problem in Two-Phase Flow Modeling." *Water Resources Research, 31,* (4), 913-924. Washington, D.C.: American Geophysical Union. TIC: 252318.

100033 Flint, L.E. 1998. *Characterization of Hydrogeologic Units Using Matrix Properties, Yucca Mountain, Nevada.* Water-Resources Investigations Report 97-4243. Denver, Colorado: U.S. Geological Survey. ACC: MOL.19980429.0512.

161743 Forsyth, P.A.; Wu, Y-S.; and Pruess, K. 1995. "Robust Numerical Methods for Saturated-Unsaturated Flow with Dry Initial Conditions in Heterogeneous Media." *Advances in Water Resources, 18,* 25-38. Southhampton, England: Elsevier. TIC: 235658.

139237 Glass, R.J.; Nicholl, M.J.; and Tidwell, V.C. 1996. *Challenging and Improving Conceptual Models for Isothermal Flow in Unsaturated, Fractured Rock Through Exploration of Small-Scale Processes*. SAND95-1824. Albuquerque, New Mexico: Sandia National Laboratories. ACC: MOL.19970520.0082.

151762 IEEE/ASTM SI 10-1997. 1997. *Standard for Use of the International System of Units (SI): The Modern Metric System.* New York, New York: Institute of Electrical and Electronics Engineers. TIC: 240989.

144612 LeCain, G.D.; Anna, L.O.; and Fahy, M.F. 2000. *Results from Geothermal Logging, Air and Core-Water Chemistry Sampling, Air-Injection Testing, and Tracer Testing in the Northern Ghost Dance Fault, Yucca Mountain, Nevada, November 1996 to August 1998*. Water-Resources Investigations Report 99-4210. Denver, Colorado: U.S. Geological Survey. TIC: 247708.

160110 Liu, H.H. and Bodvarsson, G.S. 2001. "Constitutive Relations for Unsaturated Flow in a Fracture Network." *Journal of Hydrology, 252,* (1-4), 116-125. New York, New York: Elsevier. TIC: 253269.

105729 Liu, H.H.; Doughty, C.; and Bodvarsson, G.S. 1998. "An Active Fracture Model for Unsaturated Flow and Transport in Fractured Rocks." *Water Resources Research, 34,* (10), 2633-2646. Washington, D.C.: American Geophysical Union. TIC: 243012.

166106 Liu, H-H.; Zhang, G.; and Bodvarsson, G.S. 2003. "The Active Fracture Model: Its Relation to Fractal Flow Patterns and an Evaluation Using Field Observations." *Vadose Zone Journal, 2,* ([2]), 259-269. Madison, Wisconsin: Soil Science Society of America. TIC: 255196.

100161 Montazer, P. and Wilson, W.E. 1984. *Conceptual Hydrologic Model of Flow in the Unsaturated Zone, Yucca Mountain, Nevada.* Water-Resources Investigations Report 84-4345. Lakewood, Colorado: U.S. Geological Survey. ACC: NNA.19890327.0051.

105731 Neuman, S.P. 1994. "Generalized Scaling of Permeabilities: Validation and Effect of Support Scale." *Geophysical Research Letters, 21,* (5), 349-352. Washington, D.C.: American Geophysical Union. TIC: 240142.

163274 NRC (U.S. Nuclear Regulatory Commission) 2003. *Yucca Mountain Review Plan, Final Report.* NUREG-1804, Rev. 2. Washington, D.C.: U.S. Nuclear Regulatory Commission, Office of Nuclear Material Safety and Safeguards. TIC: 254568.

100684 Pruess, K. 1987. *TOUGH User's Guide.* NUREG/CR-4645. Washington, D.C.: U.S. Nuclear Regulatory Commission. TIC: 217275.

124773 Roberson, J.A. and Crowe, C.T. 1990. *Engineering Fluid Mechanics.* 4th Edition. Boston, Massachusetts: Houghton Mifflin. TIC: 247390.

102097 Rousseau, J.P.; Kwicklis, E.M.; and Gillies, D.C., eds. 1999. *Hydrogeology of the Unsaturated Zone, North Ramp Area of the Exploratory Studies Facility, Yucca Mountain, Nevada.* Water-Resources Investigations Report 98-4050. Denver, Colorado: U.S. Geological Survey. ACC: MOL.19990419.0335.

100178 Rousseau, J.P.; Loskot, C.L.; Thamir, F.; and Lu, N. 1997. *Results of Borehole Monitoring in the Unsaturated Zone Within the Main Drift Area of the Exploratory Studies Facility, Yucca Mountain, Nevada. Milestone SPH22M3*. Denver, Colorado: U.S. Geological Survey. ACC: MOL.19970626.0351.

178762 SNL (Sandia National Laboratories) 2006. Data Qualification Plan, Qualification of Parameter Values Used to Estimate Measurement Errors for Matrix Water Saturation and Water Potential. Las Vegas, Nevada: Sandia National Laboratories. ACC: MOL.20070212.0105.

174294 SNL 2007. *Simulation of Net Infiltration for Present-Day and Potential Future Climates.* MDL-NBS-HS-000023 REV 01. Las Vegas, Nevada: Sandia National Laboratories.

175177 SNL 2007. *UZ Flow Models and Submodels.* MDL-NBS-HS-000006 REV 03. Las Vegas, Nevada: Sandia National Laboratories.

100610 van Genuchten, M.T. 1980. "A Closed-Form Equation for Predicting the Hydraulic Conductivity of Unsaturated Soils." *Soil Science Society of America Journal, 44,* (5), 892-898. Madison, Wisconsin: Soil Science Society of America. TIC: 217327.

106793 Wang, J.S.Y. and Narasimhan, T.N. 1993. "Unsaturated Flow in Fractured Porous Media." Chapter 7 of *Flow and Contaminant Transport in Fractured Rock.* Bear, J.; Tsang, C-F.; and de Marsily, G., eds. San Diego, California: Academic Press. TIC: 235461.

114295 Weast, R.C., ed. 1987. *CRC Handbook of Chemistry and Physics: 1987-1988.* 68th Edition. Pages A-1, F-72, F-185 only. Boca Raton, Florida: CRC Press. TIC: 245444.

156399 Wu, Y.S.; Liu, H.H.; Bodvarsson, G.S.; and Zellmer, K.E. 2001. *A Triple-Continuum Approach for Modeling Flow and Transport Processes in Fractured Rock.* LBNL-48875. Berkeley, California: Lawrence Berkeley National Laboratory. TIC: 251297.

178715 YMP (Yucca Mountain Site Characterization Project) 1995. *Sample Management Facility Core Processing Checklist Borehole 249 USW UZ-14 Dated January 12, 1995.* Las Vegas, Nevada: Yucca Mountain Site Characterization Office. ACC: DRC.19960416.0009.

178714 YMP (Yucca Mountain Site Characterization Project) 1996. *Sample Management Facility, Core Processing Checklist Borehole 275 USW Sd-12, Dated February 28, 1994 through February 20, 1996.* Las Vegas, Nevada: Yucca Mountain Site Characterization Office. ACC: DRC.19960226.0005.

8.2 CODES, STANDARDS, REGULATIONS, AND PROCEDURES

173273 10 CFR 63. 2005. Energy: Disposal of High-Level Radioactive Wastes in a Geologic Repository at Yucca Mountain, Nevada. ACC: MOL.20050405.0118.

IM-PRO-002, REV.000, ICN 0. *Control of the Electronic Management of Information,* Washington, D.C.: U.S. Department of Energy, Office of Civilian Radioactive Waste Management. ACC: DOC.20060927.0023.

IM-PRO-003, Rev. 002, ICN 0. *Software Management.* Washington, D.C.: U.S. Department of Energy, Office of Civilian Radioactive Waste Management. ACC: DOC.20070228.0002..

LS-PRO-0203, Rev.002, ICN 0, *Q-List and Classification of Structures, Systems, and Components.* Washington, D.C.: U.S. Department of Energy, Office of Civilian Radioactive Waste Management. ACC: DOC.20060927.0016.

SCI-PRO-001, Rev 02. *Qualification of Unqualified Data.* Washington, D.C.: U.S. Department of Energy, Office of Civilian Radioactive Waste Management. ACC: DOC.20070522.0016.

SCI-PRO-005, Rev.002. *Scientific Analyses and Calculations.* Washington, D.C.: U.S. Department of Energy, Office of Civilian Radioactive Waste Management. ACC: DOC.200704190010.

8.3 SOURCE DATA, LISTED BY DATA TRACKING NUMBER

155891 GS000608312261.001. Shut-In Pressure Data from Boreholes UE-25 NRG#2B, UE-25 NRG#5, USW SD-9, and USW UZ-7A from 4/1/95 through 12/31/95. Submittal date: 07/05/2000.

162174 GS000708312232.004. Deep UZ Surface-Based Borehole Instrumentation Program-Interim Data Submittal for Boreholes USW NRG-7A, UE-25 UZ#4, and UE-25 UZ#5. Data Were Collected between 4/1/99 and 3/31/00. Submittal date: 09/13/2000.

162175 GS010908312232.001. Deep Unsaturated Zone Surface-Based Borehole Instrumentation Program-Interim Data Submittal for Boreholes USW NRG-7A, UE-25 UZ#4, and UE-25 UZ#5. Data Were Collected between April 1, 2000 and March 31, 2001. Submittal date: 09/26/2001.

162176 GS021008312232.001. Deep Unsaturated Zone Surface-Based Borehole Instrumentation Program - Final Data Submittal for Boreholes USW NRG-7A, UE-25 UZ#4, and UE-25 UZ#5. Data Were Collected between April 1, 2001 and December 17, 2001. Submittal date: 12/12/2002.

178752 GS031208312232.001. Deep Unsaturated Zone Instrumentation Data from Boreholes USW NRG-7A, UE-25 UZ#4, UE-25 UZ#5, USW UZ-7A and USW SD-12 for 10/01/98 through 03/31/99. Submittal date: 07/15/2004.

171748 GS031208312232.002. Deep UZ Surface-Based Borehole Instrumentation Program Data from Boreholes USW NRG-7A, UE-25 UZ#4, USW NRG-6, UE-25 UZ#5, USW UZ-7A and USW SD-12 for the Time Period 4/1/98 through 9/30/98. Submittal date: 07/15/2004.

178751 GS031208312232.007. Shut-in Pressure Test Data from UE-25 NRG#5 and USW SD-7 from November, 1995 to July, 1996. Submittal date: 05/24/2004.

178750 GS031208312232.008. Deep Unsaturated Zone Surface-Based Borehole Instrumentation Program Data from Boreholes USW NRG-7A, USW NRG-6, UE-25 UZ#4, UE-25 UZ#5, USW UZ-7A, and USW SD-12 for the Time Period 10/01/95 through 3/31/96. Submittal date: 05/24/2004.

105572 GS950208312232.003. Data, Including Water Potential, Pressure and Temperature, Collected from Boreholes USW NRG-6 and USW NRG-7A from Instrumentation through March 31, 1995. Submittal date: 02/13/1995.

106756 GS951108312232.008. Data, Including Water Potential, Pressure and Temperature, Collected from Boreholes UE-25 UZ#4 & UZ#5 from Instrumentation through September 30, 1995, and from USW NRG-6 & NRG-7A from April 1 through September 30, 1995. Submittal date: 11/21/1995.

106784 GS960908312261.004. Shut-in Pressure Test Data from UE-25 NRG#5 and USW SD-7 from November, 1995 to July, 1996. Submittal date: 09/24/1996.

159525 LB0205REVUZPRP.001. Fracture Properties for UZ Model Layers Developed from Field Data. Submittal date: 05/14/2002.

159526 LB0207REVUZPRP.001. Revised UZ Fault Zone Fracture Properties. Submittal date: 07/03/2002.

159672 LB0207REVUZPRP.002. Matrix Properties for UZ Model Layers Developed from Field and Laboratory Data. Submittal date: 07/15/2002.

174491 LB0208HYDSTRAT.001. 2002 UZ Model Grid Components. Submittal date: 08/26/2002.

160108 LB02081DKMGRID.001. 2002 UZ 1-D and 2-D Calibration Grids. Submittal date: 08/26/2002.

178764 LB0208UZDSCPLI.001. Drift-Scale Calibrated Property Sets: Lower Infiltration Supporting Files. Submittal date: 08/27/2002.

161285 LB0208UZDSCPMI.001. Drift-Scale Calibrated Property Sets: Mean Infiltration Supporting Files. Submittal date: 08/27/2002.

166711 LB0208UZDSCPUI.001. Drift-Scale Calibrated Property Sets: Upper Infiltration Supporting Files. Submittal date: 08/27/2002.

161292 LB02091DSSCP3I.001. 1-D Site Scale Calibrated Properties: Supporting Files. Submittal date: 09/18/2002.

162422 LB02092DSSCFPR.001. 2-D Site Scale Calibrated Fault Properties: Supporting Files. Submittal date: 09/18/2002.

166712 LB0210AMRU0035.002. Model Validation and Parameter Uncertainty: Data Summary. Submittal date: 10/10/2002.

162378 LB0302AMRU0035.001. Model Validation and Parameter Uncertainty: Supporting Files. Submittal date: 02/07/2003.

170678 LB0401H2OPOTEN.001. Statistically Consolidated Water Potential Data. Submittal date: 01/29/2004.

153777 MO0012MWDGFM02.002. Geologic Framework Model (GFM2000). Submittal date: 12/18/2000.

177912 SN0608WEATHER1.005. Temperature, Precipitation, Wind Speed, Relative Humidity, Dew Point Temperatures, and Barometric Pressure Data Collected from 1993-2004 Measured at Yucca Mountain Weather Stations 1,2,3,6, and 9. Submittal date: 08/23/2006.

178753 SN0609T0502206.028. Present-Day Net Infiltration Results. Submittal date: 09/22/2006.

168542 TM0000SD9SUPER.002. USW SD-9 Structure Logs (53.6' to 2223.1'). Submittal date: 12/14/1995.

178755 TMUSWSD1200095.001. Logs for USW SD-12. Submittal data: 10/27/1995.

8.4 OUTPUT DATA, LISTED BY DATA TRACKING NUMBER

LB0610UZDSCP10.001. Drift-Scale Calibrated Property Set for the 10th Percentile Infiltration Map. Submittal Date: 11/02/2006.

LB0610UZDSCP30.001. Drift-Scale Calibrated Property Set for the 30th Percentile Infiltration Map. Submittal Date: 11/02/2006.

LB0611MTSCHP10.001. Mountain-Scale Calibrated Property Set for the 10th Percentile Infiltration Map. Submittal Date: 11/28/2006.

LB0611MTSCHP30.001. Mountain-Scale Calibrated Property Set for the 30th Percentile Infiltration Map. Submittal Date: 11/28/2006.

LB0611UZDSCP50.001. Drift-Scale Calibrated Property Set for the 50th Percentile Infiltration Map. Submittal Date: 11/28/2006.

LB0612MTSCHP50.001. Mountain-Scale Calibrated Property Set for the 50th Percentile Infiltration Map. Submittal Date: 12/19/2006.

LB0612MTSCHP90.001. Mountain-Scale Calibrated Property Set for the 50th Percentile Infiltration Map. Submittal Date: 12/20/2006.

LB0612MTSCHPFT.001. Calibrated Fault Property Set. Submittal Date: 12/07/2006.

LB0612UZDSCP90.001. Drift-Scale Calibrated Property Set for the 90th Percentile Infiltration Map. Submittal Date: 12/20/2006.

LB0608COORCONV.001. Coordinate Conversion for the Infiltration Model Grid. Submittal Date: 11/02/2006.

8.5 SOFTWARE CODES

155082 CORPSCON V. 5.11.08. 2001. WINDOWS NT 4.0. STN: 10547-5.11.08-00.

154787 Software Routine: 2kgrid8.for VV1.0. 2002. DEC-Alpha, PC. 10503-1.0-00.

154793 Software Code: infil2grid. V1.7. DEC-Alpha, PC. 10077-1.7-00.

160106 Software Code: iTOUGH2. V5.0. SUN UltraSparc., DEC ALPHA, LINUX. 10003-5.0-00.

160107 Software Code: TBgas3D. V2.0. SUN UltraSparc. 10882-2.0-00.

146536 Software Routine: e9-3in V1.0. 1.0. Sun workstation. 10126-1.0-00.

INTENTIONALLY LEFT BLANK

APPENDIX A
RECENT WATER-POTENTIAL DATA

This appendix describes comparisons between water potential data used in inversions (Section 6) and more recent data.

Water potential data from Boreholes USW NRG-6 and USW NRG-7a (November 1994 to March 1998), Borehole UE-25 UZ#4 (June 1995 to March 1998), and Borehole UE-25 SD-12 (November 1995 to March 1998) were used to determine the equilibrium (steady-state) water potential value, which are used as direct inputs in this report (Sections 6.2.2 and 6.3) for calibration (inverse modeling).

More-recent water potential data are available from USW NRG-7a (April 1998 to March 2001), UE-25 UZ#4 (April 1998 to December 2001), and UE-25 SD-12 (April 1998 to December 1998) (DTNs: GS031208312232.002 [DIRS 171748]; GS031208312232.001 [DIRS 178752]; GS000708312232.004 [DIRS 162174]; GS010908312232.001 [DIRS 162175]; and GS021008312232.001 [DIRS 162176]). Monthly averages of all available water potential data are plotted in Figures A-1 to A-4b, starting from October 1994 (when the boreholes were instrumented) as Month 1 until December 2001. Each plot corresponds to a given measurement station that is instrumented with two sensors. Differences between the data from the two sensors at the same position (for example, TCP 1693 and TCP 1694 in Borehole UE-25 SD-12, see Figure A-4a and A-4b) indicate the measurement error. The measured water potential reached a quasi-steady-state within the first 20 months after the instrumentations (Figures A-1 to A-4b), and the more recently measured water potentials are stable.

Newer data from two sensors in UE-25 SD-12 (TCP 1675 and TCP 1676 at 76.8 m deep and TCP 1682 at 65.2 m deep) show a slightly wetter condition than the adopted equilibrium (steady-state) value as shown in Figure A-4a and A-4b, but the difference between the adopted equilibrium water potential value and the more recent data is within the measurement error.

In general, the difference between the adopted equilibrium (steady-state) value and the more-recent data is within the range of the 95% confidence interval (plus or minus 0.2 Mpa, (Rousseau et al. 1999 [DIRS 102097], p. 144)) except for data from sensor TCP 1688 and TCP 1694 in Borehole UE-25 SD-12, which are possibly caused by measurement errors. The drastic increase in the latest water potential data from TCP 1688 is possibly caused by a sensor failure. The difference between data from TCP 1693 and TCP 1694 (Figure A-4a and A-4b) indicates a large uncertainty in the measured water potential at this particular location.

The comparisons given in Figures A-1 to A-4b indicate that the equilibrium (steady-state) water potential values used for calibration in this report (based on data collected prior to March 1998) are consistent with the more recent data.

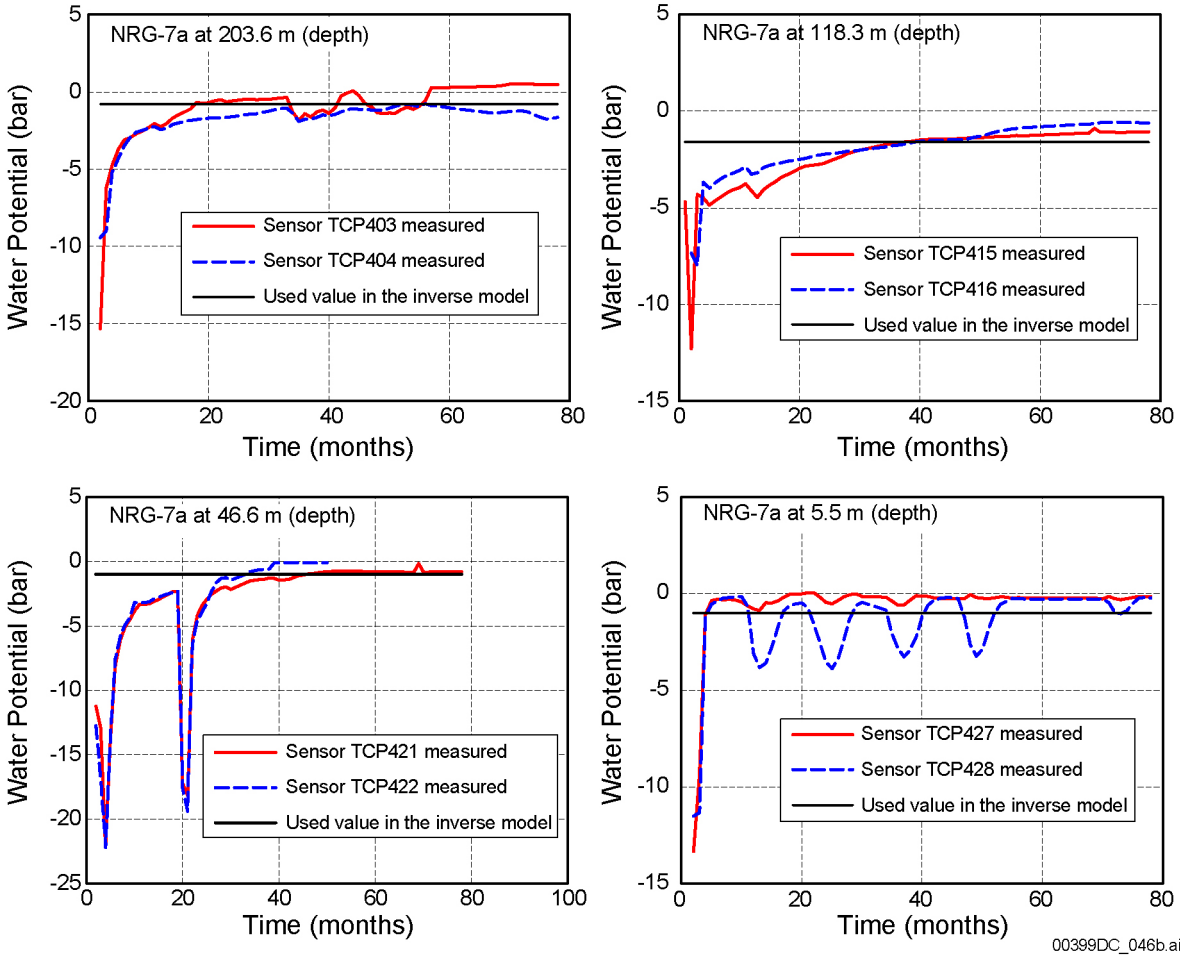

Source: DTN: LB0401H2OPOTEN.001 [DIRS 170678].

NOTE: The equilibrium water potential values used for calibration (inverse modeling) are determined using the data collected before the end of March 1998 (month 42).

Figure A-1. Measured Water Potential (from Available Instrument Stations of Borehole USW NRG-7a) Breakthrough (Starting from October 1994, as Month 1) and the Determined Steady-State Value Used for Hydraulic Property Calibration

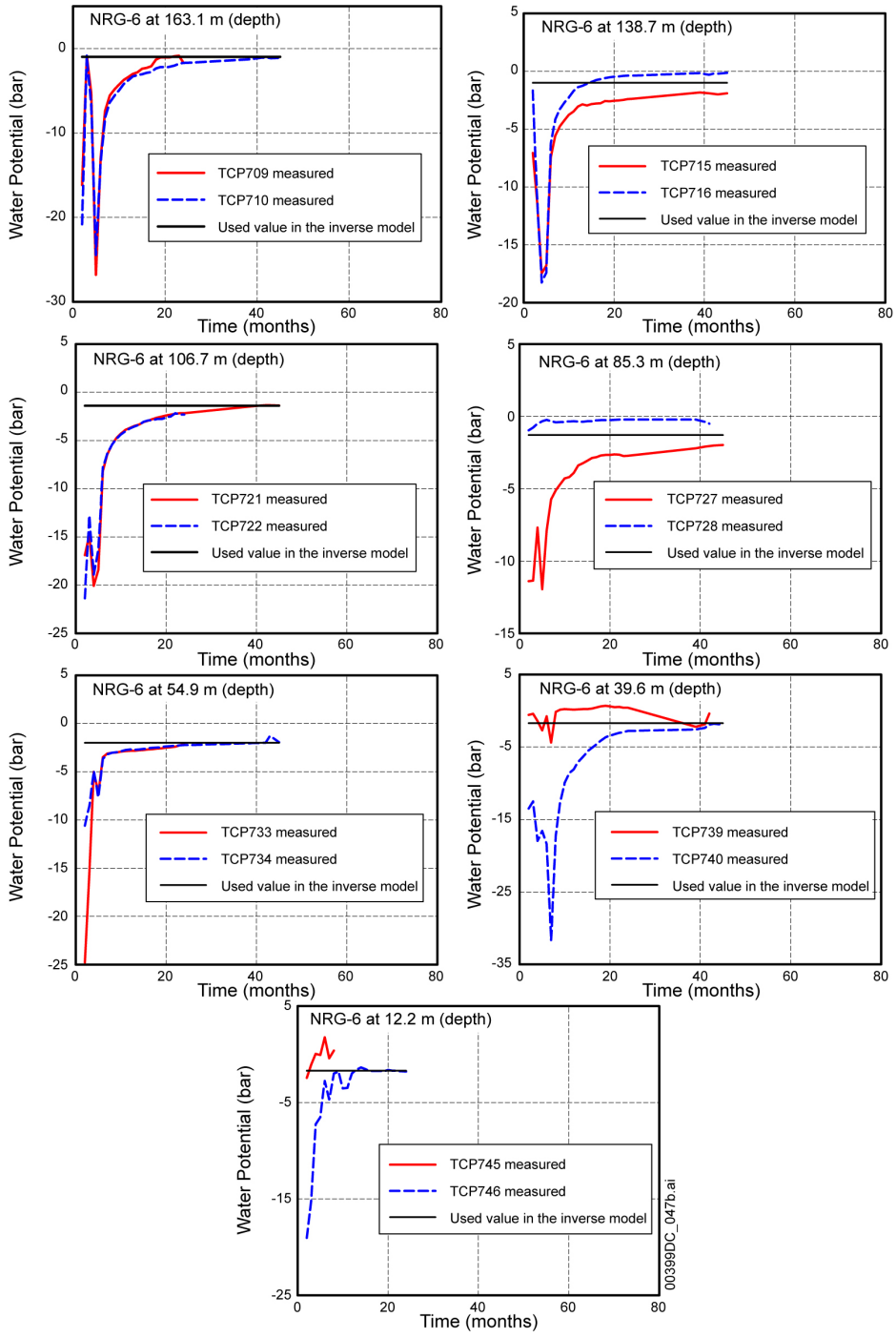

Source: DTN: LB0401H2OPOTEN.001 [DIRS 170678].

NOTE: The equilibrium water potential values used for calibration (inverse modeling) are determined using the data collected before the end of March 1998 (month 42).

Figure A-2. Measured Water Potential (from Available Instrument Stations of Borehole USW NRG-6) Breakthrough (Starting from October 1994, as Month 1) and the Determined Steady-State Value Used for Hydraulic Property Calibration

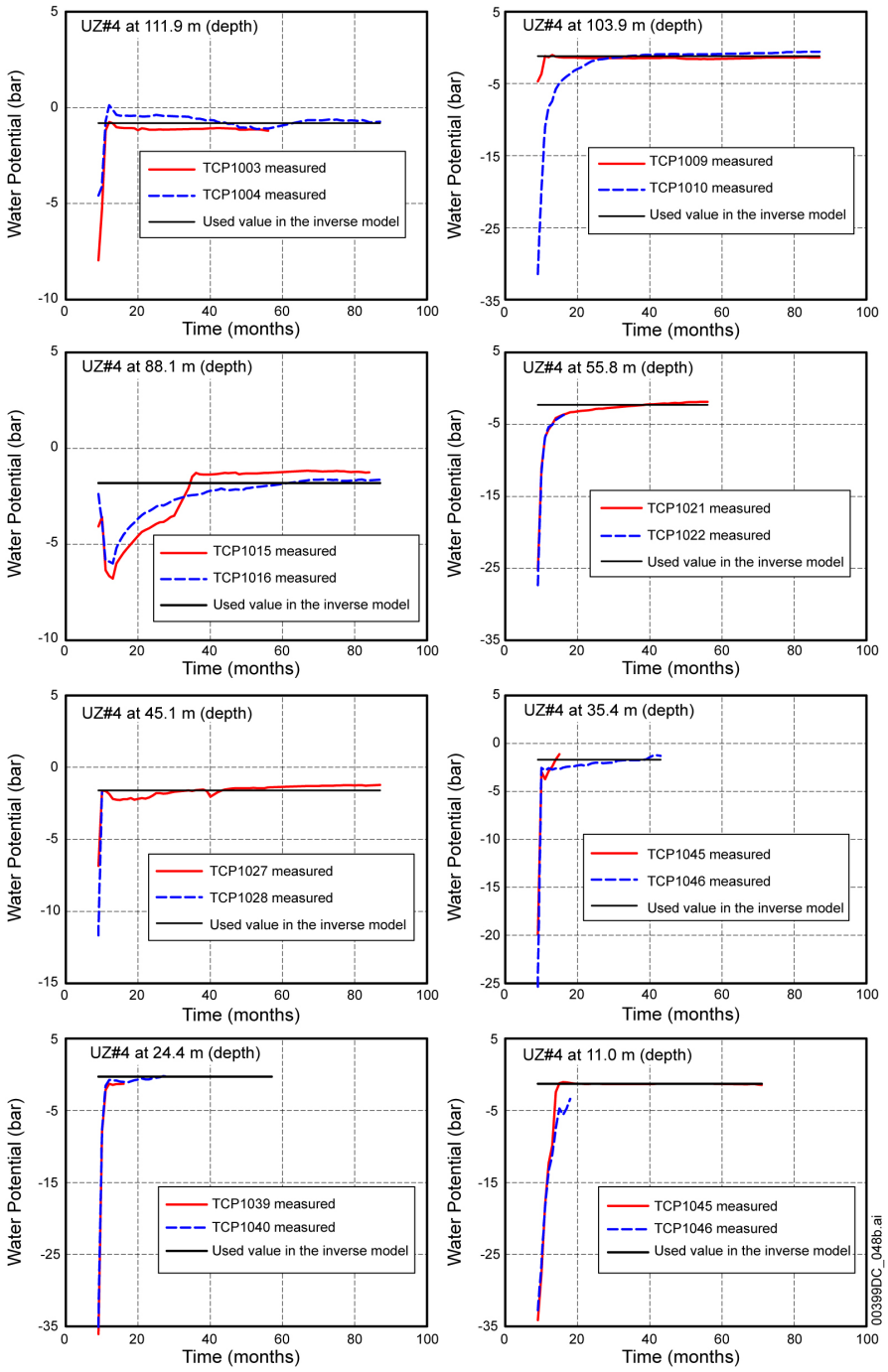

Source: DTN: LB0401H2OPOTEN.001 [DIRS 170678].

NOTE: The equilibrium water potential values used for calibration (inverse modeling) are determined using the data collected before the end of March 1998 (month 42).

Figure A-3. Measured Water Potential (from Available Instrument Stations of Borehole UE-25 UZ#4) Breakthrough (Starting from October 1994, as Month 1) and the Determined Steady-State Value Used for Hydraulic Property Calibration

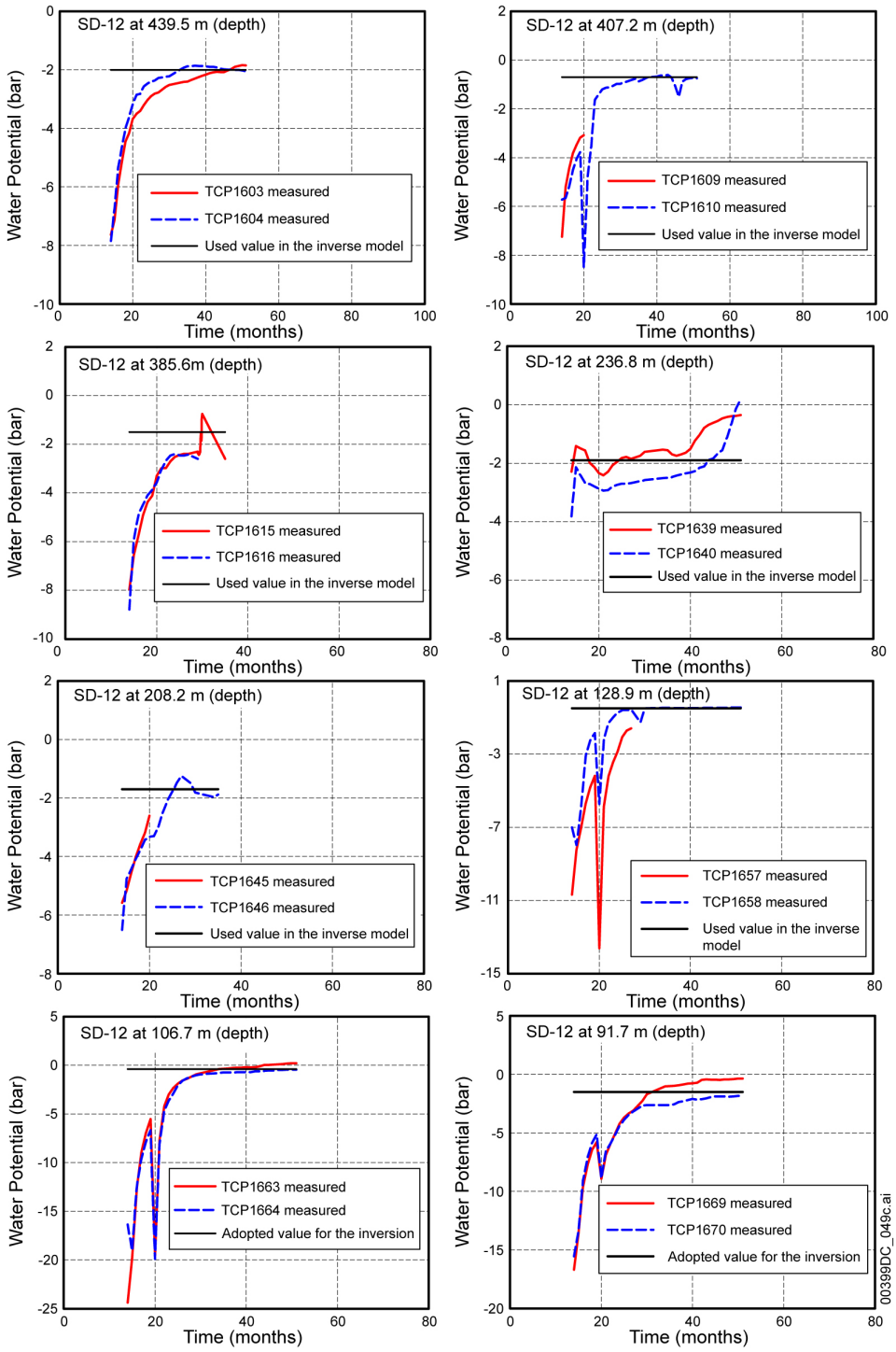

Source: DTN: LB0401H2OPOTEN.001 [DIRS 170678].

NOTE: The equilibrium water potential values used for calibration (inverse modeling) are determined using the data collected before the end of March 1998 (month 42).

Figure A-4a. Measured Water Potential (from Available Instrument Stations of Borehole UE-25 SD-12) Breakthrough (Starting from October 1994, as Month 1) and the Determined Steady-State Value Used for Hydraulic Property Calibration

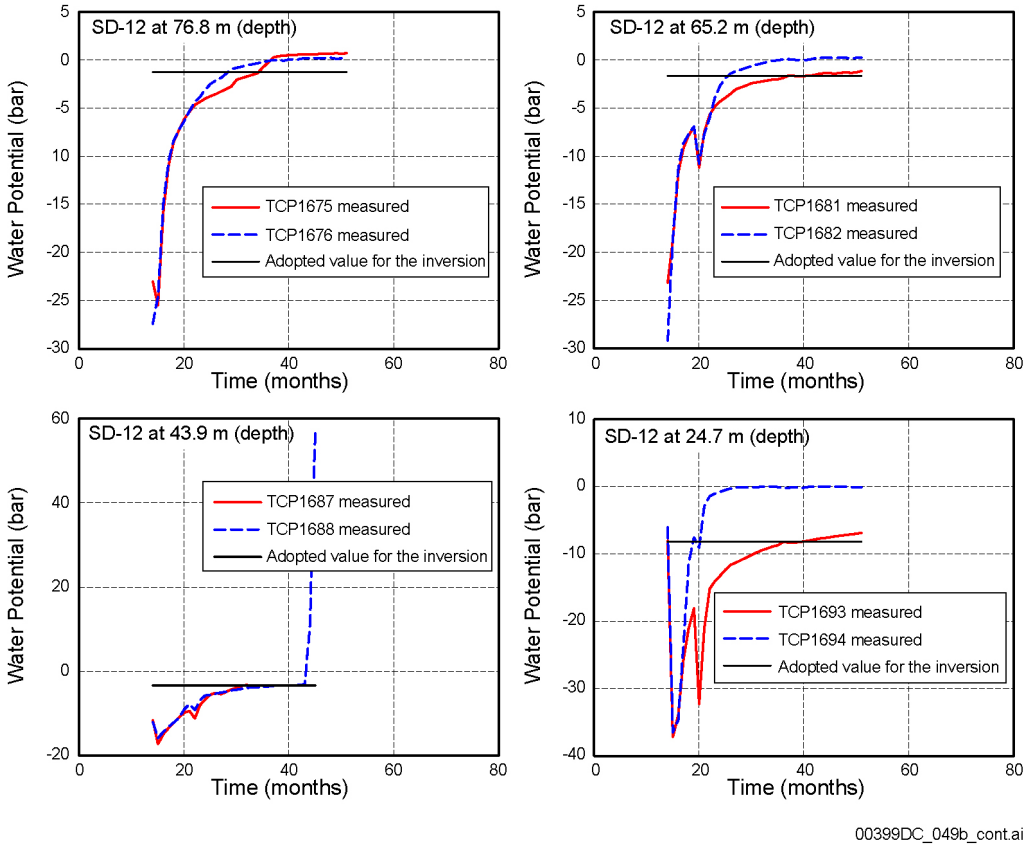

Source: DTN: LB0401H2OPOTEN.001 [DIRS 170678].

NOTE: The equilibrium water potential values used for calibration (inverse modeling) are determined using the data collected before the end of March 1998 (month 42).

Figure A-4b. Measured Water Potential (from Available Instrument Stations of Borehole UE-25 SD-12) Breakthrough (Starting from October 1994, as Month 1) and the Determined Steady-State Value Used for Hydraulic Property Calibration

APPENDIX B
MESH MODIFICATION

This appendix describes modifications of numerical grids used for inversions (Section 6).

B.1 MESHES FOR ONE-DIMENSIONAL CALIBRATION

The one-dimensional meshes for calibrating rock properties were generated from DTN: LB02081DKMGRID.001 [DIRS 160108] (*Boreholes.mesh*). *Boreholes.mesh* was converted to dual-permeability file *Mesh_1D.BOF* as the input to code 2kgrid8.for V1.0 [DIRS 154787]. *Mesh_1D.BOF* was submitted to the Technical Data Management System (TDMS) under DTN: LB0610UZDSCP10.001.

This mesh needs to be modified because:

1. The element names are in an eight-character format that is inconsistent with the five-character format used by iTOUGH2 V5.0 [DIRS 160106].

2. There are element columns that do not correspond to calibration boreholes. Extra elements need to be deleted.

Mesh Element Name Conversion

The eight-character element names in the *Mesh_1D.BOF* consist of three parts:

1. The first part is composed of the first character (F for fracture continuum or M for matrix continuum) and the second character "0".

2. The second part is composed of the third to fifth characters, representing model (material) layers and the order of elements within each model layer. The model layer order is from "01" for material layer "tcw11" to "30" for material layer "bf2". The order for elements within each material layer is from "0", "A", "B", "C"…"T".

3. The third part is composed of the sixth to eighth characters, representing the rock columns in the vertical direction. The sixth character is alphabetic and the seventh to eighth characters are numerical.

Name modification is conducted as follows:

1. Copy the element names in the ELEME block and CONNE block into a file

2. Extract the second part of each name into a second file by using column-copy

3. Delete the second character (e.g., "0") in the first name part

4. Delete the first character ("D", or "q") of the third part (i.e., the sixth character in the eight name), leaving the column number (the second and the third characters of the third part) to be still unique

5. Convert the extracted second part of three characters into a two-character name. The first character in the two-character name is for the element order in each material layer; the second character is for the material layer.

In the name-conversion process described below, "0" is used for representing character "0", NN for two-digit numbers (from 11 to 30), and N for one-digit (non-zero) numbers from 1 to 9, and E for element indicator from A to T:

6. For the 0NN format of the second part, change it into an L0 format for material layers from 10 to 30. (Here, "L" stands for "Letter")

7. For the NNE format, change it to an LE format for material layers from 10 to 30

8. For the 00N format, change it to an N0 format for material layers from 2 to 9

9. For the 0NE format, change it to an NE format for material layers from 1 to 9

10. Switch the resulting first and second characters, putting the material layer indicator after the element indicator. The final format of the converted second part is in EM format, with "E" representing element indicator from "0", "A" to "T", and "M" representing a material indicator from "1" to "9" and then "A" to "U" (see Table B-1).

Table B-1. Material Indicators in Element Names and the Corresponding Material Layer

Material Indicator in the Eight-character Name	Material Indicator in the Five-character Name	Material Layer
01	1	Tcw11
02	2	Tcw12
03	3	Tcw13
04	4	Ptn21
05	5	Ptn22
06	6	Ptn23
07	7	Ptn24
08	8	Ptn25
09	9	Ptn26
10	A	Tsw31
11	B	Tsw32
12	C	Tsw33
13	D	Tsw34
14	E	Tsw35
15	F	Tsw36
16	G	Tsw37
17	H	Tsw38
18	I	Tsw39
19	J	Chn1
20	K	Chn2
21	L	Chn3
22	M	Chn4
23	N	Chn5
24	O	Chn6
25	P	Pp4
26	Q	Pp3

Table B-1. Material Indicators in Element Names and the Corresponding Material Layer (Continud)

Material Indicator in the Eight-character Name	Material Indicator in the Five-character Name	Material Layer
27	R	Pp2
28	S	Pp1
29	T	Bf3
30	U	Bf2

Finally, combine the one-character first part, two-character second part, and two-character third part to form the five-character names. The revised mesh file is *MESH_1D_5char.DOF*, submitted to TDMS under DTN: LB0610UZDSCP10.001.

Deletion of Extra Rock Columns

The correspondence of mesh columns with calibration boreholes is obtained from DTN: LB0208UZDSCPMI.001 [DIRS 161285] (*minfI7Ddri*). This file contains the grid information for all 19 calibration boreholes (except NRG#5). The correspondence between mesh column and calibration borehole for NRG#5 is obtained from DTN: LB02091DSSCP3I.001 [DIRS 161292] (*Mgasi*). For the 20 calibration boreholes, the following table shows the correspondence between boreholes and mesh columns.

Table B-2. Correspondence between Columns and Boreholes

Rock Column in the *MESH_1D.BOF*	Rock Column in the *MESH_1D_5char.BOF*	Borehole
q26	26	NRG#5
D 5, q27 to q41	—	—
q42	42	NRG-6
q43	43	NRG-7
q44	44	SD-6
q45	45	SD-7
q46	46	SD-9
q47	47	SD-12
q48	48	UZ#4
q49	—	—
q50	50	UZ-14
q51	51	UZ#16
q52	52	UZ-N11
q53 to q55	—	—
q56	56	UZ-N31, UZ-N32
q57	57	UZ-N33
q58	—	—
q59	59	UZ-N37
q60	60	UZ-N38
q61	61	UZ-N54, UZ-N53
q62	62	UZ-N55
q63	63	UZ-N58, UZ-N57

Table B-2. Correspondence between Columns and Boreholes (Continued)

Rock Column in the *MESH_1D.BOF*	Rock Column in the *MESH_1D_5char.BOF*	Borehole
q64	64	UZ-N59, UZ-Z61
q65 to q72	—	—
q73	73	WT-24

All rock columns in the original mesh file (*Mesh_1D.BOF*) without corresponding calibration boreholes are deleted for both ELEME and CONNE blocks. The resultant mesh file is *MESH_1D_5char_for19boreholes_withoutTop.BOF,* submitted to TDMS under DTN: LB0610UZDSCP10.001.

Checking the Name Conversion

The modified mesh file is compared with the mesh file: *m1di5m.dkm.nvf.SP.nt* (DTN: LB0208UZDSCPMI.001 [DIRS 161285]). This mesh file has the correct five-character element name and the other grid information, except for the following:

(1) Added fracture-matrix connections between tcw13 and ptn21, ptn26 and tsw31, tsw38, and tsw39 in *m1di5m.dkm.nvf.SP.nt*

(2) Interface-areas changes for all vitric elements in *m1di5m.dkm.nvf.SP.nt*

(3) A 10,000 time increase in element volume in *MESH_1D_5char.BOF*.

The mesh file, *m1di5m.dkm.nvf.SP.nt*, was modified by removing the additional connections mentioned in (1) and changing the interface areas back to geometric values, as mentioned in (2) above. The modified file is *m1di5m.dkm.nvf.SP_modifiedbyzhou.nt* submitted to TDMS under DTN: LB0610UZDSCP10.001. Using the UNIX command *diff*, this file was then compared with *MESH_1D_5char.BOF* changed to the original element volumes (see (3) above). The two files were found to be identical, indicating that the modified mesh file, *MESH_1D_5char.BOF*, is accurate.

B.2 MESHES FOR TWO-DIMENSIONAL FAULT CALIBRATION

The original two-dimensional mesh is *mesh_2d.DKM* in DTN: LB02081DKMGRID.001 [DIRS 160108]. The eight-character names for each grid element are converted into five-character names using the same procedure for the one-dimensional meshes. The first three characters in the five-character names were obtained in the same way as for one-dimensional calibration. The last two characters for the vertical columns are converted as in the following table.

Table B-3. Column Indicators for 8- and 5-Character Element Names

Columns Indicator in an Eight-character Element Name	Column Indicator in a Five-character Element Name
a62	92
q40	90
a63	93
c88	88
A42	42
c87	87
e64	64
q44	44
a58	58
i24	24
i29	99
i35	35
i40	40
i41	41
i46	46
i47	97
i52	52
i56	56
i60	60
i61	61
q69	69
p 3	3
D 5	5
p 2	72
e70	70
c30	30
A13	13
c29	29
q62	62
q51	51
o 2	2
C55	55
o 1	1
a47	47
a48	48
q19	19
D63	63
q18	18
a62	92
q40	90
a63	93
c88	88
A42	42

Table B-3. Column Indicators for 8- and 5-Character Element Names (Continued)

Columns Indicator in an Eight-character Element Name	Column Indicator in a Five-character Element Name
c87	87
e64	64
q44	44
a58	58
i24	24
i29	99
i35	35

The newly modified mesh file is *Mesh_NewFaultCalibration,* submitted to TDMS under DTN: LB0612MTSCHPFT.001.

APPENDIX C
CALCULATION OF AVERAGE INFILTRATION RATES FOR SELECTED BOREHOLES

This appendix describes calculation of infiltration rates for calibration boreholes. An iTOUGH2 run generally needs two input files. One contains rock property, numerical grid, source term, and initial conditions. The other contains variables to be calibrated and data information used for calibration. For convenience, the first file is called a TOUGH2 input file, and the other an iTOUGH2 input file.

C.1. INFILTRATION MAPS AND BOREHOLE LOCATIONS

Infiltration maps with 40 realizations for the present-day climate can be found from DTN: SN0609T0502206.028 [DIRS 178753]. Infiltration rates corresponding to 10th, 30th, 50th, and 90th percentiles are used for calibration. The corresponding realization file names are listed in Table C-1.

Table C-1. Infiltration Realizations Used for Calibration

Percentile of Infiltration Rates	Realization File Name
10	*PD_R2_V18_Infiltration.dat*
30	*PD_R1_V13_Infiltration.dat*
50	*PD_R1_V18_Infiltration.dat*
90	*PD_R2_V17_Infiltration.dat*

DTN: SN0609T0502206.028 [DIRS 178753].

Boreholes selected for calibration are given in Table C-2. Element names of gridblocks containing the boreholes are given in Appendix B (Table B-2).

Table C-2. Calibration Boreholes and their Locations

	Coordinates (m)	
Borehole Name	Easting	Northing
UE-25 NRG#5	172141.9	234052.9
USW NRG-6	171964.2	233698.1
USW NRG-7	171597.5	234354.6
USW SD-6	170263.7	232385.9
USW SD-7	171066.0	231328.0
USW SD-9	171242.1	234085.8
USW SD-12	171177.5	232244.5
UE-25 UZ#4/5	172558.9	234285.9
USW UZ-1/14	170743.5	235090.3
UE-25 UZ#16	172168.4	231811.1
USW UZ-N11	170389.6	237919.0
USW UZ-N31/32	171534.1	232950.9
USW UZ-N33	171051.3	234717.3
USW UZ-N37	171820.0	233933.7
USW UZ-N38	171707.3	233923.6
USW UZ-N53/54	171983.2	231704.1
USW UZ-N55	171982.8	231801.3
USW UZ-N57/58	170945.9	230185.7
USW UZ-N59/61	170959.6	230230.2

Table C-2. Calibration Boreholes and their Locations (Continued)

	Coordinates (m)	
Borehole Name	**Easting**	**Northing**
USW WT-24	171397.9	236739.1

Source: DTN: LB0208HYDSTRAT.001 [DIRS 174491], filename: *borehole loc.xls*.

Because the infiltration map uses UTM coordinates, it should be converted into NSP coordinates before data processing. The coordinate conversion from the UTM to NSP coordinates is provided in output DTN: LB0608COORCONV.001 (filename: *PD_001.out*). This output DTN provides the infiltration model grid coordinates, converted from Universal Transverse Mercator (UTM), in meters, to Nevada State Plane (NSP), in meters. The UTM coordinates are further specified as North American Datum (NAD) 27, zone 11 (as documented in DTN: SN0609T0502206.028 [DIRS 178753], *ReadMe.doc*). The converted NSP coordinates are further specified as NAD 27, Nevada Central - 2702 (see *infl.doc* in the DTN). The coordinate conversion was carried out using CorpsCon V.5.11.08 [DIRS 155082] on a PC platform using Windows NT 4.0 operating system.

C.2 CALCULATION OF INFILTRATION RATES

New coordinates and the infiltration maps were copied to *GENER_Infil0906.xls* in worksheet *Rawdata*. Because the infiltration maps were large in terms of line numbers, exceeding the maximum line number in Excel® (65,536), the infiltration files were divided into three parts (Column A to G for 1 to 50,000, Column I to O for 50,001 to 100,000, Column Q to W for 100,001 to end) and copied into Column B to H of the three worksheets named as "*1*"**,** "*50001*", and "*100001*" in the Excel® file, respectively.

Distances from boreholes to infiltration data points were calculated using the coordinates of boreholes and data points. The calculation follows the following steps:

1. The distance between a borehole and an infiltration data point was calculated using coordinates. Borehole names and coordinates were copied into the area of Cell **Q4** through **BG6** in the three worksheets ("*1*", "*50001*", and "*100001*"), and one borehole name and coordinates were copied into three cells of **O4** to **O6.** The distance between the borehole in the cells (**O4** to **O6**) and the infiltration data points in the columns (**Column B** to **H**) were calculated using the equation (=**SQRT((O$6-$C7)^2+(O$5-$B7)^2)**) and saved to **Column O** under the cells for the borehole.

2. The spreadsheet area (**B7** to **O5006**) (including infiltration data coordinates, infiltrations and the distance) was sorted by ascending order of distance (**Column O**) to find the infiltration data points within the 200-m radius from each borehole. This sorting was executed on the three worksheets ("*1*", "*50001*", and "*100001*") separately. Average infiltrations for the infiltration points within the 200 meter radius were calculated for the 20 boreholes (listed in the table above) and copied into worksheet *Avg Inf*.

3. In most boreholes, infiltration data points within the 200-m radius are found in a worksheet, but two boreholes (SD-6, WT-24) had data points within the 200-m radius in two or three spreadsheets (*1, 50001,* or *100001*). In these cases, all the data points with infiltration were copied into another spreadsheet (*Avg Inf*) to calculate the average infiltration.

4. Average infiltrations for those data points that are within a 200-m radius from each borehole were calculated in the worksheets (*1*, *50001*, or *100001*) and copied into the worksheet "*Avg Inf*."

Because the infiltration has a unit of "mm/yr", it should be converted into "kg/s," which is accepted by TOUGH2 codes. The conversion was executed with the following equation: "Infiltration (kg/s,**Column I** to **M**)= Infiltration (mm/yr, **Column C** to **G**) × Area (m^2) of element for each borehole (**Column H**) / (365.25 × 60 × 60 × 24)" in the worksheet "**unit_conversion**" of *GENER_Infil0906.xls*.

GENER block was generated according to the prefixed TOUGH2 input format and saved as *GENER_INF0906.txt*, in which the five GENER blocks were listed.

Table 6-3 lists area-averaged infiltrations rates for the four selected infiltration maps. For the purpose of comparison, Table C-3 lists the infiltration rates for some calibration boreholes for the old USGS infiltration maps. The procedure used to calculate these rates follows the methods described above regarding unit conversion. The averaged infiltration rates for these boreholes are 0.55, 2.75, and 8.30 mm/yr for the lower-bound, base-case, and upper bound (USGS) infiltration maps, respectively. The averaged infiltration rates for the same boreholes (Table C-3) are 2.63, 6.93, 11.09, and 23.68 mm/yr for the 10th, 30th, 50th, and 90th infiltration scenarios (Table 6-3), respectively.

Table C-3. Area-Averaged Infiltration Rates (mm/yr) for USGS Infiltration Maps for Some Calibration Boreholes

Borehole	Lower Bound	Base Case	Upper Bound
USW NRG-6	10^{-4}	0.53	2.72
USW SD-6	1.17	6.54	15.33
USW SD-7	1.11×10^{-3}	1.06	2.59
USW SD-9	0.08	1.04	3.63
USW SD-12	0.80	3.37	7.95
UE-25 UZ#4	0.02	0.41	3.79
USW UZ-14	0.20	2.28	8.72
UE-25 UZ#16	10^{-4}	0.22	2.91
USW UZ-N11	3.64	10.62	22.67
USW UZ-N31	0.54	1.75	4.45
USW UZ-N33	0.08	0.53	4.76
USW UZ-N37	10^{-4}	0.07	4.40
USW UZ-N53	10^{-4}	0.16	1.45
USW UZ-N57	0.23	5.03	18.08

Table C-3. Area-Averaged Infiltration Rates (mm/yr) for USGS Infiltration Maps for Some Calibration Boreholes (Continued)

Borehole	Lower Bound	Base Case	Upper Bound
USW UZ-N61	0.15	4.84	17.58
USW WT-24	1.87	5.50	11.96

Source: DTNs: LB0208UZDSCPLI.001 [DIRS 178764]; LB0208UZDSCPMI.001 [DIRS 161285]; LB0208UZDSCPUI.001 [DIRS 166711].

APPENDIX D
INPUT AND OUTPUT FILES FOR CALIBRATION OF DRIFT-SCALE PROPERTY SETS

This appendix describes input and output files for calibrations of drift-scale properties (Section 6). An iTOUGH2 run generally needs two input files—one containing rock property, numerical grid, source term, and initial conditions; another containing variables to be calibrated and data information used for calibration. For convenience, the first file is called a TOUGH2 input file, and the other, an iTOUGH2 input file.

D.1 CALIBRATION FOR THE 10TH PERCENTILE INFILTRATION MAP

All the input and output files discussed in this section have been submitted to TDMS under DTN: LB0610UZDSCP10.001.

The infiltration maps are from DTN: SN0609T0502206.028 [DIRS 178753]. As discussed in Appendix C, GENER block is generated based on the coordinates of the 20 calibration boreholes and the 10th percentile infiltration map.

The ROCKS block in the TOUGH2 input file is constructed from the calibrated rock property set for the USGS base-case infiltration rate, corresponding to DTN: LB0208UZDSCPMI.001 [DIRS 161285] and *minfI7Ddri.par*. This is because the mean 10th percentile infiltration rate is close to the mean value for the USGS base-case infiltration map (Appendix C). The numerical grid for one-dimensional calibration is discussed in Appendix B.

The iTOUGH2 input file in DTN: LB0208UZDSCPMI.001 ([DIRS 161285], *minfI7Ddri*) is slightly modified for this calibration. The modifications include:

1. Combining the previous 16 calibration boreholes (NRG-6, SD-6, SD-7, SD-9, SD-12, UZ#4, UZ-14, UZ#16, UZN11, UZN31, UZN33, UZN37, UZN53, UZN57, UZN61, and WT-24) with the previous validation boreholes UZN32, UZN38, UZN54, UZN55, UZN58, UZN59, NRG-7a, and considering all of them to be calibration boreholes.

2. Using previous calibration results as the initial guess for property calibration (DTN: LB0208UZDSCPMI.001 [DIRS 161285], *minfI7Ddri.par*)

3. Performing minor modifications to the "first GUESS" block to avoid convergence problem.

The input and output files for the five sequential calibration runs are listed in Table D-1. The number of sequential runs is determined by the criterion that the objective function is minimized and the calibrated properties are within reasonable ranges. For each run, the calibrated results in the *.par file of its previous run is used for the "first GUESS" block in the iTOUGH2 file. During the calibration, the objective function value is changed from 0.8493×10^4 (*Sandia2R218i.out*) to 0.6620×10^4 (*Sandia2R218Di.out*).

Table D-1. Input and Output Files for 10th Percentile Infiltration Map

Run1	Run2	Run3	Run4	Run5
Sandia2R218	*Sandia2R218A*	*Sandia2R218B*	*Sandia2R218C*	*Sandia2R218D*
Sandiar2R218.out	*Sandiar2R218A.out*	*Sandiar2R218B.out*	*Sandiar2R218C.out*	*Sandiar2R218D.out*
Sandiar2R218.sav	*Sandiar2R218A.sav*	*Sandiar2R218B.sav*	*Sandiar2R218C.sav*	*Sandiar2R218D.sav*
Sandia2R218i	*Sandia2R218Ai*	*Sandia2R218Bi*	*Sandia2R218Ci*	*Sandia2R218Di*
Sandia2R218i.par	*Sandia2R218Ai.par*	*Sandia2R218Bi.par*	*Sandia2R218Ci.par*	*Sandia2R218Di.par*
Sandia2R218i.tec	*Sandia2R218Ai.tec*	*Sandia2R218Bi.tec*	*Sandia2R218Ci.tec*	*Sandia2R218Di.tec*
Sandia2R218i.out	*Sandia2R218Ai.out*	*Sandia2R218Bi.out*	*Sandia2R218Ci.out*	*Sandia2R218Di.out*

D.2 CALIBRATION FOR THE 30TH PERCENTILE INFILTRATION MAP

All the input and output files discussed in this section have been submitted to TDMS under DTN: LB0610UZDSCP30.001.

The infiltration maps are from the DTN: SN0609T0502206.028 [DIRS 178753]. As discussed in Appendix C, GENER block is generated based on the coordinates of the 20 calibration boreholes and the 30th percentile infiltration map.

The ROCKS block in the TOUGH2 input file is constructed from the calibrated rock property set for the USGS upper-bound infiltration rate, corresponding to DTN: LB0208UZDSCPUI.001 [DIRS 166711] and *UinfA1i.par*. This is because the mean 30th percentile infiltration rate is close to the mean value for the USGS upper infiltration map (Appendix C). The numerical grid for one-dimensional calibration is discussed in Appendix B.

The iTOUGH2 input file in DTN: LB0208UZDSCPUI.001 [DIRS 166711], *UinfA1i*) is slightly modified for this calibration. The modifications include:

1. Combining the previous16 calibration boreholes (NRG-6, SD-6, SD-7, SD-9, SD-12, UZ#4, UZ-14, UZ#16, UZN11, UZN31, UZN33, UZN37, UZN53, UZN57, UZN61, and WT-24) with the previous validation boreholes UZN32, UZN38, UZN54, UZN55, UZN58, UZN59, NRG-7a, and considering all of them to be calibration boreholes.

2. Using previous calibration results as the initial guess for property calibration (DTN: LB0208UZDSCPUI.001 [DIRS 166711], *UinfA1i.par*)

3. Performing minor modification in the "first GUESS" block to avoid convergence problem.

The input and output files for the two sequential calibration runs are listed in Table D-1. The number of sequential runs is determined by the criterion that the objective function is minimized and the calibrated properties are within reasonable ranges. For each run, the calibrated results in the **.par* file of its previous run is used for the "first GUESS" block in an iTOUGH2 file. During the calibration, the objective function value is changed from 0.8457×10^4 (*Sandia2R113i.out*) to 0.7551×10^4 (*Sandia2R113Ai.out*).

Table D-2. Input and Output Files for 30th Percentile Infiltration Map

Run1	Run2
Sandia2R113	*Sandia2R113A*
Sandiar2R113.out	*Sandiar2R113A.out*
Sandiar2R113.sav	*Sandiar2R113A.sav*
Sandia2R113i	*Sandia2R113Ai*
Sandia2R113i.par	*Sandia2R113Ai.par*
Sandia2R113i.tec	*Sandia2R113Ai.tec*
Sandia2R113i.out	*Sandia2R113Ai.out*

D.3 CALIBRATION FOR THE 50TH PERCENTILE INFILTRATION MAP

All the input and output files discussed in this section have been submitted to TDMS under DTN: LB0611UZDSCP50.001.

The infiltration maps are from the DTN: SN0609T0502206.028 [DIRS 178753]. As discussed in Appendix C, GENER block is generated based on the coordinates of the 20 calibration boreholes and the 50th percentile infiltration map.

The ROCKS block in the TOUGH2 input file is constructed from the calibrated rock property set for the USGS upper-bound infiltration rate, corresponding to DTN: LB0208UZDSCPUI.001 [DIRS 166711] and *UinfA1i.par*. This is because the mean 50th percentile infiltration rate is close to the mean value for the USGS upper infiltration map (Appendix C). The numerical grid for one-dimensional calibration is discussed in Appendix B.

The iTOUGH2 input file in DTN: LB0208UZDSCPUI.001 ([DIRS 166711], *UinfA1i*) is slightly modified for this calibration. The modifications include:

1. Combining the previous16 calibration boreholes (NRG-6, SD-6, SD-7, SD-9, SD-12, UZ#4, UZ-14, UZ#16, UZN11, UZN31, UZN33, UZN37, UZN53, UZN57, UZN61, and WT-24) with the previous validation boreholes UZN32, UZN38, UZN54, UZN55, UZN58, UZN59, NRG-7a and considering all of them to be calibration boreholes.

2. Using previous calibration results as the initial guess for property calibration (DTN: LB0208UZDSCPUI.001 [DIRS 166711], *UinfA1i.par*)

3. Performing minor modification in the “first GUESS” block to avoid convergence problem.

The input and output files for the three sequential calibration runs are listed in Table D-1. The number of sequential runs is determined by the criterion that the objective function is minimized and the calibrated properties are within reasonable ranges. For each run, the calibrated results in the **.par* file of its previous run is used for the “first GUESS” block in an iTOUGH2 file. During the calibration, the objective function value is changed from 0.9805×10^4 (*Sandia2R118i.out*) to 0.8460×10^4 (*Sandia2R118Bi.out*).

Table D-3. Input and Output Files for 50th Percentile Infiltration Map

Run1	Run2	Run3
Sandia2R118	*Sandia2R118A*	*Sandia2R118B*
Sandiar2R118.out	*Sandiar2R118A.out*	*Sandiar2R118B.out*
Sandiar2R118.sav	*Sandiar2R118A.sav*	*Sandiar2R118B.sav*
Sandia2R118i	*Sandia2R118Ai*	*Sandia2R118Bi*
Sandia2R118i.par	*Sandia2R118Ai.par*	*Sandia2R118Bi.par*
Sandia2R118i.tec	*Sandia2R118Ai.tec*	*Sandia2R118Bi.tec*
Sandia2R118i.out	*Sandia2R118Ai.out*	*Sandia2R118Bi.out*

D.4 CALIBRATION FOR THE 90TH PERCENTILE INFILTRATION MAP

All the input and output files discussed in this section have been submitted to TDMS under DTN: LB0612UZDSCP90.001.

The infiltration maps are from the DTN: SN0609T0502206.028 [DIRS 178753]. As discussed in Appendix C, GENER block is generated based on the coordinates of the 20 calibration boreholes and the 90th percentile infiltration map.

The ROCKS block in the TOUGH2 input file is constructed from the calibrated rock property set for the USGS upper-bound infiltration rate, corresponding to DTN: LB0208UZDSCPUI.001 [DIRS 166711] and *UinfA1i.par*. This is because the mean 90th percentile infiltration rate is close to the mean value for the USGS upper infiltration map (Appendix C). The numerical grid for one-dimensional calibration is discussed in Appendix B.

The iTOUGH2 input file in DTN: LB0208UZDSCPUI.001 ([DIRS 166711], *UinfA1i*) is slightly modified for this calibration. The modifications include:

1. Combining the previous16 calibration boreholes (NRG-6, SD-6, SD-7, SD-9, SD-12, UZ#4, UZ-14, UZ#16, UZN11, UZN31, UZN33, UZN37, UZN53, UZN57, UZN61, and WT-24) with the previous validation boreholes UZN32, UZN38, UZN54, UZN55, UZN58, UZN59, NRG-7a, and considering all of them to be calibration boreholes.

2. Using previous calibration results as the initial guess for property calibration (DTN: LB0208UZDSCPUI.001 [DIRS 166711], *UinfA1i.par*)

3. Performing some minor modifications in the "first GUESS" block to avoid convergence problem.

The input and output files for the three sequential calibration runs are listed in Table D-4. The number of sequential runs is determined by the criterion that the objective function is minimized and the calibrated properties are within reasonable ranges. For each run, the calibrated results in the **.par* file of its previous run is used for the "first GUESS" block in an iTOUGH2 file. During the calibration, the objective function value is changed from 0.1232×10^5 (*Sandia2R217i.out*) to 0.8538×10^4 (*Sandia2R217Ci.out*).

Table D-4. Input and Output Files for 90th Percentile Infiltration Map

Run1	Run2	Run3	Run4
Sandia2R217	*Sandia2R217A*	*Sandia2R217B*	*Sandia2R217C*
Sandiar2R217.out	*Sandiar2R217A.out*	*Sandiar2R217B.out*	*Sandiar2R217C.out*
Sandiar2R217.sav	*Sandiar2R217A.sav*	*Sandiar2R217B.sav*	*Sandiar2R217C.sav*
Sandia2R217i	*Sandia2R217Ai*	*Sandia2R217Bi*	*Sandia2R217Ci*
Sandia2R217i.par	*Sandia2R217Ai.par*	*Sandia2R217Bi.par*	*Sandia2R217Ci.par*
Sandia2R217i.tec	*Sandia2R217Ai.tec*	*Sandia2R217Bi.tec*	*Sandia2R217Ci.tec*
Sandia2R217i.out	*Sandia2R217Ai.out*	*Sandia2R217Bi.out*	*Sandia2R217Ci.out*

INTENTIONALLY LEFT BLANK

APPENDIX E
INPUT AND OUTPUT FILES FOR CALIBRATION OF SITE-SCALE FRACTURE PERMEABILITIES

This section describes input and output files for calibrations of the site-scale property sets (Section 6). An iTOUGH2 run generally needs two input files—one containing rock property, numerical grid, source term, and initial conditions; another containing variables to be calibrated and data information used for calibration. For convenience, the first file is called a TOUGH2 input file, and the other, an iTOUGH2 input file.

E.1 PNEUMATIC PRESSURE DATA FILES

Pneumatic pressure data exist for 22 sensors from five boreholes: NRG#5, NRG-6, NRG-7a, SD-7, and SD-12. The pressure-data file names and associated DTNs are given in Table E-1.

Table E-1. Formatted Pneumatic Pressure Data Files

Files from DTN LB02091DSSCP3I.001 [DIRS 161292]	Files from DTN: LB0302AMRU0035.001 [DIRS 162378]
NRG5_133_zone3.txt	*NRG6_130_PT737.txt*
NRG5_187_zone4.txt	*NRG6_180_PT731.txt*
NRG5_243_zone5.txt	*NRG6_280_PT725.txt*
NRG5_298_zone6.txt	*NRG6_720_PT701.txt*
NRG5_354_zone7.txt	—
NRG5_799_zone13.txt	—
nrg7a_153_PT420.txt	—
nrg7a_18_PT425.txt	—
nrg7a_388_PT413.txt	—
nrg7a_668_PT401.txt	—
SD12_1058_PT1619.txt	—
SD12_214_PT1679.txt	—
SD12_301_PT1667.txt	—
SD12_350_PT1661.txt	—
sd7_300_zone1.txt	—
sd7_350_zone2.txt	—
sd7_400_zone3.txt	—
sd7_800_zone11.txt	—

The pneumatic pressure data at the top boundary is from DTN: LB02091DSSCP3I.001 ([DIRS 161292], *timvsp.dat*). As indicated in DTNs given in Table 6-2, measurement errors (standard deviations) for all the individual pressure measurements are close to 0.001 kPa. Therefore, a constant standard deviation value was used for all the inversions using pneumatic pressure data. As a result of using a constant standard deviation, final calibration results are independent of the standard deviation value used (Equation 6-2). The same treatment was also used for fault property calibrations (Appendix F).

E.2 CALIBRATION FOR THE 10TH PERCENTILE INFILTRATION MAP

All the input and output files discussed in this section have been submitted into the Technical Data Management System (TDMS) under DTN: LB0611MTSCHP10.001.

E.2.1 Steady-State Liquid Flow Forward Run

Mesh

A numerical grid is obtained from *MESH_1D_5char.DOF* (DTN: LB0610UZDSCP10.001). The volume of each element is updated to be its original geometric value, because gas calibration involves transient flow simulations resulting in *MESH_1D_5char_for20boreholes.dat.*

GENER block

The GENER block is *GENER_Infil0906.xls* (Appendix C).

ROCK block

The matrix rock properties are from the one-dimensional calibration (*sandia2R218Di.par* from DTN: LB0610UZDSCP10.001). The mountain-scale fracture permeability values (to three digits for accuracy) for TCw11 to TCw13, PTn21 to PTn26, and TSw31 to TSw37 are obtained from previous gas-pressure calibration results (*Mgasi.par* in DTN: LB02091DSSCP3I.001 [DIRS 161292]) for the base-case USGS infiltration map, because the mean 10th percentile infiltration rate is close to the mean value for the USGS upper infiltration map (Appendix C). Since all these fracture permeability values will be calibrated, the choice of values at this stage does not impact the final calibration results. However, appropriate selection of them (such that they are close to the final calibrated results) would speed up the entire calibration procedure.

Simulation run and data file conversion

Based on the input information mentioned above, the following iTOUGH2 and TOUGH2 input files are constructed: *sandiaR218Gi* and *sandiaR218G.* A forward run for the steady-state liquid flow with EOS9 module is performed. The output file, *sandiaR218G.sav*, is used to generate the INCON block for the steady-state gas/liquid run (to be discussed later). This file is saved as *save.es9* by keeping the number of elements in the first line of *sandiaR218G.sav* and deleting the last two line starting with "+++". The e9-3in V1.0 [DIRS 146536] is used to convert *save.es9* to an EOS3 file, *save.es3*. As there is no default gas pressure in *save.es3*, the file is further updated to *save.up3* with non-zero default gas pressure.

E.2.2 Steady-State Gas and Liquid Forward Simulation

The steady-state gas and liquid forward simulation is performed to obtain the initial condition and top boundary condition (gas pressure) for the transient gas calibration.

The ROCKS block in the TOUGH2 input file (*ssgasR218*) is the same as in *sandiaR218G*, except all fracture porosity values are changed to 1.0. The INCON block is from *save.up3*.

The iTOUGH2 input file (*ssgasR218i*) is created by combining *MinfGasAi* in DTN: LB02091DSSCP3I.001 [DIRS 161292] for NRG#5, NRG-7a, SD-7, and SD-12, and *NMi* in DTN: LB0302AMRU0035.001 [DIRS 162378] for NRG-6.

The forward run is performed using the iTOUGH2 V5.0 [DIRS 160106] with the EOS3 module. The boundary condition file (*timvsp.dat*) for the transient gas calibration is determined by updating the boundary condition file mentioned in Section E.1 with steady-state gas pressure values for the top boundary elements (from *ssgasR218.sav*). The updating is performed using TBgas3D V2.0 [DIRS 160107].

E.2.3 Gas Calibration with Transient Gas and Liquid Flow Simulations

The input files are *ttgasR218i* and *ttgasR218,* in addition to those given in Table E-1. The INCON in *ttgasR218* is from the steady-state run results: *ssgasR218.sav.* The "TIMBC" block is added in *ttgasR218* for time-dependent boundary conditions presented in *timvsp.dat*. The file *ttgasR218i* is the same as *ssgasR218i*, except it includes the OBSERVATION block for all the 22 sensors. The parameters to be calibrated are the shift for the data files and fracture permeability in the TCw11 to TCw13 and PTn21 to PTn26 layers. The calibrated fracture permeability for these units is in *ttgasR218.par*.

E.2.4 Calibration of Fracture Permeability Values for the TSw Layers

Three forward runs are performed with different d-factor values: *ttgasR218Ai* and *ttgasR218A* for log(d_factor) =2.1, *ttgasR218Bi* and *ttgasR218B* for log(d_factor) =2.0, and *ttgasR218Ci* and *ttgasR218C* for log(d_factor) =1.9). The TOUGH2 input files (*ttgasR218A, ttgasR218B, ttgasR218C*) are the same as *ttgasR218.* The iTOUGH2 files (*ttgasR218Ai*, *ttgasR218Bi, ttgasR218Ci*) are prepared based on *ttgasR218i* with the following modifications; (a) the block of fracture permeability for TSw31 to TSw37 is added to the iTOUGH2 input file, and (b) the d-factor is implemented in the "first guess" block by changing the TSw31 to TSw37 fracture permeability values from their prior information as log (prior value) + log (d-factor). The F value is calculated for each of the three cases from the simulation results in *ttgasR218Ai.tec, ttgasR218Bi.tec*, and *ttgasR218Ci.tec*. The F value is then also calculated for the data between the upper sensor in the TSw32 layer and the bottom sensor in the TSw35 layer. The calculation is performed and saved in *R218_d_factor_calibration.xls.* (Details on using Excel® file to calculate F values can be found in Section E.2.). The F values for the three cases (Cases A, B, and C) are 1.298174×10^{-3}, 1.520423×10^{-3}, and 1.831912×10^{-3}, respectively. The F value for the data is 1.447850×10^{-3}, which is closest to that of Case B (*ttgasR218Bi* and *ttgasR218B*). As a result, the calibrated log (d-factor) is 2.0, and the calibrated fracture permeability values for the layers in the TCw, PTn, and TSw units are saved in *ttgasR218Bi.par*.

As shown in the above calibration process, there are two separate steps, one for calibrating fracture permeability for layers TCw11 to TCw13 and PTn21 to PTn26, and the other for d-factor calibration for TSw31 to TSw37. In the first step, the initial d-factor guess (log [d-factor] = 2.0) for layers TSw31 to TSw37 was used. The final calibrated d-factor is the same as the assumed initial guess, and therefore the iteration of the two steps in the calibration process is not needed. However, for completeness, a forward run for this check process is also performed. The input files are *ttgasR218check* and *ttgasR218checki.* As expected, the objective function (considering the output from the second step) remains the same as that from the first step.

Finally, Table E-2 lists all the TOUGH2 and iTOUGH2 input and output files for the inversion runs. During the calibration, the objective function value is changed from 0.3378×10^8 (*TtgasR218i.out*) to 0.3665×10^6 (*TtgasR218teci.out*).

Table E-2. Input and Output Files for Inversion Runs using Gas Pressure Data (10th Percentile Infiltration Case)

	Input Files	Output Files
Initial conditions for EOS3	*SandiaR218G*	*SandiaR218G.out*
	SandiaR218Gi	*SandiaR218G.sav*
		SandiaR218Gi.par
		SandiaR218Gi.tec
		SandiaR218Gi.out
		SandiaR218Gi.msg
Initial and boundary conditions for gas calibration	*ssgasR218*	*SsgasR218.out*
	ssgasR218i	*SsgasR218.sav*
		SsgasR218i.par
		SsgasR218i.tec
		SsgasR218i.out
		SsgasR218i.msg
Gas calibration for TCw and PTn fracture permeability and plotting	*TtgasR218*	*TtgasR218.out*
	TtgasR218i	*TtgasR218.sav*
		TtgasR218i.par
		TtgasR218i.tec
		TtgasR218i.out
		TtgasR218i.msg
	TtgasR218tec	*TtgasR218tec.out*
	TtgasR218teci	*TtgasR218tec.sav*
		TtgasR218teci.par
		TtgasR218teci.tec
		TtgasR218teci.out
		TtgasR218teci.msg
d-factor calibration for TSw fracture peremability	*TtgasR218A*	*TtgasR218A.out*
	TtgasR218Ai	*TtgasR218A.sav*
		TtgasR218Ai.par
		TtgasR218Ai.tec
		TtgasR218Ai.out
		TtgasR218Ai.msg
	TtgasR218B	*TtgasR218B.out*
	TtgasR218Bi	*TtgasR218B.sav*
		TtgasR218Bi.par
		TtgasR218Bi.tec
		TtgasR218Bi.out
		TtgasR218Bi.msg
	TtgasR218C	*TtgasR218C.out*
	TtgasR218Ci	*TtgasR218C.sav*
		TtgasR218Ci.par

Table E-2. Input and Output Files for Inversion Runs using Gas Pressure Data (10th Percentile Infiltration Case) (Continued)

	Input Files	Output Files
		TtgasR218Ci.tec
		TtgasR218Ci.out
		TtgasR218Ci.msg
Iterative calibration for TCw, PTn and TSw fracture permeability	*TtgasR218check*	*TtgasR218check.out*
	TtgasR218checki	*TtgasR218check.sav*
		TtgasR218checki.par
		TtgasR218checki.tec
		TtgasR218checki.out
		TtgasR218checki.msg

E.3 CALIBRATION FOR THE 30TH PERCENTILE INFILTRATION MAP

All the input and output files discussed in this section have been submitted into the Technical Data Management System (TDMS) under DTN: LB0611MTSCHP30.001.

E.3.1 Steady-State Liquid Flow Forward Run

Mesh

A numerical grid is obtained from *MESH_1D_5char.DOF* (DTN: LB0610UZDSCP10.001). The volume of each element is updated to be its original geometric value, because gas calibration involves transient flow simulations. The resulting mesh is: *MESH_1D_5char_for20boreholes.dat* (Section E.2).

GENER block

The GENER block is *GENER_Infil0906.xls* (Appendix C).

ROCK block

The matrix rock properties are from the one-dimensional calibration (*sandia2R113Ai.par* from DTN: LB0610UZDSCP30.001). The mountain-scale fracture permeability values (to three digits for accuracy) for TCw11 to TCw13, PTn21 to PTn26, and TSw31 to TSw37 are obtained from previous gas-pressure calibration result (*Mgasi.par* in DTN: LB02091DSSCP3I.001 [DIRS 161292]). Since all these fracture permeability values will be calibrated, the choice of these values at this stage does not impact the final calibration results. However, appropriate selection of them (such that they are close to the final calibrated results) would speed up the entire calibration process.

Simulation run and data file conversion

Based on the input information mentioned above, the following iTOUGH2 and TOUGH2 input files are constructed: *sandia2R113Gi* and *sandia2R113G.* A forward run for the steady-state liquid flow with EOS9 module is performed. The output file *sandia2R113G.sav* is used to generate the INCON block for the steady-state gas/liquid run to be discussed later. This file is saved as *save.es9* by keeping the number of elements in the first line of *sandia2R113G.sav* and deleting the last two line starting with "+++." The e9-3in V1.0 [DIRS 146536] is used to convert *save.es9* to an EOS3 file, *save.es3*. As there is no default gas pressure in *save.es3*, the file is further updated to *save.up3* with non-zero default gas pressure.

E.3.2 Steady-State Gas and Liquid Forward Simulation

The steady-state gas and liquid forward simulation is performed to obtain the initial condition and top boundary condition (gas pressure) for the transient gas calibration.

The ROCKS block in the TOUGH2 input file (*ssgas2R113*) is the same as in *sandia2R113*, except all fracture porosity are changed to 1.0. The INCON block is from *save.up3*.

The iTOUGH2 input file (*ssgas2R113i*) is created by combining *MinfGasAi* in DTN: LB02091DSSCP3I.001 [DIRS 161292] for NRG#5, NRG-7a, SD-7, and SD-12 and *NMi* in DTN: LB0302AMRU0035.001 [DIRS 162378] for NRG-6.

The forward run is performed using the iTOUGH2 V5.0 [DIRS 160106] with the EOS3 module. The boundary condition file (*timvsp.dat*) for the transient gas calibration is determined by updating the boundary condition file mentioned in Table E-1 with steady-state gas pressure values for the top boundary elements (from *ssgas2R113.sav*). The updating is performed using TBgas3D V2.0 [DIRS 160107].

E.3.3. Gas Calibration with Transient Gas and Liquid Flow Simulations

The input files are *ttgas2R113i* and *ttgas2R113,* in addition to those given in Table E-1. The INCON in *ttgas2R113* is from the steady-state run results: *ssgas2R113.sav.* The "TIMBC" block is added in *ttgas2R113* for time-dependent boundary conditions presented in *timvsp.dat*. *ttgas2R113i* is the same as *ssgas2R113i*, except it includes the OBSERVATION block for the 22 sensors. The parameters to be calibrated are the shift for the data files and fracture permeability in the TCw11 to TCw13 and PTn21 to PTn26 layers. The calibrated fracture permeability values for these units are in *ttgas2R113.par*.

E.3.4. Calibration of Fracture Permeability Values for the TSw Layers

Three forward runs are performed with different d-factor values: *ttgas2R113D1i* and *ttgas2R113D1* for log(d_factor) =1.8, *ttgas2R113D2i* and *ttgas2R113D2* for log(d_factor) =1.9, *ttgas2R113D3i* and *ttgas2R113D3* for log(d_factor) =2.0, and *ttgas2R113D3i* and *ttgas2R113D3* for log(d_factor) =2.1. The TOUGH2 input files are the same as *ttgas2R113.* The iTOUGH2 files are prepared based on *ttgas2R113i* with the following modifications; (a) the block of fracture permeability for TSw31 to TSw37 is added to the iTOUGH2 input file, and (b) the d-factor is implemented in the "first guess" block by changing the TSw31 to TSw37 fracture permeability values from their prior information as log (prior value) + log (d-factor). The F value is calculated for each of the four cases from the simulation results in *ttgas2R113D1i.tec,*

ttgas2R113D2i.tec, *ttgas2R113D3i.tec*, and *ttgas2R113D4i.tec*. The F value is also calculated for the data between the upper sensor in the TSw32 layer and the bottom sensor in the TSw35 layer. The calculation is performed and saved in *R113_d_factor_calibration.xls* (see Section E.3.5). The F values for the four cases (Cases 1 to 4) are 1.955292×10^{-3}, 1.622973×10^{-3}, 1.350371×10^{-3}, and 1.156127×10^{-3}, respectively. The F value for the data is 1.447850×10^{-3}, which is closest to that of Case 3 (*ttgas2R113D3i* and *ttgas2R113D3*). As a result, the calibrated log (d-factor) is 2.0, and the calibrated fracture permeability for the layers in the TCw, PTn, and TSw units are saved in *ttgas2R213Di.par*.

As shown in the above calibration process, there are two separate steps, one for calibrating fracture permeability for layers TCw11 to TCw13 and PTn21 to PTn26, and the other for d-factor calibration for TSw31 to TSw37. In the first step, the initial d-factor guess (log [d-factor] = 2.0) for layers TSw31 to TSw37 was used. The final calibrated d-factor is the same as the assumed initial guess, and therefore the iteration of the two steps in the calibration process is not needed. However, for completeness, a forward run for this check process is also performed. The input files are *sandia2R113check* and *sandia2R113checki.* As expected, the objective function (considering the output from the second step) remains the same as that from the first step.

Finally, Table E-3 lists all the TOUGH2 and iTOUGH2 input and output files for the inversion runs. During the calibration, the objective function value is changed from 0.3251×10^{8} (*Ttgas2R113i.out*) to 0.1716×10^{7} (*Ttgas2R113Di.out*).

Table E-3. Input and Output Files for Inversion Runs using Gas Pressure Data (30th Percentile Infiltration Case)

	Input Files	Output Files
Initial conditions for EOS3	*Sandia2R113G* *Sandia2R113Gi*	*Sandia2R113G.out*
		Sandia2R113G.sav
		Sandia2R113Gi.par
		Sandia2R113Gi.tec
		Sandia2R113Gi.out
		Sandia2R113Gi.msg
Initial and boundary conditions for gas calibration	*Ssgas2R113* *Ssgas2R113i*	*Ssgas2R113.out*
		Ssgas2R113.sav
		Ssgas2R113i.par
		Ssgas2R113i.tec
		Ssgas2R113i.out
		Ssgas2R113i.msg
Gas calibration for TCw and PTn fracture permeability and plotting	*Ttgas2R113* *Ttgas2R113i*	*Ttgas2R113.out*
		Ttgas2R113.sav
		Ttgas2R113i.par
		Ttgas2R113i.tec
		Ttgas2R113i.out
		Ttgas2R113i.msg
	Ttgas2R113A *Ttgas2R113Ai*	*Ttgas2R113A.out*
		Ttgas2R113A.sav

Table E-3. Input and Output Files for Inversion Runs using Gas Pressure Data (30th Percentile Infiltration Case) (Continued)

	Input Files	Output Files
		Ttgas2R113A.par
		Ttgas2R113Ai.tec
		Ttgas2R113Ai.out
		Ttgas2R113Ai.msg
	Ttgas2R113B	*Ttgas2R113B.out*
	Ttgas2R113B	*Ttgas2R113B.sav*
		Ttgas2R113Bi.par
		Ttgas2R113Bi.tec
		Ttgas2R113Bi.out
		Ttgas2R113Bi.msg
	Ttgas2R113C	*Ttgas2R113C.out*
	Ttgas2R113C	*Ttgas2R113C.sav*
		Ttgas2R113Ci.par
		Ttgas2R113Ci.tec
		Ttgas2R113Ci.out
		Ttgas2R113Ci.msg
	Ttgas2R113D	*Ttgas2R113D.out*
	Ttgas2R113D	*Ttgas2R113D.sav*
		Ttgas2R113Di.par
		Ttgas2R113Di.tec
		Ttgas2R113Di.out
		Ttgas2R113Di.msg
d-factor calibration for TSw fracture peremability	*Ttgas2R113D1*	*Ttgas2R113D1.out*
	Ttgas2R113D1	*Ttgas2R113D1.sav*
		Ttgas2R113D1i.par
		Ttgas2R113D1i.tec
		Ttgas2R113D1i.out
		Ttgas2R113D1i.msg
	Ttgas2R113D2	*Ttgas2R113D2.out*
	Ttgas2R113D2	*Ttgas2R113D2.sav*
		Ttgas2R113D2i.par
		Ttgas2R113D2i.tec
		Ttgas2R113D2i.out
		Ttgas2R113D3i.msg
	Ttgas2R113D3	*Ttgas2R113D3.out*
	Ttgas2R113D3	*Ttgas2R113D3.sav*
		Ttgas2R113D3i.par
		Ttgas2R113D3i.tec
		Ttgas2R113D3i.out
		Ttgas2R113D3i.msg
	Ttgas2R113D4	*Ttgas2R113D4.out*
	Ttgas2R113D4	*Ttgas2R113D4.sav*
		Ttgas2R113D4i.par
		Ttgas2R113D4i.tec

Table E-3. Input and Output Files for Inversion Runs using Gas Pressure Data (30th Percentile Infiltration Case) (Continued)

	Input Files	Output Files
		Ttgas2R113D4i.out
		Ttgas2R113D4i.msg
Iterative calibration for TCw, PTn and TSw fracture permeability	*Ttgas2R113check* *Ttgas2R113checki*	*Ttgas2R113check.out*
		Ttgas2R113check.sav
		Ttgas2R113checki.par
		Ttgas2R113checki.tec
		Ttgas2R113checki.out
		Ttgas2R113checki.msg

E 3.5 Description of *R113_d_factor_gascalibration.xls* to Determine F Values

The Excel® file: *R113_d_factor_gascalibration.xls* was used to determine F values. Input files for *R113_d_factor_gascalibration.xls* are *ttgas2R113D1i.tec*, *ttgas2R113D2i.tec*, *ttgas2R113D3i.tec*, and *ttgas2R113D4i.tec*, which are submitted under the DTN: LB0611MTSCHP30.001. In these four extension *.tec* files, only the last four zones (Zone 41 to 44) were used in the calculation. The four zones consist of two zones for data and two zones for simulation, each zone for the upper layer TSw32 and the bottom layer TSw35. The second column in the Zone 41 and Zone 43 for TSw32 Data (line 9,540 to 9,779) and TSw35 Data (line 10,020 to 10,261) in *ttgas2R113D1i.tec* were copied into Column B and C, respectively, in *R113_d_factor_gascalibration.xls*. These data was the same in all four *.tec* files. The second columns in the next zone (Zone 42 and Zone 44) for TSw32 Simulation (line 9781 to 10,020) and TSw35 Simulation (line 10,263 to 10,502) were copied into Column E and F in *R113_d_factor_gascalibration.xls*. The same lines from the other extension *.tec* files (*ttgas2R113D2i.tec*, *ttgas2R113D3i.tec*, and *ttgas2R113D4i.tec*) were copied into *R113_d_factor_gascalibration.xls* for different cases with log d values (−1.9 to −2.0) on Columns H, I, K, L, N, and O. Column D, G, J, M, and P in *R113_d_factor_gascalibration.xls* contains the squared difference of pressure variance between the upper layer (TSw32) and the bottom (TSw35), as presented in the equation:

$$F = \frac{1}{N}\left\{\sum_{i=1}^{N}\left[\left(P_u(t_i) - P_u(t_1)\right) - \left(P_b(t_i) - P_b(t_1)\right)\right]^2\right\}^{1/2} \qquad \text{(Eq. 6-12)}$$

In the Row 243 of the four columns (Column D, G, J, M, and P), the summation was calculated for the Row 3 to 242 (for example, =SUM(D3:D242)). The Cells D244, G244, J244, M244, and P244 were to calculate F using the equation: (=D243^(1/2)/240). In this equation, number 240 is the number (*N*) of data points in the equation above.

The same process has been used for determining the d factor for the other infiltration cases.

E.4 CALIBRATION FOR THE 50TH PERCENTILE INFILTRATION MAP

All the input and output files discussed in this section have been submitted into the Technical Data Management System (TDMS) under DTN: LB0612MTSCHP50.001.

E.4.1 Steady-State Liquid Flow Forward Run

Mesh

A numerical grid is obtained from file *MESH_1D_5char.DOF* (DTN: LB0610UZDSCP10.001). The volume of each element is updated to be its original geometric value, because gas calibration involves transient flow simulations. The resulting mesh is: *MESH_1D_5char_for20boreholes.dat* (Section E.2).

GENER block

The GENER block is *GENER_Infil0906.xls* (Appendix C).

ROCK block

The matrix rock properties are from the one-dimensional calibration (*sandia2R118Bi.par* from DTN: LB0610UZDSCP50.001). The mountain-scale fracture permeability values (with three digits for accuracy) for the TCw11 to TCw13, PTn21 to PTn26, and TSw31 to TSw37 used are from previous gas-pressure calibration result (*Ugasi.par* in DTN: LB02091DSSCP3I.001 [DIRS 161292]). As these fracture permeability values will be calibrated, the choice of these values at this stage does not impact the final calibration results. However, appropriate selection of them (such that they are close to the final calibrated results) would speed up the whole calibration procedure.

Simulation run and data file conversion

Based on the input information mentioned above, the following iTOUGH2 and TOUGH2 input files are constructed: *sandiaR118Gi* and *sandiaR118G.* A forward run for the steady-state liquid flow with EOS9 module is performed. Output file *sandiaR118G.sav* is used to generate the INCON block for the steady-state gas/liquid run to be discussed later. This file is saved as *save.es9* by keeping the number of elements in the first line of *sandiaR118G.sav* and deleting the last two line starting with "+++." The e9-3in V1.0 [DIRS 146536] is used to convert *save.es9* to an EOS3 file, *save.es3*. Since there is no default gas pressure in *save.es3*, the file is further updated to *save.up3* with non-zero default gas pressure.

E.4.2 Steady-State Gas and Liquid Forward Simulation

The steady-state gas and liquid forward simulation is performed to obtain the initial condition and top boundary condition (gas pressure) for the transient gas calibration.

The ROCKS block in the TOUGH2 input file (*ssgasR118*) is the same as in *sandiaR118G*, except all fracture porosity are changed to 1.0. The INCON block is from *save.up3*.

The iTOUGH2 input file (*ssgasR118i*) is created by combining *MinfGasAi* in DTN: LB02091DSSCP3I.001 [DIRS 161292] for NRG#5, NRG-7a, SD-7, and SD-12, and *NMi* in DTN: LB0302AMRU0035.001 [DIRS 162378] for NRG-6.

The forward run is performed using the iTOUGH2 v5.0 with the EOS3 module. The boundary condition file (*timvsp.dat*) for the transient gas calibration is obtained by updating the boundary

condition file mentioned in Table E-1 with steady-state gas pressure values for the top boundary elements (from *ssgasR118.sav*). The updating is performed using TBgas3D V2.0 [DIRS 160107].

E.4.3 Gas Calibration with Transient Gas and Liquid Flow Simulations

The input files are *ttgasR118i* and *ttgasR118,* in addition to those given in Table E-1. The INCON in *ttgasR118* is from the steady-state run results: *ssgasR118.sav.* The "TIMBC" block is added in *ttgasR118* for time-dependent boundary conditions presented in *timvsp.dat*. The file *ttgasR118i* is the same as *ssgasR118i*, except including the OBSERVATION block for all the 22 sensors. The parameters to be calibrated are the shift for the data files and fracture permeability in the TCw11 to TCw13 and PTn21 to PTn26 layers. The calibrated fracture permeability values for these units are in *ttgasR118.par*.

E.4.4 Calibration of Fracture Permeability Values for the TSw Layers

Three forward runs are performed with different d-factor values: *dfgasR118Bi* and *dfgasR118B* for log(d_factor) =2.0, *dfgasR118Ci* and *dfgasR118C* for log(d_factor) =1.9, and *dfgasR118Di* and *dfgasR118D* for log(d_factor) =1.8. The TOUGH2 input files are the same as *ttgasR118.* The iTOUGH2 files are prepared based on *ttgasR118i* with the following modifications; (a) the block of fracture permeability for the TSw31 to TSw37 is added to the iTOUGH2 input file, and (b) the d-factor is implemented in the "first guess" block by changing the TSw31 to TSw37 fracture permeability values from their prior information as log (prior value) + log (d-factor). The F value is calculated for each of the three cases from the simulation results in *dfgasR118Bi.tec, dfgasR118Ci.tec*, and *dfgasR118Di.tec*. The F value is also calculated for the data between the upper sensor in the TSw32 layer and the bottom sensor in the TSw35 layer. The calculation is performed and saved in *R118_d_factor_calibration.xls* (see Section E.3.5). The F values for the three cases (Cases B, C, and D) are 1.134926×10^{-3}, 1.354402×10^{-3}, and $1.624276E \times 10^{-3}$, respectively. The F value for the data is 1.447850×10^{-3}, which is closest to that of Case C (*dfgasR118Ci* and *dfgasR118C*). As a result, the calibrated log (d-factor) is 1.9, and the calibrated fracture permeability for the layers in the TCw, PTn, and TSw units are saved in *dfgasR118Ci.par*.

As shown in the above calibration process, there are two separate steps, one for calibrating fracture permeability for layers TCw11 to TCw13 and PTn21 to PTn26, and the other for d-factor calibration for TSw31 to TSw37. In the first Step, the initial d-factor guess (log [d-factor] = 1.9) for layers TSw31 t0 TSw37 was used. The final calibrated d-factor is the same as the assumed initial guess, and therefore the iteration of the two steps in the calibration process is not needed.

Finally, Table E-4 lists all the TOUGH2 and iTOUGH2 input and output files for the inversion runs. During the calibration, the objective function value is changed from 0.3274×10^{8} (*TtgasR118i.out*) to 0.3805×10^{6} (*TtgasR118teci.out*).

Table E-4. Input and Output Files for Inversion Runs using Gas Pressure Data (50th Percentile Infiltration Case)

	Input Files	Output Files
Initial conditions for EOS3	*SandiaR118G*	*SandiaR118G.out*
	SandiaR118Gi	*SandiaR118G.sav*
		SandiaR118Gi.par
		SandiaR118Gi.tec
		SandiaR118Gi.out
		SandiaR118Gi.msg
Initial and boundary conditions for gas calibration	*SsgasR118*	*SsgasR118.out*
	SsgasR118i	*SsgasR118.sav*
		SsgasR118i.par
		SsgasR118i.tec
		SsgasR118i.out
		SsgasR118i.msg
Gas calibration for TCw and PTn fracture permeability and plotting	*TtgasR118*	*TtgasR118.out*
	TtgasR118i	*TtgasR118.sav*
		TtgasR118i.par
		TtgasR118i.tec
		TtgasR118i.out
		TtgasR118i.msg
	TtgasR118A	*TtgasR118A.out*
	TtgasR118Ai	*TtgasR118A.sav*
		TtgasR118Ai.par
		TtgasR118Ai.tec
		TtgasR118Ai.out
		TtgasR118Ai.msg
	TtgasR118B	*TtgasR118B.out*
	TtgasR118Bi	*TtgasR118B.sav*
		TtgasR118Bi.par
		TtgasR118Bi.tec
		TtgasR118Bi.out
		TtgasR118Bi.msg
	TtgasR118C	*TtgasR118C.out*
	TtgasR118Ci	*TtgasR118C.sav*
		TtgasR118Ci.par
		TtgasR118Ci.tec
		TtgasR118Ci.out
		TtgasR118Ci.msg
	TtgasR118tec	*TtgasR118tec.out*
	TtgasR118teci	*TtgasR118tec.sav*
		TtgasR118teci.par
		TtgasR118teci.tec
		TtgasR118teci.out
		TtgasR118teci.msg
d-factor calibration for TSw	*dfgasR118B*	*dfgasR118B.out*

Table E-4. Input and Output Files for Inversion Runs using Gas Pressure Data (50th Percentile Infiltration Case) (Continued)

	Input Files	Output Files
fracture peremability	*dfgasR118Bi*	*dfgasR118B.sav*
		dfgasR118Bi.par
		dfgasR118Bi.tec
		dfgasR118Bi.out
		dfgasR118Bi.msg
	dfgasR118C	*dfgasR118C.out*
	dfgasR118Ci	*dfgasR118C.sav*
		dfgasR118Ci.par
		dfgasR118Ci.tec
		dfgasR118Ci.out
		dfgasR118Ci.msg
	dfgasR118D	*dfgasR118D.out*
	dfgasR118Di	*dfgasR118D.sav*
		dfgasR118Di.par
		dfgasR118Di.tec
		dfgasR118Di.out
		dfgasR118Di.msg

E.5 CALIBRATION FOR THE 90TH PERCENTILE INFILTRATION MAP

All the input and output files discussed in this section have been submitted into the Technical Data Management System (TDMS) under DTN: LB0612MTSCHP90.001.

E.5.1 Steady-State Liquid Flow Forward Run

Mesh

A numerical grid is obtained from file *MESH_1D_5char.DOF* (DTN: LB0610UZDSCP10.001). The volume of each element is updated to be its original geometric value, because gas calibration involves transient flow simulations. The resulting mesh is: *MESH_1D_5char_for20boreholes.dat* (Section E.2).

GENER block

The GENER block is file *GENER_Infil0906.xls* (Appendix C).

ROCK block

The matrix rock properties are from the one-dimensional calibration (*sandia2R217Ci.par* from DTN: LB0610UZDSCP90.001). The mountain-scale fracture permeability values (with three digits for accuracy) for the TCw11 to TCw13, PTn21 to PTn26, and TSw31 to TSw37 used are from previous gas-pressure calibration result (file: *Ugasi.par* in DTN: LB02091DSSCP3I.001 [DIRS 161292]). Since all these fracture permeability values will be calibrated, the choice of these values at this stage does not impact the final calibration results. However, appropriate

selection of them (such that they are close to the final calibrated results) would speed up the entire calibration process.

Simulation run and data file conversion

Based on the input information mentioned above, the following iTOUGH2 and TOUGH2 input files are constructed: *sandiaR217Hi* and *sandiaR217H.* A forward run for the steady-state liquid flow with EOS9 module is performed. The output file *sandiaR217H.sav* is used to generate the INCON block for the steady-state gas/liquid run to be discussed later. This file is saved as *save.es9* by keeping the number of elements in the first line of the *sandiaR118G.sav* file and deleting the last two line starting with "+++". The e9-3in V1.0 [DIRS 146536] is used to convert *save.es9* to an EOS3 file *save.es3*. Since there is no default gas pressure in *save.es3*, the file is further updated to *save.up3* with non-zero default gas pressure.

E.5.2 Steady-State Gas and Liquid Forward Simulation

The steady-state gas and liquid forward simulation is performed to obtain the initial condition and top boundary condition (gas pressure) for the transient gas calibration.

The ROCKS block in the TOUGH2 input file (*ssgasR217*) is the same as in *sandiaR217H*, except all fracture porosity are changed to 1.0. The INCON block is from *save.up3*.

The iTOUGH2 input file (*ssgasR217i*) is created by combining *MinfGasAi* in DTN: LB02091DSSCP3I.001 [DIRS 161292] for NRG#5, NRG-7a, SD-7, and SD-12, and file *NMi* in DTN: LB0302AMRU0035.001 [DIRS 162378] for NRG-6.

The forward run is performed using the iTOUGH2 V5.0 [DIRS 160106] with the EOS3 module. The boundary condition file (*timvsp.dat*) for the transient gas calibration is determined by updating the boundary condition file mentioned in Table E-1 with steady-state gas pressure values for the top boundary elements (from *ssgasR217.sav*). The updating is performed using TBgas3D V2.0 [DIRS 160107].

E.5.3 Gas Calibration with Transient Gas and Liquid Flow Simulations

The input files are *ttgasR217i* and *ttgasR217,* in addition to those given in Table E-1. The INCON in *ttgasR217* is from the steady-state run results: *ssgasR217.sav.* The "TIMBC" block is added in *ttgasR217* for time-dependent boundary conditions presented in *timvsp.dat*. The file *ttgasR118i* is the same as *ssgasR217i*, except including the OBSERVATION block for all the 22 sensors. The parameters to be calibrated are the shift for the data files and fracture permeability in the TCw11 to TCw13 and PTn21 to PTn26 layers. The calibrated fracture permeability for these units are in *ttgasR217i.par*.

E.5.4. Calibration of Fracture Permeability Values for the TSw Layers

Three forward runs are performed with different d-factor values: *dfgasR217Bi* and *dfgasR217B* for log(d_factor) =2.0, *dfgasR217Ci* and *dfgasR217C* for log(d_factor) =1.9, and *dfgasR217Di* and *dfgasR217D* for log(d_factor) =1.8. The TOUGH2 input files are the same as *ttgasR217.* The iTOUGH2 files are prepared based on *ttgasR217i* with the following modifications; (a) the

block of fracture permeability for TSw31 to TSw37 is added to the iTOUGH2 input file, and (b) the d-factor is implemented in the "first guess" block by changing the TSw31 to TSw37 fracture permeability values from their prior information as log (prior value) + log (d-factor). The F value is calculated for each of the three cases from the simulation results in *dfgasR217Bi.tec, dfgasR217Ci.tec*, and *dfgasR217Di.tec*. The F value is also calculated for the data between the upper sensor in the TSw32 layer and the bottom sensor in the TSw35 layer. The calculation is performed and saved in *R217_d_factor_calibration.xls* (see Section E.3.5). The F values for the three cases (Cases B, C, and D) are 1.097547×10^{-3}, 1.315879×10^{-3}, and 1.585255×10^{-3}, respectively. The F value for the data is 1.447850×10^{-3}, which is closest to that of Case C (*dfgasR217Ci* and *dfgasR217C*). As a result, the calibrated log (d-factor) is 1.9, and the calibrated fracture permeability for the layers in the TCw, PTn, and TSw units are saved in *dfgasR217Ci.par*.

As shown in the above calibration process, there are two separate steps, one for calibrating fracture permeability for layers TCw11 to TCw13 and PTn21 to PTn26, and the other for d-factor calibration for TSw31 to TSw37. In the first Step, the initial d-factor guess (log [d-factor] = 1.9) for layers TSw31 t0 TSw37 was used. The final calibrated d-factor is the same as the assumed initial guess, and therefore the iteration of the two steps in the calibration process is not needed.

Finally, Table E-5 lists all the TOUGH2 and iTOUGH2 input and output files for the inversion runs. During the calibration, the objective function value is changed from 0.3296×10^{8} (*TtgasR217i.out*) to 0.5484×10^{6} (*TtgasR217teci.out*).

Table E-5. Input and Output Files for Inversion Runs using Gas Pressure Data (90th Percentile Infiltration Case)

	Input Files	Output Files
Initial conditions for EOS3	*SandiaR217H*	*SandiaR217H.out*
	SandiaR217Hi	*SandiaR217H.sav*
		SandiaR217Hi.par
		SandiaR217Hi.tec
		SandiaR217Hi.out
		SandiaR217Hi.msg
Initial and boundary conditions for gas calibration	*SsgasR217*	*SsgasR217.out*
	SsgasR217i	*SsgasR217.sav*
		SsgasR217i.par
		SsgasR217i.tec
		SsgasR217i.out
		SsgasR217i.msg
Gas calibration for TCw and PTn fracture permeability and plotting	*TtgasR217*	*TtgasR217.out*
	TtgasR217i	*TtgasR217.sav*
		TtgasR217i.par
		TtgasR217i.tec
		TtgasR217i.out
		TtgasR217i.msg
	TtgasR217A	*TtgasR217A.out*

Table E-5. Input and Output Files for Inversion Runs using Gas Pressure Data (90th Percentile Infiltration Case) (Continued)

	Input Files	Output Files
	TtgasR217Ai	*TtgasR217A.sav*
		TtgasR217Ai.par
		TtgasR217Ai.tec
		TtgasR217Ai.out
		TtgasR217Ai.msg
	TtgasR217B	*TtgasR217B.out*
	TtgasR217Bi	*TtgasR217B.sav*
		TtgasR217Bi.par
		TtgasR217Bi.tec
		TtgasR217Bi.out
		TtgasR217Bi.msg
	TtgasR217C	*TtgasR217C.out*
	TtgasR217Ci	*TtgasR217C.sav*
		TtgasR217Ci.par
		TtgasR217Ci.tec
		TtgasR217Ci.out
		TtgasR217Ci.msg
	TtgasR217tec	*TtgasR217tec.out*
	TtgasR217teci	*TtgasR217tec.sav*
		TtgasR217teci.par
		TtgasR217teci.tec
		TtgasR217teci.out
		TtgasR217teci.msg
d-factor calibration for TSw fracture peremability	*dfgasR217B*	*dfgasR217B.out*
	dfgasR217Bi	*dfgasR217B.sav*
		dfgasR217Bi.par
		dfgasR217Bi.tec
		dfgasR217Bi.out
		dfgasR217Bi.msg
	dfgasR217C	*dfgasR217C.out*
	dfgasR217Ci	*dfgasR217C.sav*
		dfgasR217Ci.par
		dfgasR217Ci.tec
		dfgasR217Ci.out
		dfgasR217Ci.msg
	dfgasR217D	*dfgasR217D.out*
	dfgasR217Di	*dfgasR217D.sav*
		dfgasR217Di.par
		dfgasR217Di.tec
		dfgasR217Di.out
		dfgasR217Di.msg

APPENDIX F
INPUT AND OUTPUT FILES FOR TWO-DIMENSIONAL FAULT PROPERTY CALIBRATION

This appendix describes all the input and output files for calibration of fault properties (Section 6). All the relevant input and output files discussed in this appendix were submitted to the TDMS under DTN: LB0612MTSCHPFT.001. An iTOUGH2 run generally needs two input files—one containing rock property, numerical grid, source term, and initial conditions; another containing variables to be calibrated and data information used for calibration. In this appendix, the first file is called TOUGH2 input file, and the other, iTOUGH2 input file, for convenience.

F.1 GENERAL INPUTS

Numerical grids are from DTN: LB02081DKMGRID.001 [DIRS 160108] (*mesh_2d.DKM*). The eight-character element-name format was changed into a 5-character element-name format (see Appendix B). The final mesh file is *Mesh_NewFaultCalibration*.

The infiltration map (present day) is from SN0609T0502206.028 [DIRS 178753]. The GENER blocks are determined using infil2grid V1.7 [DIRS 154793]. Inputs are the grids and the infiltration maps. The outputs are *2D_EW_10.GEN* for the 10th percentile, *Q_EW_30.GEN* for the 30th percentile, *2D_EW_50.GEN* for the 50th percentile, and *2D_EW_90.GEN* for the 90th percentile, respectively.

For the moisture calibration, the moisture (and capillary pressure) data are from file *MFA*i in DTN: LB02092DSSCFPR.001 [DIRS 162422]. The initial guesses for the fault properties in moisture calibration are from uncalibrated fault property sets (DTN: LB0207REVUZPRP.001 [DIRS 159525]). Property sets for non-fault parts are LB0611MSTCHP10.001 for the 10th percentile case, LB0611MSTCHP30.001 for the 30th percentile case, LB0611MSTCHP50.001 for the 50th percentile case, and LB0611MSTCHP90.001 for the 90th percentile case, respectively. The output from this calibration is fracture alpha and the active fracture parameter.

For pneumatic data calibration, the files with extension "*prn*" from DTN: LB02092DSSCFPR.001 [DIRS 162422] were used as pneumatic data input. iTOUGH2 input file is from file *LMGi* in the above DTN. The top boundary gas-pressure condition is determined from file *timvspF.dat* from the above DTN. The code used to determine top boundary conditions is TBgas3D V2.0 [DIRS 160107]. The code used to convert eos9 results to eos3 results is e9-3in V1.0 [DIRS 146536].

F.2 CALIBRATION SIMULATIONS

The iTOUGH2 V5.0 [DIRS 160106] is used for inversion. In the calibration against moisture and water potential data, fracture alpha and active fracture model parameters are determined. The calibrated parameter sets are then used in the pneumatic data calibration for fracture permeability. In the pneumatic calibration, the fracture residual was set to zero to avoid numerical convergence problems, while this treatment has negligible effect. This is because the residual saturation has little effect on the absolute permeability for dry fractures. After that, the simulation run is performed using new fracture permeabilities to again check the match with moisture and water potential data.

(1) The 10th percentile case

Input/output files for moisture and water potential data calibration:

Input: *test10, test10i*
Output: *test10.sav; test10.out; test10i.par; test10i.out*
During this calibration step, the objective function value is changed from 0.3538×10^3 to 0.3502×10^3 (*test10i.out*).

The file *test10.sav* was converted to eos3 format: *save10.es3*. Then 9.2×10^5 is added to the pressure column and the new file *save10.up3* is used as INCON block for file *try10*. This file was used to run initial conditions for gas calibration. Output files are *try10.sav* and *try10.out*.

The top boundary condition file is *timvsp10.dat* for the gas calibration. Input files for the gas calibration are: *testGas10*; *testGAS10i*; *testGAS10A*; and *testGAS10Ai*. Output files are: *testGAS10.out*, *testGAS10.sav*; *testGAS10i.out*; *testGAS10i.par*; *testGAS10i.tec*; *testGAS10A.out*; *testGAS10Ai.out*; *testGAS10Ai.par*; *testGAS10Ai.tec*. During the gas calibration, the objective function value is changed from 0.2032×10^7 (*testGAS10i.out*) to 0.5730×10^4 (*testGAS10Ai.out*).

After gas calibration, a forward run is performed to check if the objective function (for moisture and water potential calibration) is significantly increased using the new gas calibrated fracture permeability. If not, the results are acceptable. In this case, the check results are satisfactory. The input file for the check run is *Check10* and *Check10i*. Outputs are *Check10.out*; *Check10i.out* and *Check10i.par*.

The final calibration results are in *Check10i.par*.

(2) The 30th percentile case

Input/output files for moisture and water potential data calibration:

Input: *test30, test30i*
Output: *test30.sav*; *test30.out*; *test30i.par*; *test30i.out*

During this calibration step, the objective function value is changed from 0.5063×10^3 to 0.4926×10^3 (*test30i.out*).

The file *test30.sav* was converted to eos3 format: *save30.es3*. Then 9.2×10^5 is added to the pressure column and the new file *save30.up3* is used as INCON block for file *try30*. This file was used to run initial conditions for gas calibration. Output files are *try30.sav* and *try30.out*.

The top boundary condition file is *timvsp30.dat* for the gas calibration. Input files for the gas calibration are: *Gas30; GAS30i*. Output files are: *GAS30.out, GAS30.sav; GAS30i.out; GAS30i.par; GAS30i.tec.* During the gas calibration, the objective function value is changed from 0.2032×10^7 to 0.5730×10^4(*GAS30i.out*).

After gas calibration, a forward run is performed to check if the objective function (for moisture and water potential calibration) is significantly increased using the new gas calibrated fracture permeability. If not, the results are acceptable. In this case, the check results are satisfactory.

The input file for the check run is *Check30* and *Check30i*. Outputs are *Check30.out*; *Check30i.out* and *Check30i.par.*

The final results are in *Check30i.par*.

(3) The 50th percentile case

Input/output files for moisture and water potential data calibration:

Input: *Atest50, Atest50i*
Output*: Atest50.sav; Atest50.out; Atest50i.par; Atest50i.out*
During this calibration step, the objective function value is changed from 0.5374×10^3 to 0.4971×10^3 (*Atest50i.out*).

The file *Atest50.sav* was converted to eos3 format: *save50.es3*. Then 9.2×10^5 is added to the pressure column and the new file *save50.up3* is used as INCON block for file *try50*. This file was used to run initial conditions for gas calibration. Output files are *try50.sav* and *try50.out*.

The top boundary condition file is *timvsp50.dat* for the gas calibration. Input files for the gas calibration are: *Gas50; GAS50i*. Output files are: *GAS50.out, GAS50.sav; GAS50i.out; GAS50i.par; GAS50i.tec.* During the gas calibration, the objective function value is changed from 0.1971×10^7 to 0.5938×10^4 (*GAS50i.out*).

After gas calibration, a forward run is performed to check if the objective function (for moisture and water potential calibration) is significantly increased using the new gas calibrated fracture permeability. If not, the results are acceptable. In this case, the check results are satisfactory. The input file for the check run is *Check50* and *Check50i*. Outputs are *Check50.out*; *Check50i.out*, and *Check50i.par*.

The final results are in *Check50i.par*.

(4) The 90th percentile case

Input/output files for moisture and water potential data calibration:

Input: *test90, test90i*
Output: *test90.sav*; *test90.out*; *test90i.par*; *test90i.out*

During this calibration step, the objective function value is changed from 0.7455×10^3 to 0.6399×10^3 (*test90i.out*).

test90.sav was converted to eos3 format: *save90.es3*. Then 9.2×10^5 is added to the pressure column and the new file *save90.up3* is used as INCON block for file *try90*. This file was used to run initial condition for gas calibration. Output files are *try90.sav* and *try90.out*.

For the gas calibration, the top boundary condition file is *timvsp90.dat*. Input files for the gas calibration are: *Gas90; GAS90i*. Output files are: *GAS90.out, GAS90.sav; GAS90i.out;*

GAS90i.par; GAS90i.tec. During the gas calibration, the objective function value is changed from 0.2012×10^7 to 0.6368×10^4 (*GAS90i.out*).

After gas calibration, a forward run is performed to check if the objective function (for moisture and water potential calibration) is significantly increased using the new gas calibrated fracture permeability. If not, the results are acceptable. In this case, the check results are satisfactory. The input file for the check run is *Check90* and *Check90i*. Outputs are *Check90.out; Check90i.out and Check90i.par.*

The final results are in *Check90i.par*.

APPENDIX G
QUALIFICATION OF UNQUALIFIED DATA

G.1 PURPOSE

This appendix documents qualification of data used to calculate weights given to observations in inverse modeling in Section 6.2.2. The values to be qualified are (a) the relative humidity, wind speed, and air temperature (of the environment in which samples were handled in the field) of 25%, 3 km/hr, and 30°C, respectively; (b) the core surface area available for evaporative loss of moisture of 297 cm^2; (c) a 95% confidence for in situ measurement of water potential of ±0.2 MPa; (d) a sample handling time in the field of 5 min; and (e) error in measurement of saturation of 0.5%.

G.2 QUALIFICATION PLAN AND CRITERIA

Data Qualification Plan, Qualification of Parameter Values Used to Estimate Measurement Errors for Matrix Water Saturation and Water Potential (SNL 2006 [DIRS 178762]), hereafter called the data qualification plan, states that the qualification process will be according to Method 2 "Corroborating Data" in SCI-PRO-001, *Qualification of Unqualified Data,* Attachment 3, because data are available to conduct data comparisons that can be shown to substantiate or confirm parameter values. In addition, the data qualification plan (SNL 2006 [DIRS 178762]) states that Qualification Process Attribute 6 "the extent to which conditions under which the data were generated may partially meet the QA program that supports the YMP License Application process or post closure science" is used.

G.3 DATA QUALIFICATION DETAIL

G.3.1 Relative Humidity, Temperature, and Wind Speed

Corroborating data that support the relative humidity, temperature, and wind speed values used in the calculations in Section 6.2.2 were recorded at six sites at Yucca Mountain (DTN: SN0608WEATHER1.005 [DIRS 177912]). This qualified DTN was used in lieu of the DTNs provided in the data qualification plan (SNL 2006 [DIRS 178762]), which are not available for viewing. Sites 1, 2, and 9 were used for corroborating the unqualified data.

From the hourly-averaged relative humidity, temperature, and wind-speed data, those collected during daytime (8:00 AM to 6:00 PM, the most likely times of field work) were selected. From these, the minimum and maximum values of relative humidity, wind-speed data, and temperature for each site and year were identified and are summarized in Tables G-1, G-2, and G-3, respectively. The relative humidity, wind speed, and air temperature values used in the calculations of moisture loss in Section 6.2.2 (25%, 30°C, and 3 km/hr, respectively) are all within the range of observations obtained from the qualified data source and, therefore, meet the criteria for qualification of unqualified data provided in the data qualification plan (SNL 2006 [DIRS 178762]).

Calculation Procedures

The data reduction procedures employed were identical for all the three quantities (relative humidity, temperature, and wind speed). The following steps are used to calculate temperature:

Step 1. Create a new blank Excel® Workbook. Rename the first worksheet at Site 1 (same applies for Sites 2 and 9). Save as *Temperature-hourly-site 1.xls*.

Step 2. From the DTN open the file Site 1 *SmyQry_Aug23.xls*. The file consists of separate worksheets with hourly weather data for years ranging from 1993 to 2004. From these worksheets, copy columns A to D (corresponding to site, year, Julian day, and time) of 1993 and paste in worksheet "Site 1" of *Temperature-hourly-site 1.xls*. Repeat copying the same data for with years 1994 through 2004 and paste them in columns J to M, S to V, etc. of "Site 1" of *Temperature-hourly-site 1.xls*.

Step 3. Copy the column containing temperature of 1993 in *SmyQry_Aug23.xls*and paste column E of "Site 1" of *Temperature-hourly-site 1.xls*. Repeat copying the same data for with years 1994 through 2004 and paste them in columns N, W, etc. of "Site 1" of *Temperature-hourly-site 1.xls*.

Step 4. In column G (and P, Y etc) calculate the date and time in the Excel® Serial Format (Year + Julian_Day−1+Time_of_day/100/24). The exact formula used is "DATE(B6,1,1)+C6-1+D6/100/24".

Step 5. In column H (and Q, Z, etc) copy the temperature from column E (and N, W, etc.) if the time is between 8:00AM and 6:00 PM.

Step 6. For each year identify the maximum and minimum temperature using the max() and min() functions of Excel®. These values are tabulated in Table G-2.

In the DTN files, the wind speed is recorded in m/s. These values were converted to km/hr by multiplying the DTN values by a factor of 3.6.

Table G-1. Maximum and Minimum of Hourly-Averaged Day-Time Relative Humidity (%)

Site		1993	1994	1995	1996	1997	1998	1999	2000	2001	2002	2003	2004
1	Max							97.6	99.5	100	93.5	96.7	97.2
	Min							2.9	2.3	3.0	3.2	3.6	4.0
2	Max	100	100	100	100	100	100	100	100	100	92.9	96.3	96.6
	Min	2.8	1.6	1.8	2.1	1.8	2.4	2.6	2.0	3.1	2.1	2.5	2.9
9	Max	98.8	96.5	100	100	100	100	98.0	98.8	100	95.8	99.0	99.6
	Min	2.3	1.5	1.0	1.3	1.0	1.5	1.4	0.9	1.4	1.7	2.2	2.5

Table G-2. Maximum and Minimum of Hourly-Averaged Day-Time Wind Speed (km/hr)

Site		1993	1994	1995	1996	1997	1998	1999	2000	2001	2002	2003	2004
1	Max	50.90	48.13	56.48	51.30	50.26	57.35	49.82	49.32	46.55	63.50	57.78	64.22
	Min	1.08	1.04	1.04	1.50	1.98	1.81	2.34	2.00	1.63	1.88	2.32	1.91
2	Max	75.02	76.57	81.68	73.44	67.03	82.12	71.86	71.17	69.98	85.28	83.34	69.98
	Min	0.04	2.71	2.54	2.02	2.55	1.89	2.56	2.47	2.24	2.45	2.65	2.46
9	Max	48.20	55.08	58.54	56.92	53.86	55.80	57.82	61.45	53.75	69.80	54.68	66.35
	Min	2.31	2.10	2.68	1.43	2.62	2.31	1.82	2.98	2.28	1.80	2.20	2.25

Table G-3. Maximum and Minimum of Hourly-Averaged Day-Time Temperature (°C)

Site		1993	1994	1995	1996	1997	1998	1999	2000	2001	2002	2003	2004
1	Max	39.4	39.8	40.2	39.8	39.5	41.5	40.5	41.0	41.1	42.3	41.6	39.6
	Min	−6.2	−3.7	−2.6	−5.5	−7.7	−7.6	−2.3	−2.5	−2.7	−4.8	−3.2	−5.4
2	Max	36.4	38.8	38.3	38.2	37.8	39.8	38.3	38.8	38.9	39.9	39.7	37.5
	Min	−6.3	−4.4	−2.3	−5.1	−9.3	−7.4	−4.5	−2.6	−4.8	−5.8	−5.2	−4.7
9	Max	43.1	43.9	43.8	43.2	42.7	44.7	43.2	43.4	43.6	44.5	44.3	42.3
	Min	−7.1	−5.7	−1.7	−5.0	−5.0	−8.1	−3.2	−2.7	−2.3	−6.8	−3.9	−4.2

G.3.2 Surface Area of Core Samples Available for Evaporative Moisture Loss

Corroboration of the core surface area available for evaporation (297 cm²) used in the calculations in Section 6.2.2 is done by referencing drilling instructions that specify the diameter of core to be obtained and core logs that provide elevations of core top and bottom depths, from which the core lengths can be calculated. Core top and bottom depths were recorded in *Sample Management Facility, Core Processing Checklist* (YMP 1996 [DIRS 178714], 1995 [DIRS 178715]). Drilling instructions recorded in DTN: TM0000SD9SUPER.002 [DIRS 168542] (Subpart DRC.19960819.0022, requirement # 3.1.6) specifies minimum core diameter of 2.4 in (6.1 cm), and DTN: TMUSWSD1200095.001 [DIRS 178755] (subpart DRC.19960926.0092, requirement # 3.12.1) specifies core diameter of 2.4 in.

Core length information is recorded in the Core Processing Checklist of the Sample Management Facility. Specific information on cores retrieved from boreholes SD-12 and UZ-14 and sent to A. Flint are recorded in *Sample Management Facility, Core Processing Checklist* (YMP 1996 [DIRS 178714], 1995 [DIRS 178715]) and listed in Table G-4. The geometric and arithmetic means of the core lengths are 11.9 and 14.1 cm, respectively. The corresponding core-surface areas are 287 and 329 cm^2, respectively. The unqualified surface of 297 cm² used in the calculations in Section 6.2.2 is within 50% of the corroborating surface areas calculated above and, therefore, meets the criteria for qualification of unqualified data provided in the data qualification plan (SNL 2006 [DIRS 178762]).

Table G-4. Lengths of Cores Retrieved from Wells SD-12 and UZ-14

Well	SMF ID	Top (ft)	Bottom (ft)	Length (cm)
SD-12[a]	26480[a]	13.4[a]	13.7[a]	9.144[a]
SD-12[a]	26481[a]	13.7[a]	14.2[a]	15.24[a]
UZ-14	28953	1,725.8	1,726.3	15.24
UZ-14	28954	1,726.3	1,726.6	9.144
UZ-14	28956	1,728.1	1,728.8	21.336
UZ-14	28957	1,728.5	1,728.8	9.144
UZ-14	28924	1,716.4	1,716.6	6.096
UZ-14	28925	1,716.6	1,717.1	15.24
UZ-14	28927	1,718.9	1,719.4	15.24
UZ-14	28928	1,719.4	1,719.6	6.096
UZ-14	28958	1,731	1,731.3	9.144

Table G-4. Lengths of Cores Retrieved from Wells SD-12 and UZ-14 (Continued)

Well	SMF ID	Top (ft)	Bottom (ft)	Length (cm)
UZ-14	28959	1,731.3	1,731.7	12.192
UZ-14	28945	1,721.9	1,722.4	15.24
UZ-14	28946	1,722.4	1,722.7	9.144
UZ-14	28948	1,723.3	1,723.6	9.144
UZ-14	28976	1,743	1,743.2	6.096
UZ-14	28977	1,743.2	1,743.7	15.24
UZ-14	28984	1,746.7	1,747.1	12.192
UZ-14	28985	1,747.1	1,747.8	21.336
UZ-14	28965	1,734.5	1,734.7	6.096
UZ-14	28966	1,734.7	1,735.1	12.192
UZ-14	28970	1,737.1	1,737.4	9.144
UZ-14	28971	1,737.4	1,737.9	15.24
UZ-14	28987	1,749.8	1,750.1	9.144
UZ-14	28988	1,750.1	1,750.6	15.24
UZ-14	28990	1,752.3	1,752.7	12.192
UZ-14	28991	1,752.7	1,753	9.144
UZ-14	28973	1,740.2	1,740.4	6.096
UZ-14	28974	1,740.4	1,740.8	12.192
UZ-14	29031	1,761.8	1,762.1	9.144
UZ-14	29032	1,762.1	1,762.7	18.288
UZ-14	29038	1,765.5	1,765.7	6.096
UZ-14	29039	1,765.7	1,766.1	12.192
UZ-14	29204	1,755.6	1,756	12.192
UZ-14	29205	1,756	1,757.8	54.864
UZ-14	29042	1,768	1,768.6	18.288
UZ-14	29043	1,768.6	1,770.8	67.056
UZ-14	29208	1,758.5	1,758.8	9.144
UZ-14	29209	1,758.8	1,759	6.096

Sources: [a]YMP 1996 [DIRS 178714]; all others, YMP 1995 [DIRS 178715].

G.3.3 Confidence for in situ Measurement of Water Potential

In situ water potentials were measured with thermocouple psychrometers. Corroborating data that support the 95% confidence for in situ measurement of water potential of 0.2 MPa is available in Theormocouple Psychrometer Calibration Control Forms. The calibration data for two psychrometers are recorded in DTN: GS950208312232.003 [DIRS 105572] (subparts MOL.19950412.0198 and MOL.19950412.0213). The sensors were calibrated against standards in the ranges –7.4098 to –0.0904 MPa and –6.7547 to –0.0904 MPa, respectively. There were 107 and 90 calibration points, respectively, for each of the sensors. Measurement errors were documented in the calibration records for each calibration point. The 95% confidence intervals range from 0.1031 to 0.1487 MPa and 0.1018 to 0.1043 MPa. The corroborating 95% confidence interval of in situ water potential measurements is within the interval used in the calculations in Section 6.2.2 (0.2 MPa) and, therefore, meets the criteria for qualification of unqualified data provided in the data qualification plan (SNL 2006 [DIRS 178762]).

G.3.4 Sample Handling Time

Instruction on special handling for core samples from borehole USW NRG-6 (Edwards 1992 [DIRS 178718]) direct that samples should be placed in metal tins within five minutes of the opening of the split inner core barrel. This instruction corroborates the estimated sample handling time of five minutes used in the calculation in Section 6.2.2.

G.3.5 Measurement Error of Sample Saturation

Saturation was measured by method HP-266. In this method, the sample is weighed four times. First, it is weighed as received (D). Lettering is reversed to agree with the notation of *Standard Test Method for Density, Relative Density (Specific Gravity), and Absorption of Coarse Aggregate* (ASTM 2001 [DIRS 159569]). It is then saturated with water and weighed under water (C). This gives an apparent weight, which is the weight of the saturated sample minus the weight of an equal volume of water. Then the surface is saturated surface dried (SSD) and the sample is weighed in air (B). The weight of an equal volume of water is therefore (B–C). Finally, the sample is oven dried and weighed (A). Of these four weighings, the greatest error occurs with (B), because of the irreproducibility of the step in which the core outer surface is dried; the sample may be partially desaturated or excess water may remain on the surface. All the other weighings are relatively error-free.

The measurement error for the density of a saturated core (SSD density) is discussed in the ASTM standard (2001 [DIRS 159569], Section 11). The SSD density in kg/m^3 is calculated as ($\rho B/(B–C)$) (ASTM 2001 [DIRS 159569]), Equation (6)), where ρ is the density of water). The standard deviation of repeated measurements by a single operator using this method is 7 kg/m^3, equal to 0.007 g/cm^3 (ASTM 2001[DIRS 159569], Table 1). For a typical rock with SSD density of 2.33 g/cm, this results in a percentage error of 0.3%. The density of water is known exactly; therefore, the percentage error of (B/(B–C)) is also 0.3%. The effect of error in B on the calculated SSD is partly mitigated by the fact that B appears in the numerator and denominator.

This measurement error can be used to estimate the error in measurement of the saturation calculated from these weighings: saturation is (D–A)/(B–A). Because B does not appear in the numerator, the effect of error in B on the calculated saturation is greater than its effect on calculated SSD density, typically (depending upon grain density, porosity, and saturation) about twice as great, or about 0.6%. Thus, the standard deviation of measurements reported in *Standard Test Method for Density, Relative Density (Specific Gravity), and Absorption of Coarse Aggregate* (ASTM 2001 [DIRS 159569], Table 1) corroborates the estimate of 0.5% measurement error in saturation.

G-4 CONCLUSION

The unqualified data in Section 6.2.2 meet all criteria outlined in the data qualification plan (SNL 2006 [DIRS 178762]) and, therefore, are qualified for use in this report. The qualification provides a desired level of confidence that the data are suitable for their intended use for the work documented in this report (Section 6).

INTENTIONALLY LEFT BLANK